Investigating the role of chloride in endocytic organelle acidification

By
Mary R. Weston

A dissertation submitted to Johns Hopkins University in conformity with the requirements for the degree of Doctor of Philosophy

Baltimore, Maryland
December 2017

ABSTRACT

Endocytic organelles maintain their characteristic, essential internal pH using the V-type ATPase H^+-pump. Accumulation of H^+ generates a voltage across the membrane; an additional ion, known as a counterion, must move to dissipate charge buildup. Chloride (Cl^-) has been hypothesized to be an important counterion in the endosomal pathway, but its role is still debated. This thesis seeks to explore the role of counterions and the proteins that facilitate their movements in the acidification of clathrin-coated vesicles (CCVs), a subset of early endosomes, and lysosomes. We confirmed previous work showing that isolated bovine brain CCVs acidify in the presence of external Cl^-, independent of the monovalent cations present. While unsuccessful at identifying the protein responsible for the observed anion transport, we used a new approach to confirm that most brain CCVs are synaptic vesicles. Secondly, because acidification in isolated lysosomes is Cl^--dependent and the lysosomal protein ClC-7, a Cl^-/H^+ antiporter, moves Cl^- into the organelles, this protein has been suggested to mediate such counterion movement. However, live cell ClC-7 knockout (KO) mouse lysosomes have the same pH as WT. We generated mice with a liver-specific deletion of ClC-7 to test these results in isolated lysosomes and live cells in parallel. While isolated ClC-7 KO lysosomes showed a drastic decrease in Cl^--facilitated acidification, lysosomal pH was similar in WT and KO hepatocytes, even during metabolic and base challenges. Lastly, we present two patients with an identical pathogenic *de novo* variant in *CLCN7*, who display hypopigmentation, a delay in motor skills, abnormal liver/spleen/kidneys, and failure to thrive, but no osteopetrosis. Patient fibroblasts contain large vacuoles scattered throughout the cytoplasm that do not consistently stain for lysosomal markers, and

possess a vast increase in the lysosomal-like compartments that stain for Lamp1, a lysosomal protein. Lysosomal pH in cultured patient fibroblasts are more acidic than the neonatal controls and heterologous expression of the mutant ClC-7 in *Xenopus* oocytes revealed substantial increases in transport activity. These results suggest a novel gain-of-function for this Cl^-/H^+ antiporter, one of the first reported instances of lysosomal hyperacidification, and shows that ClC-7 plays a role in lysosomal pH. Overall, this work contributes to the field of organelle acidification and brings us closer to understanding how organelles use counterions to assist in and regulate pH.

Advisor/primary thesis reader: Joseph Mindell, M.D., Ph.D.

Secondary thesis readers: Kenton Swartz, Ph.D.
Beverly Wendland, Ph.D.

Acknowledgements

Graduate school has been a great challenge and an adventure. I have learned so much and am grateful to all those who helped and supported me over the years.

First and foremost, I would like to thank my mentor, Dr. Joseph Mindell, for providing me with support and guidance throughout my graduate work. I am so thankful that I had the opportunity to work with someone who constantly challenged me to develop a thoughtful and rigorous approach to science. Thank you for your patience, encouragement, and for knowing that I would come out on the other side.

The Mindell lab has been a fun place to scientifically “grow up”. Thank you to the current and past members for the atmosphere, the advice, and the food (specifically, birthday cakes, bagels, and babkas). I am especially grateful to Dr. Sara Lioi for teaching me about cells and to Dr. Christopher Mulligan for acting as my surrogate "older graduate student" when I first started. Additional thanks go to the members of the 3B and 3D pods. It has been amazing to be surrounded by so many kind people who foster a creative and collaborative scientific environment.

Thank you to all my collaborators. It has been lovely working with and learning from you all, especially Dr. Anowarul Amin and Dr. Ralu Nicoli.

Thank you to my wonderful thesis committee. Dr. Kenton Swartz and Dr. Beverly Wendland have provided constant support and guidance throughout my graduate work and I am grateful for their helpful scientific discussions and mentorship. Additionally, I received a lot of support from the kind people in the GPP, the professors and administrators at the JHU program, and OITE. I would specifically like to thank Dr. Orna Cohen-Fix and Julia Jarvis for listening to my science woes and encouraging me to carry on.

I had some lovely and encouraging teachers during my high school and undergrad years who encouraged me on my path. Of those, I would like to specifically thank Mr. Kennedy for sparking my interest in science and Dr. Frank Roberto for keeping that spark alive.

I have been fortunate to have had so many amazing friends over the years and many of you have made a lasting impact. Throughout graduate school, I am so happy that Senta, Kristie, Annie, Angel, and Sara shared in this adventure.

Thank you to Gobi Thillai for being my person. I am eternally grateful for your advice, support, and patience through this graduate process. Thank you for making me laugh, for your healthy dose of reality through this process, and the constant reminder to enjoy life and not take things too seriously.

I am so blessed to have my family. Thank you to my parents, Jeff and Karen. Thank you for providing me a solid foundation in both learning and in life. You always provided unwavering support and taught me to approach the world with kindness. I am grateful for my grandparents who are so encouraging and are some of my life role models. I strive to be as wise and humble as you. Then there are my crazy/fun/weird siblings, Rachel, David, and Eve. Thank you for being my biggest, most consistent cheerleaders, especially during those late-night phone calls. They say you can't choose your family but, given the option, I could not have done better.

TABLE OF CONTENTS

LIST OF FIGURES

Science is a collaborative effort and some of the work presented in this thesis has been performed by others.

In chapter 3, Anorawul Amin did all the experiments in isolated lysosomes while I performed experiments related to measuring lysosomal pH in cultured hepatocytes.

Chapter 4 is a highly collaborative effort between several different research groups. Others were responsible for sequencing and clinically characterizing the patients, isolating patient fibroblasts, and measuring the electrophysiological differences between the mutant and WT proteins. I was responsible for experiments related to the behavior of cultured cells and lysosomal pH of patient fibroblasts. The figures that were contributed to by others are marked as follows:

*Figures with work from both Mary Weston and a collaborator
**Figures contributed solely by a collaborator

Chapter 1: Introduction

pH in the endocytic pathway

From prokaryotes to multicellular organisms, function and behavior is dictated by, and has evolved from, interactions with the pH of external and internal environments. For example, the human body carefully regulates the pH of its various systems to ensure proper function, ranging from the slightly basic pH of blood, where even small deviations can result in detrimental symptoms, to the extremely acidic pH of the stomach. On a cellular level, processes such as the generation of ATP in the mitochondria, the glycosylation and transport of proteins from the trans-Golgi network, and macromolecule degradation in lysosomes depend on precise pHs for proper function. Various diseases arise when pH is improperly regulated, with symptoms ranging from tolerable to life threatening.

Careful regulation and maintenance of luminal pH is crucial for the function of the organelles that comprise the endocytic pathway, a transport network used to recycle or degrade various solutes and macromolecules within a cell (Figure 1). These membrane-delimited organelles consist of early endosomes, recycling endosomes, late endosomes, and lysosomes. The pathway begins with the fusion of endocytic vesicles to early endosomes, providing them with cargo and internal solutes. Early endosomes sort the internalized material, lipids, and membrane proteins, where they are sent to be degraded or recycled back to the plasma membrane, the trans-Golgi network (TGN), or recycling endosomes. After a short period of cargo accumulation and recycling, early endosomes undergo a maturation process and eventually transition to late endosomes.

Late endosomes fuse with lysosomes to become endolysosomes and these hybrid organelles ultimately mature into lysosomes, acidic compartments containing hydrolytic enzymes that degrade macromolecules.

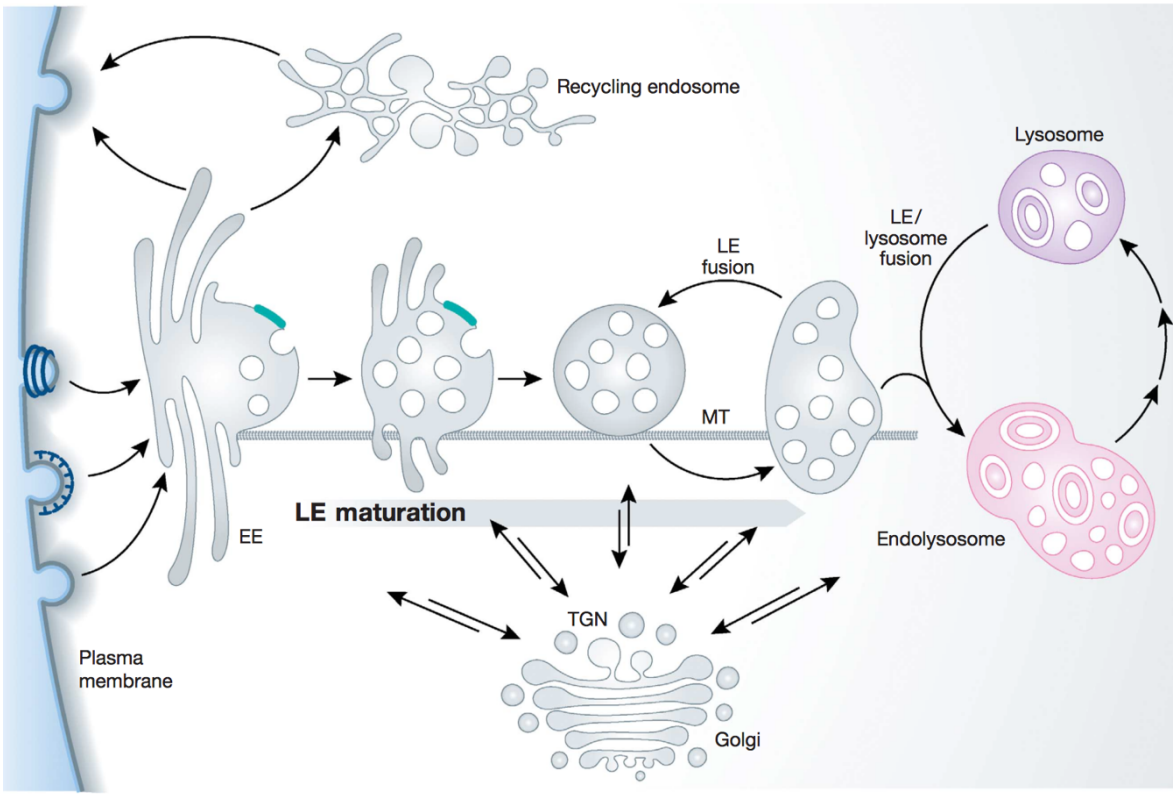

Figure 1: The endosome/lysosome system.
Endocytic vesicles, typically originating from the plasma membrane and the trans-Golgi network (TGN) deliver their cargo to early endosomes (EEs). After a short period where EEs accumulate cargo and sort some away for recycling, the EEs mature into late endsosomes (LEs). Lysosomes fuse with LEs to form endolysosomes, which ultimately mature into lysosomes. pH progressively decreases along the endosomal pathway. EEs typically maintain a pH near 6.5, LE have a pH between 5.0-5.5, and lysosomes typically have a pH around 4.0-5.0.

The endosomal organelles progressively become more acidic, a process essential to their function. The pathway starts with early endosomes near pH 6.5 and end with lysosomes whose pH ranges from 4.0-5.0. In early and late endosomes, the decrease in pH to specific values induces conformation changes that trigger the release of ligands from their respective transmembrane receptor proteins. Once released, cargo remains in the organelle lumen and the receptors are recycled back to the plasma membrane or TGN. In the lysosome, the extremely acidic pH is vital to optimally activate internal hydrolyses and to provide the protons necessary to drive the transport of catabolites back into the cytoplasm.

In this thesis, I explore mechanisms related to how pH is established/maintained in two endocytic compartments: clathrin-coated vesicles, a subset of early endosomes, and lysosomes. Although these organelles have drastically different internal pH values and function, both appear to utilize Cl^- transporting membrane proteins to assist with maintaining internal acidification.

The V-ATPase generates a pH gradient in endocytic organelles

The acidic pH of endocytic organelles is generated and maintained by the vacuolar H^+-ATPase (V-ATPase), a membrane protein that utilizes the metabolic energy from ATP hydrolysis to unidirectionally pump protons into the lumen. It is a multisubunit complex composed of a membrane-embedded V_0 subcomplex (consisting of eight subunits, A-H) that contains a central stock attached to the soluble, cytoplasmic V_1 subcomplex (made up of five subunits, a,c,c'',d, and e) (4). Hydrolysis of ATP drives the rotation of the V_1 domain around the central stock, forcing protons to move through the V_0 domain and into the lumen. Unlike the structurally-related F_0F_1 ATPases that both

synthesize and hydrolyze ATP, the V-ATPases only unidirectionally rotate to hydrolyze ATP. Assuming the efficiency of the V-ATPase is 2 protons pumped for every ATP hydrolyzed, Grabe et al. calculated that an ideal rotary pump could theoretically create up to a 4 pH unit gradient between the organelle lumen and the cytosol (5), a wide range that encompasses all of the pHs found within the endocytic pathway.

The V-ATPase is responsible for acidifying various intracellular organelles, including clathrin-coated vesicles, endosomes, lysosomes, secretory vesicles, and the Golgi apparatus, yet each compartment maintains its own unique internal pH (4). Although the mechanisms that control internal organellar pH are unclear, one possible method is to regulate the H^+ pump. Several potential mechanisms of V-ATPase activity have been observed, but none have been shown to directly regulate organelle pH. These mechanisms occur on both functional and transcriptional levels and include the reversible inactivation of the pump, utilization of different isoforms that control cellular localization and/or modify ATP hydrolysis-proton transport coupling efficiency, and interaction with regulating partners (4, 6).

One form of V-ATPase regulation occurs at the functional level, where the soluble V_1 subcomplex reversibly dissociates from the membrane-embedded V_0 complex, resulting in the loss of both its ATP hydrolysis and H^+ translocation capabilities. This process was first observed in the yeast *S. cerevisiae* upon glucose starvation and in the tobacco hornworm *Manduca sexta* (*M. sexta*) in response to molting or starvation (7, 8). Addition of glucose/nutrients reversed this process, inducing the reassembly of V_1 with V_0 and restoring H^+ pumping without the need for synthesis of new protein (7). Renal cells also display some V-ATPase dissociation in response to glucose starvation, although

the physiological significance of this has yet to be determined (9). The dissociation process is regulated and aided by various protein and protein complexes, including the RAVE complex, microtubules, and the glycolytic enzyme aldolase (6). Thus, V-ATPase activity acts as a metabolic sensor regulated by nutrient availability, although whether this specifically influences pH in different organelles is unknown. Additional instances of V-ATPase functional regulation have been observed in various mammalian cells. For example, maturing dendritic cells activate the proton pump on late endosomes/lysosomes to acidify the organelle and process antigens (10).

Another mechanism of V-ATPase regulation is control of cellular localization. This regulation has been most studied in yeast, where two different isoforms of subunit a, Vph1p and Stv1p, dictate whether the protein is targeted to the vacuole or the TGN, respectively (11-13). To compare the properties of the two isoforms, the Forgac lab overexpressed one of the isoforms in a yeast strain where the genes of both isoforms had been disrupted. By only expressing one isoform, Kawasaki-Nishi et al. measured the kinetic properties of the two complexes and measured coupling efficiency of ATP hydrolysis, the ability of the pump to couple ATP hydrolysis to the pumping of H^+ (13). While having similar rates of hydrolysis, complexes containing the Vph1p were 4-5 times more efficient at coupling ATP hydrolysis to H^+ pumping than the Stv1p-containing complexes, indicating that the latter complexes slip and hydrolyze ATP without pumping H^+. While this change to the pump mechanism seems inefficient, the lower pH in the vacuole compared to the Golgi complex mirrors the V-ATPase distribution and may assist in pH regulation in the compartments.

In addition to cellular localization, isoforms of certain subunits have been observed to be tissue specific. The most studied subunit is a, which has 4 isoforms in mammalian cells. These isoforms are heavily expressed in specific tissues, including a3 in osteoclasts, a4 in renal tissue, and a1 in synaptic vesicles of neuronal tissues (14). These isoforms appear to be important for targeting the V-ATPase to specific locations, such as the plasma membrane during bone resorption or synaptic vesicles in neurons, where their function is required in a tissue specific manner. Besides subunit a, at least 6 of the 14 V-ATPase subunits have multiple isoforms (14). In these cases, typically one subunit tends to be ubiquitously expressed and trafficked, while another directly targets a specific compartment. For example, the d1 subunit is ubiquitously expressed but the d2 subunit has limited tissue distribution, expressed primarily in bone osteoclasts and kidney (15, 16), and mice lacking the subunit have increased bone mass due to defective osteoclasts (17). While their individual effects have been observed, combinations of isoforms may be an additional type of regulation that is unexplored.

Therefore, while many mechanisms regulate activity on both transcriptional and functional levels, none directly show that the V-ATPase affects pH levels. It is possible cells may employ various combinations of isoforms to tune the targeting and coupling efficiency of the pump's activity to certain tissues/locations, but these approaches have yet to be identified. Therefore, other mechanisms must be investigated in order to determine how different organelles maintain their various internal pHs.

The electrogenic V-ATPase requires counterions to allow organelle acidification

The proton pumping action of the V-ATPase is electrogenic because it translocates charge across the lumen of the membrane, creating a voltage difference. This electrogenic property was established in isolated lysosomes by experiments performed by Ohkuma et al. and Harikumar & Reeves using the voltage-sensitive fluorescent dye diS-C_3(5) (18, 19). This positively charged dye accumulates in the membrane of compartments with negative transmembrane voltages, resulting in the quenching of fluorescence. In their experiments, the fluorescence signal of the dye increased upon the activation of the V-ATPase (by ATP addition), indicating that H^+ pumping shifts the lysosomal lumen from negative internal voltages to more positive ones. The change in membrane potential clearly shows that the H^+ pump is electrogenic. The accumulation of charge from the continuous pumping of the V-ATPase eventually builds to the point where net transport is inhibited because it is no longer favorable to pump an additional H^+ across the membrane. Thus, to efficiently acidify an organelle an additional ion, known as a counterion, must simultaneously move to dissipate charge buildup and allow bulk acidification. The counterion could be a cytoplasmic anion entering the organelle, a luminal cation exiting the organelle, or a combination of both mechanisms. If counterion movement is a rate-limiting step in acidification, this too could be a mechanism of regulation of organelle pH.

The ions most likely to behave as counterions are Na^+, K^+, Cl^-, and Ca^{2+}, due to their relative cellular abundance. The identity of the counterion(s) utilized by the organelles in the endosomal pathway has been studied in various systems, but is still not fully understood. Most of the initial studies investigating the importance and identity of counterions were performed on isolated organelles, an approach that allows for precise

control over the external ion composition. These experiments revealed that in isolated clathrin-coated vesicles (CCVs), endosomes, and lysosomes, the presence of anions in the bathing solution, specifically Cl^-, facilitate acidification when measured with pH sensitive dyes (20-24). Subsequent studies over the years show that CCVs and endosomes rely on Cl^- to act as the primary counterion in acidification, but the ions utilized by lysosomes are less clear (25-27). In the following sections I will expand upon the potential counterion mechanisms used by organelles in the endosomal pathway, focusing on early endosomes and lysosomes.

Endosomal acidification

Early endosomes serve as the sorting hub of the endocytic pathway. They receive macromolecules and other cargo from endocytic vesicles formed at the plasma membrane or TGN, which then either fuse with existing early endosomes or with each other to generate early endosomes. Upon receiving cargo, early endosomes direct internal solutes to various locations in the cell using the same vesicles. The internal pH of ~6-6.5 of the early endosome induces the detachment of certain substrates from their transmembrane receptors, allowing for the recycling of receptors back to the plasma membrane/TGN. Those cargos that are not recycled in either the early or late endosomes are moved to the lysosome for degradation. Early endosomes mature into late endosomes through a series of fission and fusion events involving the modification or exchange of multiple organelle-specific lipids and membrane proteins. Because of their diverse inputs and continuous maturation, endosomes tend to have an extremely heterogeneous composition. Consequentially, studying their acidification properties using a biochemical approach is

challenging because it is difficult to separate them from other endosomal organelles to obtain a well-defined population. Despite these barriers, it is well established that endosomes utilize the V-ATPase to acidify (28). Additionally, Cl^- has emerged as the primary counterion that facilitates acidification, but some significant questions remain in the process. In the following sections, I will detail some of the proteins thought to be important in endosomal acidification, primarily focusing on the endosomal members of the chloride channel (ClC) superfamily, and propose a method to biochemically investigate early endosomal acidification.

Early study of endosomal acidification

The discovery of endocytic organelles occurred throughout the 1950s-60s, assisted by the technological advancements in ultracentrifugation and electron and fluorescence microscopy. While lysosomes were discovered in 1955 (29), endosomes were not characterized until 1964 when Werner Straus observed that internalized proteins passed through intermediate structures ('prelysosomal vacuoles') prior to reaching lysosomes (30). He noted a progression of protein localization from the peripheral cytoplasm at early time points to the perinuclear area near lysosomes at later time points (later defined as early and late endosomes). Twenty years later, Tycko and Maxfield incubated cultured cells with a fluorescein-labeled α2-macroglobulin to measure the pH changes in endosomes following receptor-mediated endocytosis, the process by which cells uptake extracellular solutes (31). They observed that after 15-20 min, the fluorescent ligand was contained in an acidic compartment with a pH of 5.0 +/- 0.2, in contrast to a fluorescein-dextran, which reached lysosomes after approximately 30-35 min and had a

pH of 4.6 +/- 0.2. These results were shortly verified both *in viv*o by Van Renswoude et al., who observed the acidification of internalized substrate prior to reaching the lysosome, and *in vitro* by Galloway et al., who demonstrated that isolated endosomes acidify in an ATP-dependent manner (32, 33). Thus, endosomes were discovered as intermediate transport vesicles that are not quite as acidic as lysosomes.

Subsequent studies of endosomal pH acidification properties employed more precise methods to examine the organelles in both isolated and live cell settings. Obtaining a well-defined population of isolated endosomes is challenging due to their constant, rapid maturation process. To evaluate the acidification properties *in vitro,* isolated endosomes are either harvested after a brief exposure to a pH sensitive dye that is rapidly internalized via endocytosis or harvested and subsequently incubated with a membrane permeable dye. These studies have shown that the V-ATPase is responsible for acidification (28, 33, 34). Van Dyke and colleagues examined the counterions required for endosomal acidification, finding that the organelles primarily relied on Cl^- for acidification, but also displayed a permeability to Na^+ and a substantial H^+ leak (23, 34).

In vivo methods used to characterize endosomal pH typically involve using a pH-sensitive dye taken up by endocytosis, fluorescently-labeled compartment specific proteins, or expression of a GFP/GFP-variant attached to an endosomal-specific membrane protein. These studies have shown that early endosomes tend to have a pH of 5.9-6.8 and late endosomes range between 5.0-6.0 (2). Additionally, several proteins have been found that contribute to the maintenance of endosomal acidification, some of which may provide a counterion current. These proteins include some members of the

ClC family, the Cl^- channel Cystic Fibrosis Transmembrane Conductance Regulator (CFTR), and sodium-proton exchangers (NHEs). These family members will be discussed in detail in the next sections.

The diverse family of ClC transporters and channels

The ClC family is a diverse group of Cl^- channels and secondary active transporters. ClCs are well conserved and found in yeast, bacteria, archaea, plants, and invertebrates. There are nine isoforms in mammals, located in the plasma membrane and intracellularly, where they participate in a wide range of physiological functions. ClC family members play critical roles in the cell and their mutations cause various diseases (35). ClC-0, the first known member of the family, was characterized by White and Miller as a voltage-gated anion channel in the electric organ of the *Torpedo* ray, but an additional ten years passed before it was identified and cloned by Jentsch et al. (36, 37). Crystal structures of both prokaryotic and eukaryotic ClCs reveal that they are homodimers with a functional ion-translocating pathway in each monomer (3, 38-40) (Figure 2). Surprisingly, while all mammalian isoforms share the same basic structure, half of the family members function as channels and the rest are $2Cl^-/H^+$ antiporters. This distinction between Cl^- channels and transporters was discovered by Accardi and Miller in the bacterial ecClC (41), and confirmed a year later in the eukaryotic homologs ClC-4 and -5 (42, 43). Subsequent studies demonstrated the same antiporter function for ClC-6 and -7, with ClC-3 presumably being an antiporter as well (25, 44, 45).

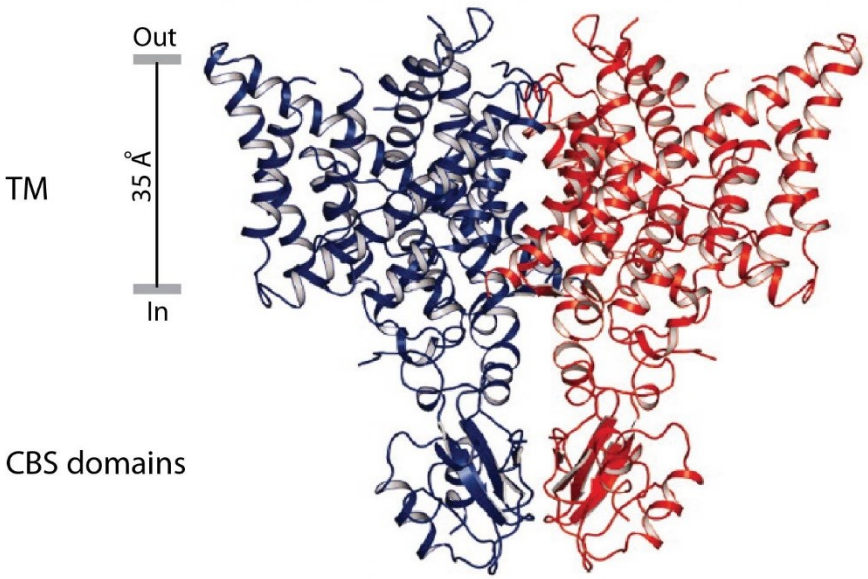

Figure 2: Structure of CmClC
Ribbon representation of the eukaryotic CmClC dimer from the side of the membrane. The CBS domains, found only in eukaryotic ClCs, are located below the TM domain and reside in the cytoplasm. The individual monomers are colored in blue and red, respectively. Figure adapted from Feng et al. (2010); PDB: 3ORG. Full citation: (3).

In addition to being separated into channels and transporters, these two groups of the ClC family are also spatially segregated. The channels, ClC-1, -2, -Ka, and -Kb, are found in the plasma membrane while the transporters, ClC-3 to ClC-7, are found intracellularly within endocytic organelles (Figure 3). The antiporter ClC-3 is found primarily in endosomes and synaptic vesicles, ClC-4 and ClC-5 in endosomes, ClC-6 in neuronal late endosomes, and ClC-7 in lysosomes (35). Additionally, four of the mammalian ClCs (ClC-Ka and -Kb, ClC-2, and ClC-7) possess auxiliary β subunits that are essential for their associated ClC's function (46-48).

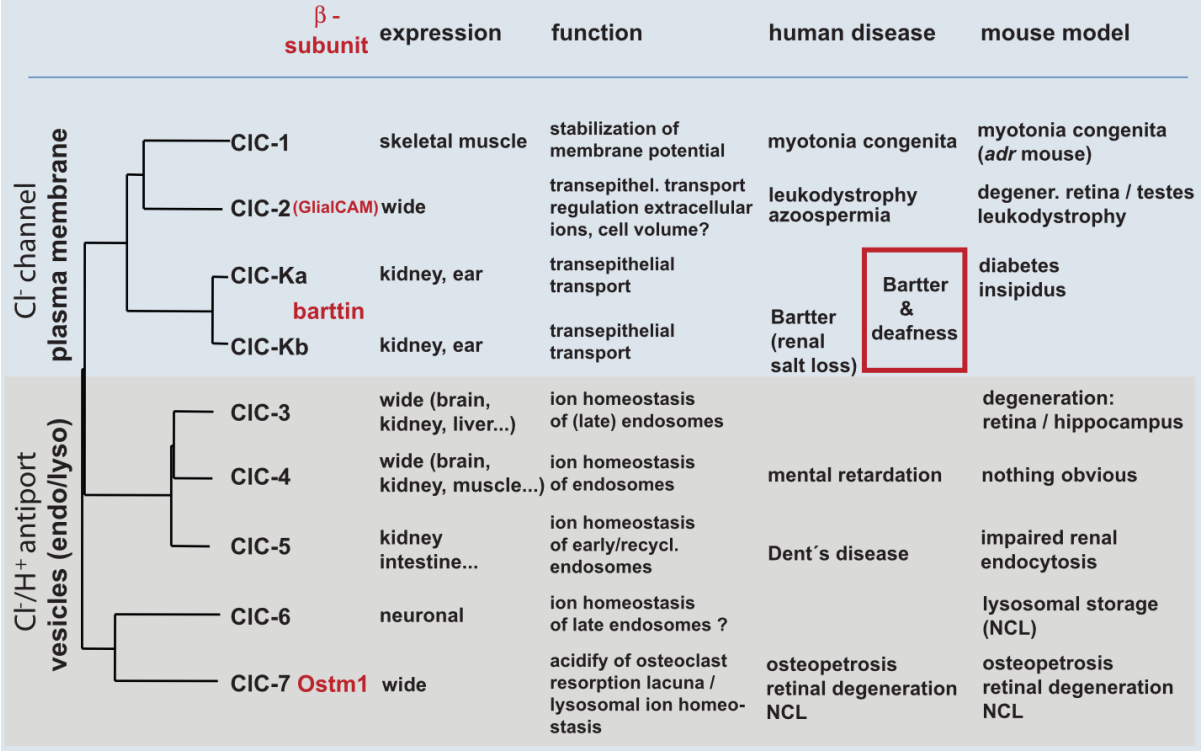

Figure 2: The ClC family of channels and transporters
An overview of the currently known expression patterns of mammalian ClC proteins, their presumed functions, and pathologies upon loss-of-function mutations. The proteins have been segregated into channels and antiporters. Any associated β-subunits are shown in red. Figure from Thomas Jentsch (2015). Full citation: (1).

Crystal structures of the ClCs reveal that both channels and transporters have a similar basic architecture. Therefore, the structural mechanism used by ClCs to dictate channel versus transporter function is not entirely clear. In the transporters, there are three conserved Cl^- binding sites, the external, central, and internal sites, which are thought to be responsible for anion transporting activity (3, 38-40). Mutating some of these key residues converts the transporter into a passive Cl^- channel (39, 41), suggesting an importance of the pathway for channel vs. transporter distinction. A new structure

recently published by the MacKinnon group suggests that a conserved loop in the Cl^- transport pathway is shifted to widen the ion transport pathway in channels, removing the transporter activity (40).

While the prokaryotic and eukaryotic ClCs have a similar structure, the eukaryotic proteins have an additional large carboxyterminus with two cystathionine-β-synthase (CBS) domains that presumably regulate protein activity and trafficking, although their function is not well understood (1). The domains interact with both the transmembrane portion of their respective subunit and each other, in addition to interacting with the CBS domains of the partner monomer (3). Some studies have shown that the binding of ATP affects the activity of several ClCs in different fashions (some are inhibited, while others are activated), but their role regulating ClC activity is not yet clear (49). However, many human disease-causing mutations reside in these domains, highlighting their importance in function of ClCs.

ClC-5 facilitates Cl^--dependent acidification in early endosomes

Cl^- has long been hypothesized to be an important counterion in the endosomal pathway, a model supported by considerable experimental data. Much of Cl^--related counterion research has examined the properties of ClC-5, a $2Cl^-/H^+$ antiporter (42, 43, 50, 51). ClC-5 has a restricted tissue distribution and is found primarily in epithelia, most prominently in kidney and intestine, with some expression in the brain and liver (52). The transporter is predominately localized to early endosomes and found transiently in the plasma membrane. Mutations in ClC-5 cause Dent's disease, characterized by recurrent kidney stones, nephrocalcinosis, and possibly renal failure (53). On a cellular level, the

absence of the transporter leads to a broad defect in proximal tubular endocytosis, potentially due to a loss in acidification of renal endosomes (54).

Several early papers characterized endosomal pH in ClC-5 knockout mice, observing a more basic luminal pH when the protein was absent (50, 51, 53). In one experiment, the Verkman group fed a pH sensitive dye attached to transferrin, a glycoprotein that trafficks to early/recycling endosomes, to wild-type (WT) and ClC-5 KO proximal tubule cell cultures (50). Initial pH in transferrin-labeled endosomes was ~7.2, decreasing to 6.0 and 6.5 in WT and ClC-5 deficient cells, respectively. Additionally, the ClC-5 deficient cells had a lower endosomal Cl^- concentration compared to WT cells, suggesting that the protein moves Cl^- into the organelle. In contrast, acidification and Cl^- accumulation were not impaired in late endosomes or the Golgi. Therefore, ClC-5 was proposed to be necessary for proper acidification of early endosomes and efficient endocytosis.

To determine if Cl^-/H^+ antiport is essential for acidification, the Jentsch lab created a knock-in mouse containing a mutation that converts ClC-5 from a transporter to a chloride channel ("Unc" mouse) (51). In comparison to the reduced acidification in KO endosomes, the Unc and WT acidified to a similar level, indicating that a Cl^- shunt provides a sufficient counterion current and the transporting activity of ClC-5 is not required for acidification. However, the Unc mouse displayed the same endocytosis defects as the KO mouse, specifically proteinuria, impaired receptor-mediated and fluid-phase endocytosis, and reduced levels of endocytic receptors. Because a single internal point mutation is unlikely to cause enough of a structural change in ClC5 to disrupt its macromolecular interactions, it is likely that the concentration of luminal Cl^- is essential

for the proper function of the endosome (3). The Verkman group noted that KO endosomes had a lower internal Cl^- concentration compared to WT (50), although the Cl^- concentration in Unc endosomes was not measured.

Recently, even the mechanism by which ClC-5 functions has been questioned. In contrast to the proposal that ClC-5 provides chloride to assist in acidification, recent work by Smith and Lippiatt observed that ClC-5 only facilitates outwardly rectifying currents when overexpressed at the plasma membrane of HEK293 cells (55). Outward rectification implies that ClC-5 is moving Cl^- out of the organelle lumen and moving H^+ into the organelle, starkly contrasting the proposed role of Cl^- acting as an electrical shunt for the proton pump, and contradictory to the aforementioned experimental data showing that the concentration of Cl^- is higher in ClC-5 expressing endosomes compared to KO (51). Therefore, this group is suggesting that ClC-5 is involved in endosomal acidification by exchanging endosomal Cl^- for H^+, the opposite of proving a counterion for the V-type ATPase (55, 56). However, these experiments were conducted on transporters expressed at the plasma membrane, and it is possible that ClC-5 behaves differently when expressed in the endosomes. Thus, although ClC-5 is involved in endosomal acidification, much remains unknown about how it functions in the organelle.

Additional proteins with known and suggested roles in endosomal acidification

While ClC-5 is important to endosomal acidification, it is predominately expressed in kidney and intestine, and the counterion mechanisms other tissues use to achieve sufficient acidification are unclear. ClC-3 and ClC-4 are closely related family members, sharing about 80% sequence identity with ClC-5, and are also localized to

endosomal compartments (57). ClC-4, has a broad tissue distribution and is thought to be localized to endosomal compartments. Anti-sense c-DNA knockdowns of ClC-4 in cultured epithelial cells resulted in more alkalized endosomes with a reduction in receptor-mediated uptake of transferrin, an iron binding glycoprotein, hinting it may play a similar role as ClC-5 (58). The same group, by breeding *Mus spretus* with *Mus musculus*, created male hybrids that were ClC-4 null, due to the different chromosomal localization of the *ClCn4* gene (59). These mice were infertile, but displayed no additional aberrant phenotypes. Cell lines, generated from both null and WT, again showed more alkalized endosomes with a reduced receptor-mediated uptake of transferrin when ClC-4 was absent. However, conventionally created ClC-4 knockout mice from the Jentsch lab showed no defect in endocytosis (60). Additionally, no disease phenotype resulting from a ClC-4 mutation has been reported in humans. Thus, the physiological function of the transporter remains unclear.

ClC-3 is widely expressed and primarily resides in intracellular trafficking vesicles, specifically in endsosomes, synaptic vesicles (SVs), and synaptic-like microvesicles (57). During membrane recycling, ClC-3 also transiently appears at the plasma membrane (61). ClC-3 KO mice display severe degeneration of the retina and neuronal tissue, specifically in the hippocampus, although the molecular mechanism resulting in this phenotype remains undetermined (62-64). Among an array of functions attributed to ClC-3, some of which have been disproved over the years, it has been suggested to play a role in the acidification of endosomes and SVs, transport vesicles that store neurotransmitters for release at the neuronal synapse. Using cultured hepatocytes from ClC-3 KO mice, Hara-Chikuma et al. found reduced acidification and decreased

luminal Cl^- in the early and late endosomes of KO compared to WT (65). Additionally, they found the inverse effect when ClC-3A was overexpressed in Chinese hamster ovary cells, observing slightly more acidic endosomes with a higher concentration of luminal Cl^- when compared to the control. In addition to affecting the pH of endosomes, isolated ClC-3 KO SVs also display reduced acidification compared to WT (62). However, the loss of ClC-3 coincides with a decrease in a glutamate transporter, vGLUT1, and a respective decrease in SV glutamate uptake (62). Recent studies have shown that instead of ClC-3, vGLUT1 is responsible for the majority of observed Cl^- conductance in SVs (66, 67). In an elegant set of experiments, Preobraschenski et al. used both purified vGLUT1 reconstituted in proteoliposomes and proteoliposome/SV fusion vesicles to address the controversial role of the transporter, employing a system that allows strict control over external and internal buffer composition (67). They found that vGLUT1 contains two anion binding sites that facilitate the movement of glutamate or Cl^- and a flexible cation binding site that allows H^+ antiport or K^+/H^+ exchange. Therefore, ClC-3 does not appear to be the primary source of Cl^- in SV acidification, but its role in ensuring proper trafficking of vGLUT1 is still not well understood. Additionally, the role that ClC-3 still appears to play in endosomal acidification has not been extensively explored.

The Cystic Fibrosis Transmembrane Conductance Regulator (CFTR) is a Cl^- channel whose malfunction results in the multisystemic disease cystic fibrosis (68). CFTR belongs to the ATP-binding cassette (ABC) transporter family but, unlike most members that function as transport ATPases, it is the only one that functions as an ion channel (69, 70). This channel is cAMP-regulated and expressed in the epithelial cells of

various tissues (71). CFTR is an attractive candidate for an organellular anion shunt, although its role in this position has been highly debated (70). Using immortalized epithelial cells from cystic fibrosis and healthy patients, one study found that a lack of CFTR resulted in small increases in pH in the TGN and endosomes, which could explain some symptoms that CF patients display (72). However, subsequent studies from several groups have directly contradicted those claims and concluded that CFTR does not affect endosomal pH levels, nor does it participate in TGN luminal pH (reviewed in (70)).

The family of Na^+/H^+ exchangers (NHEs) are secondary active ion transporters that assist in cytosolic and organellar pH homeostasis, Na^+ absorption, and cell volume (73). The 13 family members (NHE1-9, NHA1-2, and SLC9C1-2) are localized to the plasma membrane and intracellular organelles. In general, the plasma membrane NHE isoforms (NHE1-5) exchange Na^+ for H^+ in a 1:1 manner, typically moving extracellular Na^+ into the cytoplasm, although the reverse ion movement also occurs in certain tissues (74, 75). The intracellular NHEs, NHE6 and NHE9, localized to early and recycling endosomes assist in pH regulation and luminal cation levels by exchanging H^+ generated by the V-ATPase for either Na^+ or K^+ ions (74). Loss-of-function mutations in NHE6 or NHE9 result in hyper-acidified endosomes (76) and mutations in these proteins have been linked to autism and other neurodevelopmental disorders (73-75). Thus, while endosomal NHEs assist in the regulation of luminal pH, they do so by exchanging H^+ in an electroneutral fashion, and do not provide a counterion to assist in V-ATPase facilitated acidification.

In summary, while much is known about endosomal acidification, the precise mechanisms and proteins responsible for counterion transport are not fully understood.

Additional study in this field will expand upon the general knowledge in the study of ion channels and transporters, potentially suggesting mechanisms by which cells regulate their organellar pH.

CCVs display Cl^--dependent acidification via an unidentified protein

To study the counterions important for acidification, it is advantageous to examine the properties of isolated organelles, an approach that allows precise control over buffer conditions. However, endosomes are very heterogenous due to their constant, rapid maturation and isolating a well-defined, consistent population is challenging. However, a subpopulation of early endosomes, clathrin-coated vesicles (CCVs), may provide an interesting way to circumvent this problem. CCVs are responsible for trafficking proteins to various locations in the cell, including newly synthesized proteins from the TGN to either endosomes or the plasma membrane, and the endocytosis of proteins from the plasma membrane to endosomes. Clathrin is a coat protein that promotes the curvature of the membrane to create vesicles from donor membranes. CCVs were first described by Roth and Porter in 1964, who observed bristle-like coats at invaginations of the plasma membrane (clathrin pits) and on vesicles in the cytosol in electron micrographs (77). The assembly unit of clathrin is the triskelion, which is composed of three clathrin heavy chains and three clathrin light chains (78). Triskelia attach to both cargo-bound adaptor proteins on a patch of the membrane and one another, forming a rounded lattice of hexagons and pentagons that draws the membrane out into a bud shape (79). After scission from the membrane, the result is a basket-like structure surrounding the vesicle. The coat is subsequently removed by specialized proteins to

allow the vesicle to fuse with another compartment. As a primary source of cargo to and from early endosomes, these vesicles represent a sub-population of early endosomes and studying their acidification properties could provide a more readily isolatable population for studying endosomal counterion requirements.

In the 1980s, several papers reported that CCVs contained a Cl^--transporting protein important for V-ATPase facilitated acidification (21, 22, 24, 80). In the first study to report this activity, Xie and colleagues were monitoring the ionic requirements and energy source of a H^+-translocating ATPase, later determined to be the V-ATPase, in brain CCVs (24). Vesicle acidification was monitored using acridine orange (AO), a metachromic dye whose absorbance decreases when vesicular pH becomes more acidic. They found that ATP-driven H^+ translocation occurs when Cl^- or Br^- are present in the bathing media or, to a lesser extent, when the membrane potential ($\Delta\psi$) is dissipated by potassium (K^+) and valinomycin, an ionophore that moves K^+ freely across the membrane. These results were confirmed by other groups using both bovine brain and rat liver CCVs (21, 22).

Xie et al. further characterized the Cl^- transporting protein by examining its biochemical properties in proteoliposomes. The group solubilizing uncoated CCVs in detergent, column-separated the sample into 12 fractions, and after a glycerol gradient, reconstituted each fraction into liposomes (80, 81). To evaluate functional protein, they measured radiolabeled Cl^- uptake of all proteolipsomes, finding maximal activity in the later portion of the fractions (80). In addition to isolating fractions containing Cl^- transporting activity, they found several fractions possessing V-ATPase activity that acidified the proteoliposomes when K^+ was provided as a counterion in the presence of

valinomycin. When the ATPase fraction was co-reconstituted with the Cl^--transporting fraction, the proteoliposomes acidified in the presence of Cl^-, similar to the activity observed in CCVs. However, this protein was not identified.

In the second chapter of my thesis, using CCVs as our endosomal model system, we investigated the role of Cl^- transport with the intention of identifying the protein responsible for facilitating acidification. We aimed to take advantage of the technological advancements made over the last 20 years that have significantly increased the ability of mass spectrometry to identify membrane proteins (82). This approach is advantageous in that it makes no assumption as to the identity of the CCV Cl^- transporting protein. Although none have been suggested to be important for CCV acidification, ClC-3,-4, and -5, have all been shown to associate with clathrin (83), and are potential candidates.

Lysosomal acidification

Lysosomes are dynamic signaling centers that rely on pH for function

Lysosomes, the terminal organelle of the endocytic pathway, are acidic compartments that degrade macromolecules into their basic building blocks for the cell to recycle. Greek for 'digestive body', lysosomes were first identified by Christian De Duve and colleagues in the early 1950s while investigating acid phosphatase activity in fractionated rat liver homogenate (84). They observed that enzymatic activity of a specific fraction increased after several days, indicating that the phosphatase was likely contained inside an additional compartment or sac that degraded over time (85). Subsequent studies confirmed the presence of these compartments (lysosomes) using biochemical and electron microscope techniques. Currently, over 60 soluble hydrolases

have been discovered to reside in the lysosome and are responsible for breaking down various macromolecules, including carbohydrates, amino acids, lipids, and nucleic acids, or engulfed bacteria and viruses (86). In addition to digestive enzymes, lysosomes rely on many integral lysosomal membrane proteins to perform various functions, including luminal acidification, protein import from the cytosol, membrane fusion, and transport of basic catabolites from the lumen to the cytoplasm.

Lysosomes are found in nearly every mammalian cell type and are typically defined by an extremely acidic pH, degradative function, the presence of specific membrane proteins, and physical appearance (87). They are cytoplasmic dense bodies surrounded by a delimiting membrane that can appear spherical, ovoid, or tubular in shape (87). Lysosomes, the most acidic organelles in the cell, maintain an internal pH of 4.0-5.0 that is critical their catabolic functions. While lysosomes have long been primarily classified as sites for degradation and recycling, recent discoveries have expanded their cellular role, and they appear to function as signaling centers that monitor and regulate lysosomal status, autophagy, and cellular metabolism (27).

Lysosomes receive cargo from various sources, including vesicles originating from the endocytic pathway, phagocytosis, and autophagy. The first involves sorting and trafficking cargo through the endosomal pathway, as has been discussed in earlier sections. This pathway also provides both the digestive enzymes and the integral membrane proteins required for creating and maintaining lysosomal function. Phagocytosis is a process where specialized cells engulf a large, extracellular particle, such as pathogens or cell debris, at the plasma membrane by forming an endocytic compartment called a phagosome (88). Once internalized, the phagosome fuses with

lysosomes to form a phagolysosome and the engulfed material is rapidly degraded. Autophagy, specifically macroautophagy, is an intracellular process where the cell engulfs cytoplasmic constituents into a structure entitled the autophagosome, which then fuses with lysosomes to break down the luminal contents (89). This response is crucial for the degradation of malfunctioning organelles and for providing cellular energy under starvation conditions.

Given the crucial roles performed by the lysosome, malfunctions in lysosomal-related proteins can result in a range of moderate to severe disorders, collectively known as lysosomal storage diseases (LSDs). They are characterized by a massive accumulation of materials in enlarged, dysfunctional lysosomal compartments. LSDs can be caused by a defect in trafficking, degradation, ion homeostasis, or catabolite export (27). Because lysosomal functions are closely coupled, a defect in one role of the lysosomes affects its other functions, exacerbating and amplifying the problem in a cyclic fashion. For example, the malfunction of a hydrolase could result in the accumulation of undigested material. This buildup of internal solutes enlarges the compartment and increases the osmolarity, causing improper ionic regulation, which then further reduces the catabolic abilities of the lysosome and increases the internal material accumulation (27). There are approximately 50 identified lysosomal storage diseases, many of which result from defects in a specific hydrolase (90).

The acidic pH of lysosomes is required for the optimal function of the internal hydrolases and H^+ also provide the energy to pump catabolites out of the lysosomal lumen. Most lysosomal hydrolases are active only in highly acidic solutions, requiring the lysosome to maintain a pH around 4.5 for optimal function (91). It is well established that

lysosomal pH is created and maintained by the V-ATPase (20, 92), but the identity of the required counterions, ions that move to compensate for the membrane voltage created by the V-ATPase pumping protons into the lumen, is unclear and highly debated (26, 93). Various studies examining the counterions utilized in isolated and *in vivo* lysosomes have yielded varying and, at times, conflicting results.

Acidification and counterion study in isolated lysosomes

Lysosomes are a much more easily isolated organelle than endosomes and early studies of their acidification properties involved evaluating their biochemical properties *in vitro*. Initially these studies focused on characterizing the acidification properties of the then unknown V-ATPase, but inevitably shifted to evaluating the counterions required to facilitate acidification (20, 23, 44, 92, 94). The acidification properties of isolated rat liver lysosomes were first characterized by Dell'Antonne, who evaluated acidification with acridine orange, a membrane permeable, pH sensitive dye, finding that lysosomes relied on Cl^- for acidification (92). The lysosomes displayed no acidification when Cl^- was substituted with SO_4^{2-}, but this activity could be rescued by adding Cl^- to the system. Subsequent experiments by Okhuma et al. confirmed these observations using isolated lysosomes containing the pH sensitive FITC-dextran dye (20). In these experiments, removing external Cl^- from the bathing media substantially slowed and reduced acidification, but exchanging the cation had little effect. Additional studies have confirmed these results (23, 44, 94, 95), arguing that anions act as the primary counterions in lysosomal acidification.

While cations may also act as counterions, their contribution is harder to decipher because the positively charged ions must leave the lysosomal lumen to facilitate bulk acidification, and luminal buffer is very difficult to modify while retaining functional organelles. However, ion permeability can be studied by monitoring changes in the steady-state fluorescence of a pH-sensitive dye, indicative of the movement of H^+, upon addition of an ionophore, a small molecule that creates a pathway for a specific ion(s) to traverse the membrane. If one ion is highly membrane permeable, then providing a counterion, using an ionophore, will make it favorable for the permeable species to traverse the membrane. Okhuma et al. used lysosomes loaded with FITC-dextran to investigate ion permeability (20). To isolated lysosomes, they added valinomycin to allow K^+ to act as a counterion, but observed little change in fluorescence, indicating that H^+ were not highly permeable to the membrane. Subsequent addition of the H^+ ionophore FCCP (carbonylcyanide p-trifluoromethoxyphenylhydrazone) to the reaction resulted in a rapid increase in fluorescence, indicating the movement of K^+ into and H^+ out of the lysosomal lumen. Performing the experiment with the ionophore addition order reversed yielded the same outcome and, because neither ionophore individually facilitated large ion movements, this indicates that the permeability of H^+ and K^+ across the lysosomal membrane is low.

Additional experiments investigating ion permeability were performed by monitoring changes in the membrane potential using voltage sensitive dyes. A commonly employed voltage-sensitive dye is Dis-C_3(5), a positively charged dye that accumulates in the membrane of compartments with negative transmembrane voltages, resulting in the quenching of fluorescence. In experiments by Harikumar and Reeves, the fluorescence

signal of the dye increased upon addition of K^+ to the lysosome, even in the absence of valinomycin, indicating the cation can partially dissipate membrane potential and has a small permeability in lysosomes (19). Okuma et al. reported a slightly higher K^+ permeability, but this is likely due to differences in their methodology. Their experiments were conducted with tritosomes, lysosomes with altered buoyant density due to the addition of triton WT-1339, a detergent that can change K^+ permeability (18). Cuppoletti et al. used merocyanine 540, an anionic potential-sensitive dye, to see that Cl^- was able to reduce ATP-induced luminal-positive membrane potential, whereas no change occurred upon SO_4^- addition (95). They reported that K^+ can facilitate acidification when the luminal concentration of K^+ is higher than the external buffer. They too performed these experiments on tritosomes, so the actual magnitude of K^+ permeability is unclear. Van Dyke generated a comprehensive investigation of endosomal and lysosomal acidification (23). She found that lysosomal acidification was reduced when either K^+ or Cl^- was replaced with another ion, indicating the importance of both ions. Additionally, the most acidification was seen when both K^+ and Na^+ were present. The combined results from these experiments on isolated lysosomes indicate that both Cl^- and K^+ are permeable to the membrane and assist in acidification (18, 19, 23), although Cl^- appears to function as the primary counterion.

Candidate proteins that may facilitate counterion flux

Given the Cl^--dependent acidification properties of lysosomes, the Cl^- transporting proteins CFTR and ClC-7 have been suggested as the primary candidates for providing counterion flux, although their roles are highly debated (26, 93). Additionally, recent

work is revealing the increasingly important role that cations play regarding lysosomal pH and ion homeostasis. Transmembrane protein 175 (TMEM175), transient receptor potential channel mucolipin subfamily 1 (TRPML1) and two-pore channels 1-2 (TPC1-2) (K^+, Ca^{2+}, and Na^+ channels, respectively) have been found to influence lysosomal pH under certain conditions. The role of these channels and transporters will be described in the following sections.

CFTR

As mentioned in the endosome section, CFTR is a c-AMP regulated Cl^- channel whose malfunction causes the multisystemic disease cystic fibrosis (71). Di et al. suggested that CFTR acts as an organellular anion shunt to assist with lysosomal acidification after observing that alveolar macrophages from CFTR-null mice had phagolysosomes with a more alkaline pH compared to WT (96). However, this study measured pH with fluorescein-based probes, which have poor sensitivity at the low pH values of the lysosome. Follow up studies from several groups using a small molecule inhibitor of CFTR and more quantitative pH measurements reported no pH changes (70, 94, 97). Additionally, CFTR is only expressed in a limited number of tissues and, if it were important for lysosomal acidification, would only affect a small subset of organelles. Thus, while the intracellular role(s) of CFTR may still be debated, it is unlikely to facilitate lysosomal acidification.

CLC-7

ClC-7 facilitates acidification in isolated lysosomes

Due to their distribution throughout the endosomal pathway, intracellular ClCs have long been suggested to be involved in the acidification of various endocytic organelles. ClC-7, a $2Cl^-/H^+$ transporter found in lysosomes, has been a particularly attractive protein to provide counterions given the need for Cl^- in isolated lysosomal acidification. ClC-7's role in isolated lysosomes was characterized by Graves et al. when studying Cl^- flux across the membrane (44). While numerous experiments on isolated lysosomes have suggested Cl^--dependent lysosomal acidification, none provided direct evidence that Cl^- moved across the membrane. Graves et al. used isolated rat lysosomes to demonstrate this flux by monitoring the uptake of $^{36}Cl^-$ into lysosomes. After finding that the rate of uptake was enhanced in acidic conditions, they measured reversal potentials in isolated lysosomes to determine that the primary pathway of Cl^- flux was not via a channel, but instead through a transporter exchanging two Cl^- ions for one H^+ moving in the opposite direction. To identify the protein, they used siRNA to transiently knockdown ClC-7 in HeLa cells and found that the Cl^- flux was abolished, demonstrating that ClC-7 is the primary pathway of Cl^- movement into lysosomes. Additionally, the knockdown cells appear to have less acidic lysosomes when evaluated using a qualitative, pH-sensitive dye. When combined with isolated lysosomal data indicating the importance of Cl^- in acidification, these experiments suggest that Cl^- acts as a major lysosomal counterion using ClC-7 to move across the membrane.

Loss of ClC-7 causes osteopetrosis and neurodegeneration:

ClC-7 is a broadly expressed transporter that is localized to late endosomes and lysosomes (98, 99). ClC-7 KO mice are gravely ill, only living a maximum of 6-7 weeks

past birth, and suffer from retarded growth, deformation, retinal degeneration, lysosomal storage disease, and neurodegeneration (99, 100). Analysis of the disease pathology revealed the KO mice suffered from severe osteopetrosis, or hypercalcification of bone, explaining the stunted growth and deformation. This disease occurs upon a loss of function in osteoclasts, multinucleated cells responsible for bone resorption (101). In WT animals, osteoclasts attach to the bone matrix and form an acidic external compartment that uses hydrolytic enzymes to degrade bone. It is acidified by the fusion of acidic lysosome-related organelles to a polarized portion of the plasma membrane, called the ruffled border, which has similar features to the lysosomal membrane. In KO animals, the osteoclasts were unable to resorb bone, due to an underdeveloped ruffled border that was under-acidified when measured with the qualitative, pH dye acridine orange (99). These data suggest that because ClC-7 is localized to the ruffled border, a lysosomal-like membrane, and the compartment is underacidified, the transporter likely contributes counterions to assist in its acidification and may act similarly in lysosomes.

ClC-7 is not required for lysosomal acidification in live cells?

Although ClC-7 appears important for lysosomal pH, measurements in live cell ClC-7 KO lysosomes complicate its presumed role. In 2005, Kasper et al. showed that while ClC-7 KO mice have neurodegeneration and accumulate electron-dense storage materials in lysosomes, the lysosomal pH in cultured neurons was unchanged when measured with a quantitative fluorescent dye (100). Several papers have reported a similar unchanged pH in ClC-7 KO lysosomes (47, 94, 102). Additionally, mice lacking osteopetrosis-associated transmembrane protein 1 (Ostm1), ClC7's beta subunit required

for proper trafficking to the lysosomes, also developed LSD and neurodegeneration, but maintained an unchanged lysosomal pH (47).

After observing that knocking out ClC-7 did not result in a lysosomal pH change, the Grinstein lab sought to study counterion conductances in the lysosomes of live cultured macrophages, as opposed to isolated lysosomes. To assess the ionic dependence of acidification, the external buffer composition of the lysosomes, in this case the cytosol, must be controlled. To achieve this, Steinberg et al. stimulated the plasma membrane $P2X_7$ receptor for a prolonged period of time, opening small, well-defined pores that allow for the selective permeabilization and dialysis of cytosolic ions (94). To test for the importance of Cl^- in lysosomal acidification, they dialyzed the cells in Cl^--free media and neutralized the pH of the lysosome using the ionophore FCCP. After removing FCCP and resealing the membrane, they found that lysosomes reacidified similarly in the presence or absence of cytosolic Cl^-, arguing that the anion is not necessary for acidification. However, quantitative chemical analysis showed that cytoplasm dialysis only reduced Cl^- concentration from 70 mM to 9 mM, a concentration sufficient to allow lysosomal acidification in isolated lysosomes (23). Thus, the need for cytosolic Cl^- in lysosomal acidification is still in question.

Importance of ClC-7 as a transporter vs. channel

To further explore the role of ClC-7 in the lysosome, Weinert et al. introduced a single point mutation to the gating glutamate in ClC-7 to convert the protein from an antiporter to an uncoupled Cl^- uniporter (Unc) (102). The Unc mice displayed more mild osteopetrosis and had no change in coat color, but still possessed severe LSD and

neurodegeneration symptoms. The acidification behavior of the lysosomes was complicated. Isolated Unc lysosomes acidified to a greater extent than WT, whereas KO organelles had a much smaller acidification capacity, similar to the no external Cl^- buffer control. However, the lysosomal pH measured in fibroblasts cultured from the Unc, WT, and KO was similar between all cells. They also suggest that the KO and Unc lysosomes appeared to accumulate less luminal Cl^- than WT mice, although this experiment was conducted with fibroblasts grown in a low Cl^- media while using a novel Cl^- sensor whose sensitivity range could not be calibrated to measure higher Cl^- concentrations.

Results from the Unc mutant indicate that proper lysosome and osteoclast function not only require that ClC-7 mediates Cl^-, but must exchange Cl^- for H^+. The authors postulate that proper lysosomal function depends on an appropriate luminal Cl^- concentration. The Jentsch lab further investigated the role of ClC-7 in lysosomal degradation using pulse-chase endocytosis experiments on renal cells isolated from mice carrying a chimeric deletion of ClC-7. A side-by-side comparison showed that WT and ClC-7 deficient cells could endocytose protein similarly, but the material was not properly degraded and accumulated in the KO cells, indicating that ClC-7 is important for lysosomal degradation of proteins (103). The authors mention that *in vitro* biochemical studies of Cathepsin C, a lysosomal protease, has $[Cl^-]$-dependent activity (104, 105), arguing that the regulation of intralysosomal $[Cl^-]$ may be a central role for ClC-7.

To explore the importance of various parameters of lysosomal acidification, Ishida et al. created a mathematical model of acidification that incorporates the *in vitro* results from isolated lysosomes along with several transporters and channels (106). They simulate the presence of various combinations of Na^+, K^+, and Cl^- ions and

channels/transporters in the lysosomal membrane, finding that only Cl^- can function as a counterion to achieve robust acidification over a wide range of starting luminal and cytosolic ion concentrations. Additionally, not only does a Cl^- transporter acidify the lysosome to a more acidic pH than a channel, but only a transporter can explain some of the experimental results seen in isolated lysosomes. They predict that K^+ can function as a counterion, but only if a K^+ channel is present and luminal [K^+] is high, a currently unknown value due to a lack of physiological indicators. They also simulate the effects of relying on only one counterion pathway, finding that it may result in a change in lysosomal volume. The influx of Cl^- as a counterion could result in lysosomal swelling, whereas efflux of cations likely leads to shrinking since H^+ are continuously exported when coupled to catabolite export, implicating that a combination of counterion pathways may work best to maintain lysosomal physiology. Therefore, employing both mechanisms may be important to balance these opposite osmotic forces.

Since the ClC-7 antiporter is predicted to facilitate a higher luminal Cl^- concentration than a channel, this property suggests that the concentration of luminal [Cl^-] may be important. In a recent paper, Chakraborty et al. suggest a link between luminal [Cl^-] and lysosomal degradation capacity using a recently developed DNA-based, fluorescent Cl^- reporter that allows for ion measurements in a living organism (107). Using live *C. elegans*, they observed that reducing the high levels of Cl^- (~120 mM) lowered the degradation capabilities of the lysosome. Additionally, they observe that luminal Cl^- is depleted in mammalian cell culture models of LSDs. To link high luminal [Cl^-] to lysosomal function, they show that the enzymatic capabilities of Cathepsin C and Arylsulfatase B, enzymes previous shown *in vitro* to have [Cl^-]-dependent enzymatic

activity (105), were reduced when lysosomal [Cl^-] concentration was lowered using the Cl^- channel blocker 5-nitro-2-(3-phenylproyl-amino) benzoic acid (NBBP). While these results need additional verification, they suggest an interesting role of luminal Cl^- and a potential physiological reason for why a Cl^- shunt does not sufficiently substitute for ClC-7.

Cation channels that may assist in lysosomal acidification

In addition to Cl^-, cations are also permeable to the lysosomal membrane and are likely to participate in acidification. As described above, Steinberg et al. attempted to determine the ionic dependence of Cl^- in lysosomal acidification by reversibly dialyzing the cytoplasm. Additionally, they devised a method to selectively dialyze the lysosomal compartments to investigate the cation contribution as well (94). They activated $P2X_7$ receptors to permeabilize the cytoplasm, as explained above. After inactivating the channels and resealing the membrane, they used osmotic swelling induced by glycyl-L-phenylalanine 2-napthylamide (GPN), small peptide that is specifically cleaved by Cathepsin C upon entering the lysosomal compartment, to increase osmolarity and partially rupture the lysosome. Loss of lysosomal membrane integrity allows buffer exchange with the cytosol and surprisingly, once the peptide is rinsed out, the lysosomal membrane appears to reseal and reacidify while retaining a previously loaded fluorescent dye. These ratiometric dyes monitor lysosomal pH, indicating that replacing cytosolic Cl^- with impermeant anions did not significantly alter acidification, although residual cytosolic Cl^- is likely present. However, the lysosomes did utilize K^+ and, to a lesser extent, Na^+ to facilitate acidification. Although lysosomes are known to store Ca^{2+}, which

may act as a counterion, its omission had no discernible effect on the rate of reacidification. Additionally, the substitution of Cl^- for cations allowed for acidification as well. Thus, these experiments, in agreement with data from other isolated lysosome measurements, argue that lysosomes may use both cations and anions to acidify, although they assert that cations act as the primary counterion while Cl^- acts in a secondary fashion. The authors also note that osmotic changes related to the influx/efflux of counterions may also influence the lysosome and employing both mechanisms may be important to balance these opposite osmotic forces.

Therefore, while the role of cations in lysosomal acidification is becoming more apparent, and candidates for the cation-transporting protein are becoming more established, none have been shown to regulate lysosomal pH in quiescent conditions. However, there are several candidate channels, including TMEM175, TRPML1 and TPC1-2, which appear to primarily transport K^+, Ca^{2+} and Na^+ (respectively).

TRPML1 (also known as MCOLN1) is a cation channel that is ubiquity expressed and located predominately on late endosomes and lysosomal (LEL) membranes (108). Mutations in the protein cause the lysosomal storage disorder mucolipidosis type IV (MLIV), an autosomal recessive disease that manifests as a gradually progressing neurodegenerative disorder (108). It is an inwardly rectifying channel (inward meaning cations are moving out of the lumen), permeable to Ca^{2+}, Fe^{2+}, Zn^{2+}, Na^+, and K^+, but impermeable to H^+ (109). Currently, TRPML1 is thought to mediate the release of Ca^{2+} in response to regulatory changes in LEL-specific phosphoinositides or other cellular signals, resulting in fusion/fission events (27). Its influence on lysosomal pH is unclear,

and studies from patients with mutated TRPML1 report that pH is lowered, unchanged, or increased (26).

Two-pore channels 1 and 2 (TPC1 and TPC2) are ubiquitously expressed transmembrane channels that come together to form a highly selective Na^+ channel complex on endolysosomal membranes (110-112). The TPCs receive physiological inputs from both the inside and outside of the lysosome, including luminal H^+, lysosomal $\Delta\psi$, cytosolic ATP, extracellular nutrients, lysosome-attached protein kinases, LEL-specific phosphoinositides, and Mg^{2+} ions (27). TPC1 is highly sensitive to luminal pH, becoming hyperpolarized when pH shifts to more basic pH (112). It is postulated that the increase in Na^+ conductance depolarizes the membrane and makes H^+ pumping more favorable (27, 110, 112). Thus, the pH-$\Delta\psi$ feedback loop may assist in the stability of lysosomal pH or may help with setting the resting $\Delta\psi$ during organellular maturation. In TPC KO macrophages, the pH is only slightly alkalinized by ~0.1 pH units, when compared to WT, which is consistent with previously published work arguing that TPC has little activity in nutrient-replete cells (110). Upon nutrient starvation, the KO lysosomes are significantly alkalinized by ~0.6 pH units, whereas the WT lysosomes remain similar to the fed state. This lysosomal pH increase may be due to the lack of TPCs' depolarizing abilities, which seem to contribute to pH stability. Therefore, it is likely that TPC helps influence lysosomal pH indirectly, rather than providing a cation as a counterion.

While TRPML1 and TPC1-2 are important for maintaining the homeostasis of the lysosome, neither of the two seem to be the primary cation contributor for acidification. These conclusions are supported by counterion conductance experiments, where cation

permeability experiments argue that the primary cation is likely to be from K^+ (18, 19, 23). Recently, two K^+ channels, TMEM175 and Ca^{2+}-activated potassium (BK) channels, have been suggested to be responsible for lysosomal K^+ permeability (113, 114). Cang et al. evaluated the effects of TMEM175 on lysosomal pH by knocking out the protein using CRISPR (113). The KO and control lysosomal pH are similar, but starvation caused the KO lysosomes to become alkalinized by ~0.7 pH units, whereas the control lysosomal pH was unchanged. These results suggest a role for the protein in lysosomal pH stability. However, the steady-state lysosomal pH was unchanged. Alternatively, experiments by Cao et al. with the BK channels do not detect the K^+ permeability from TMEM175, but they suggest that the BK channels are a voltage-dependent K^+ required for refilling lysosomal Ca^{2+} stores (114). More experimentation is needed to determine the exact contribution of these proteins for both lysosomal K^+ membrane permeability and how they may contribute to lysosomal pH maintenance.

Thus, although several candidate channels have been suggested to act as the main contributors to the lysosomal counterion pathway, none appear to be crucial for maintaining steady state lysosomal pH under quiescent conditions.

Other roles for ClC-7: tissue/condition specific?

While the data on the role of ClC-7 is conflicting, one possibility is that ClC-7 is significantly more important in certain cell types or conditions than others. One example of this comes from the Maxfield lab, who studied the ability of microglia, the main immune cells of the brain, to clear Alzheimer's amyloid fibrils (115). Under nonpathological conditions, the cells are inactivated and maintain their lysosomes at an

unusually high pH near ~6.0. While these cells could internalize fibrillar Alzheimer's amyloid β peptides (fAβ), they only partially digested the material. However, activation by macrophage colony-stimulating factor (MCSF) induced lysosomal acidification, reduced luminal pH to ~pH 5.0, and increased the level of fAβ peptide degradation. Majumdar et al. found that inactivated cells express ClC-7, but it is mistargeted and degraded due to low levels of Ostm1 (115). Upon activation, expression of both Ostm1 and ClC-7 increases and the Ostm1/ClC-7 interaction allows for proper lysosomal trafficking. siRNA knockdown of ClC-7 blocks lysosomal acidification and fAβ degradation in activated mouse microglia, indicating that proper ClC-7 targeting is important for lowering lysosomal pH. These results suggest a dynamic mechanism of lysosomal pH regulation and activity, dependent on the presence of ClC-7, which may be tissue specific.

Other roles for ClC-7: protein/protein interactions

To further elucidate the role of ClC-7, the Jentsch lab generated a transport-deficient (Td) ClC-7 mouse, which expresses a ClC-7 mutation that has been electrophysiologically shown to have no ion conductance (116). They found that similar to KO, the Td mouse experienced no change in lysosomal pH, had reduced luminal Cl^-, and displayed severe osteopetrosis (102, 116). The severity of the osteopetrosis further strengths the proposition that the Unc ClC-7 provides an electrical shunt to partially recover osteoclast function. However, the presence of the Td mutant protein was sufficient to recover hair pigmentation and mice had a normal coat color, indicating a more signaling based role for ClC-7. While the Td was unable to prevent LSD and CNS

degeneration, there was no increase in neurodegeneration in specific portions of the brain like the ClC-7 Unc mutant, suggesting a strict regulation of luminal Cl^- concentration is critical in this tissue. However, it is possible the Td mutant may mediate some low level of current below their detection limit of 3% of WT, an alternative explanation as to the recovered hair pigmentation and less severe neurodegeneration (compared to Unc). Yet, if the Td mutant does not conduct ions, then these results indicate that ClC-7 KO phenotypes cannot be regarded as solely due to a loss of ion transport activity and show that ClC-7 is likely required for both ion transport and protein-protein interactions.

A potential new role of ClC-7 in lysosomal physiology has been hinted at in a paper studying the effects of a drug that inhibits the endolysosomal lipid kinase PIKfyve (phosphatidylinositol-3-phosphate 5-kinase) (117). The enzyme phosphorylates the D-5 position in phosphatidylinositol-3-phosphate (PI3P) at the late endosome, generating $PI(3,5)P_2$, which assists in endolysosomal trafficking (118). Additionally, PIKfyve has also been shown to phosphorylate and interact with other lysosomal proteins. The whole-body knockout of the gene is embryonic lethal, but knockdown or drug inhibition of PIKfyve results in cytosolic vacuoles (119). Gayle et al. found that the PIKfyve inhibitor Apilimod has selective cytotoxic activity in B-cell non-Hodgkin lymphoma (B-NHL) compared to normal cells (117). Interestingly, a genome-wide CRISPR screen revealed that this killing effect was abolished when transcription factor EB (TFEB), a master transcriptional regulator of lysosomal biogenesis, and the endolysosomal genes CLC-7, Ostm1, and Snx10 were knocked out. In agreement with the loss of the killing activity, CRISPR knockouts of ClC-7 or Ostm1 displayed no vacuole formation. Although the signaling pathway and mechanism by which PIKfyve interacts with these proteins is

unknown, it hints at a potential role for ClC-7 in kinase signaling and/or protein-protein interactions.

What is the role of ClC-7?

Given the various reports on ClC-7, its role in acidification and the lysosome in general is unclear. The osteopetrosis and other lysosomal storage disease symptoms from knockout of the protein clearly show its physiological importance. Results from multiple studies using isolated lysosomes depend on Cl^- to act as a counterion in V-ATPase facilitated acidification, which was confirmed when ClC-7 was knocked down in both microglia and HeLa cells, and yielded lysosomes that appeared to have a more basic pH. However, quantitative measurements from several different studies evaluating lysosomal pH of ClC-7 KO primary cells reveal no significant pH change compared to WT, even though the mice themselves have severe osteopetrosis, lysosomal storage defects, and only live a maximum of 6 weeks (94, 99, 100, 102, 116). Several possibilities may explain this discrepancy. First, the HeLa cell ClC-7 knockdown (KD) experiments were performed using only one siRNA and measured with a non-quantitative dye, casting doubt on the results (44). However, unpublished data from our lab indicates this result is reproducible when performed with a pool of siRNAs and measured with a quantitative, pH-sensitive dye (S.B. Lioi and J.A. Mindell, unpublished results). Secondly, the *in vivo* effects on lysosomal pH have been observed when ClC-7 is knocked down via siRNAs. It is possible that KO mice have established a mechanism to compensate for the loss of ClC-7 that a short-term knockdown has not/cannot develop, potentially due to insufficient time. For example, the ClC-7 KO mouse has been shown to retarget other members of the

ClC family, ClC-3 and ClC-6, to lysosomes (120). Third, the mechanism by which various tissues and cell types compensate for the loss of ClC-7 is unknown. Perhaps tissues/cell types most affected by a loss of ClC-7, such as microglia and bone, either compensate differently or place a higher demand on their lysosomes than macrophages and fibroblasts, where KO lysosomal pH has primarily been evaluated. Finally, perhaps the role that ClC-7 plays in certain cell types becomes apparent when the lysosomes are exposed to a substantially more demanding environment, similar to the role of TPCs during nutrient deprivation.

Is ClC-7 important for lysosomal pH maintenance?

In the third chapter of my thesis, I explored the effects of ClC-7 on lysosomal acidification using hepatocytes isolated from a liver-specific ClC-7 KO mouse. This approach allowed us to evaluate the acidification of isolated lysosomes in parallel to measuring lysosomal pH in primary hepatocytes, a cell type where ClC-7 KO pH has not been previously characterized. If lysosomal pH in the WT and KO are similar, we postulate that the role ClC-7 plays in lysosomal pH maintenance could become apparent when the workload demand on lysosomes is increased. To test this, we stressed lysosomes using autophagy, a catabolic mechanism used to degrade dysfunctional or unnecessary cellular components, to increase the volume of material targeted to the lysosome. Additionally, we tested the ability of ClC-7 KO hepatocytes to regenerate an acidic pH after alkalization by a weak base.

Autophagy is an intracellular degradation system that plays a variety of roles in physiological pathways in the cell. Of the many autophagy subsets, the most common

form is macroautophagy (henceforth referred to as autophagy), where cells consume protein aggregates and damaged organelles for clearance and also in response to starvation. During autophagy, fragments of membrane surround protein aggregates and damaged organelles, forming a double-sided membrane vesicle called an autophagosome (89). After formation, the autophagosome fuse with either an endosome (which then fuses to a lysosome) or a lysosome, delivering the sequestered cytosolic proteins and organelles for degradation. Autophagy is primarily regulated by mTOR, the mechanistic target of rapamycin, an evolutionarily conserved serine/threonine kinase that regulates cell growth and division in response to energy levels, growth signals, and nutrients (particularly amino acids) (121, 122). mTOR is found in two complexes, mTORC1 and mTORC2, which regulate many processes within the cell. mTORC1 resides in its inactivated form on the lysosomal membrane, where it receives a multitude of microenvironmental inputs, resulting in a wide range of outputs. In response to starvation, mTORC1 disassociates from the membrane, triggering a cascade of signals resulting in changes in enzyme phosphorylation status, protein localization, and mRNA translation (123). Recently, the position that mTORC1 occupies at the lysosomes has been found to be important and various proteins, including the V-ATPase itself, interact with mTOR and sense amino acids levels, as well as the general metabolic state of the lysosome (121, 122).

The effects of autophagy on lysosomal pH are understudied and not well characterized. Zoncu et al. performed the first set of experiments on HEK293 cultured cells, where cells were incubated for 50 min in the presence of amino acids, amino acid esters, or no amino acids at all (121). They observed no significant change in lysosomal pH. The second experiments were performed by Cang et al. and evaluated the effects of

starvation in mouse peritoneal macrophages (110). They found that after two hours of starvation, the distribution of lysosomal pHs slightly broadened in the starved cells, but they still maintained the same average pH. However, upon disruption of TPC1/2, pH was shifted to become more alkaline. The same group also showed that RAW macrophages had no change in pH upon lysosomal starvation (113). All three sets of experiments used a quantitative, pH-sensitive dye to evaluate lysosomal pH. In a fourth set of experiments, Zhou et al. tested the effects of starvation and chemicals that affect mTOR on MEF cells for three hours (124). They monitored lysosomal pH using a qualitative dye that accumulates in acidic compartments (the more acidic, the more dye accumulation and the brighter the fluorescence). They found that starvation and treatment with Torin-1 and PP242, mTOR inhibitors, drastically increased fluorescence in cellular organelle compartments. Exposure to rapamycin, a less potent mTOR inhibitor, partially increased fluorescence as well. These experiments show that lysosomal pH is increased during autophagy. In summary, experiments evaluating the effect of starvation on lysosomes have been performed in a variety of ways using all different cell types, yielding differing and somewhat conflicting results. Therefore, the effects of autophagy on lysosomal pH of hepatocytes, with and without functional ClC-7, will be explored.

Characterizing a *de novo* ClC-7 mutation in patients

In addition to studying the effects of a ClC-7 knockout, we have also investigated the effects of a *de novo* mutation of ClC-7 on lysosomal pH. This work was done in collaboration with several research groups who are members of the NIH undiagnosed disease program. As previously mentioned, lysosomal storage diseases (LSDs) are rare,

metabolic disorders caused by deleterious mutations in lysosomal-related proteins (125). Symptoms vary greatly depending on the tissue-specific expression and function of the gene, but are typically characterized by an accumulation of undigested products in the lysosome, which subsequently alter cellular function. Disease-causing mutations in ClC-7 are primarily characterized by the symptoms of osteopetrosis and neurodegeneration (99, 100, 126). In humans, Albers-Schonberg disease, or autosomal dominant osteopetrosis type II, is the most common form of osteopetrosis caused by mutations in ClC-7 (127). Of the more than 40 different reported mutations in ClC-7, found in various positions within the transporter, all result in osteopetrosis (128). In chapter 4, we report a novel mutation in only one allele of ClC-7 that results in patients with severe lysosomal storage disease phenotypes and partial albinism, but no osteopetrosis. The patients possess highly vacuolated cells throughout the body. Because the other ClC-7 allele is unmodified, the single point mutation in the other allele suggests some sort of gain of function mutation, and we explore its cellular and biophysical effects.

Aims of the thesis:

This thesis explores the role of Cl^- as a counterion and the proteins that transporter during endosomal acidification. In chapter 2, we look at the Cl^--dependent acidification of clathrin-coated vesicles, a subset of early endosomes. Next, we explored the role of ClC-7 in two capacities. In chapter 3, we describe the creation of a ClC-7 liver specific KO and investigated additional roles that ClC-7 may play in lysosomal pH maintenance. In chapter 4, we characterized a novel mutation in ClC-7 where, unlike every other reported

ClC-7 mutation, the patient does not have osteopetrosis, but displays various other LSD symptoms.

CHAPTER 2

Characterizing chloride-dependent acidification in brain clathrin-coated vesicles

Contributing authors: Mary R. Weston and Joseph A. Mindell

ABSTRACT:

Endocytic organelles maintain their characteristic internal pH using the V-type ATPase, a membrane protein that pumps protons (H^+) into the organelle lumen. Accumulation of H^+ generates a voltage across the membrane; an additional ion, known as a counterion, must move to dissipate any charge buildup. Chloride (Cl^-) has been hypothesized to be an important counterion in the endosomal pathway, a model supported by substantial experimental data. However, the role of counterion movement in endosomes is still poorly understood, largely due to their heterogeneous composition and the difficulty of isolating a well-defined population. Fortunately, a more readily isolatable sub-population of early endosomes, clathrin-coated vesicles (CCVs), has been shown to use external Cl^- to allow V-type ATPase-dependent acidification. We aimed to confirm the vesicle counterion requirements and extend the studies to probe the role of Cl^- transport in endosomal acidification using a CCV model system and identify the Cl^- protein. Our sample of highly enriched bovine brain CCVs exhibited V-ATPase facilitated acidification in the presence of external Cl^- that was independent of the monovalent cations present. We attempted to characterize and identify the protein responsible for Cl^- transport using various methods, but were unsuccessful. A previous study determined that brain CCVs are mostly composed of synaptic vesicles (SVs) based on membrane protein

content similarity. We functionally tested this conclusion, finding that brain CCVs acidify similarly to SVs in the presence of glutamate, and we were unable to extract an acidifying sub-population of CCVs that contained no characteristic SV proteins using immunoprecipitation and density gradient-based approaches. Mass spectroscopy indicates that CCVs contain many SVs-related proteins including vGLUT1, a SV glutamate transporter with a known Cl^- permeability. Thus, we used a functional approach to show that most CCVs are SVs and the source of Cl^--dependent acidification in brain CCVs is likely to be vGLUT1, although CCVs in other tissues are likely to utilize different proteins to facilitate acidification.

Introduction:

Cells utilize the endosomal pathway to perform vital functions including protein sorting, trafficking, and cell signaling. The initial step of the pathway involves endocytic vesicles, largely originating from clathrin-coated vesicles (CCVs), merging with early endosomes. Early endosomes mature into late endosomes, which ultimately mature into lysosomes, the terminal organelle of the endocytic pathway. These organelles progressively become more acidic and each compartment strictly maintains an internal pH essential for its function. Acidic luminal pH is generated and maintained by the V-type ATPase (V-ATPase), a multi-subunit membrane protein that utilizes the free energy of ATP hydrolysis to pump protons (H^+) into the organelle against its electrochemical gradient (4). The action of the V-ATPase is electrogenic: H^+-pumping generates a voltage across the membrane and an additional ion, known as a counterion, must move to dissipate the charge buildup and allow additional proton pumping (18, 19). The counterion could be an anion moving into the organelle lumen, a cation exiting the lumen, or a combination of both. Although various organelles appear to utilize the same V-ATPase for luminal acidification, they all maintain different internal pH values. Investigating the counterion requirements of organelles could provide useful not only for understanding the ions and proteins involved, but could also hint at how organelles sense and maintain their specific internal pH, a question that has persisted in the field for 40 years. One possibility is that the regulation and movement of counterions helps determine the internal pH levels, although the identity of the counterion(s) used in different organelles is not well understood. Substantial experimental data generated from endosomal and lysosomal studies suggest that chloride (Cl^-) is an important counterion in

the endocytic pathway (20, 26, 51), but there is still debate over the identity of the counterion(s). Counterion movement in endosomes is particularly challenging to study, largely due to their extremely heterogeneous composition and the difficulty of isolating a consistent, distinct population. To study counterions in a well-defined endosomal system, we evaluated clathrin-coated vesicles (CCVs), a sub-population of early endosomes.

Previously, Xie, et al. observed that isolated brain CCVs required external Cl^- to acidify (24). Subsequent studies by Van Dyke and colleagues confirmed this Cl dependent acidification activity in both bovine brain and rat liver CCVs (21, 22). Expanding on their previous work, Xie et al. solubilized, column-separated, and reconstituted CCV protein fractions into proteoliposomes, identifying a specific fraction that facilitated Cl^- movement across the membrane (80, 81). Co-reconstitution of the Cl^- transporting fraction with a V-ATPase containing fraction yielded proteoliposomes that acidify upon addition of ATP in the presence of Cl^-, similar to the activity observed in CCVs (80). However, this protein was not identified. Using CCVs as our endosomal model system, we investigated the role of Cl^- transport during acidification with the intention of identifying the protein responsible for facilitating counterion movement. We aimed to take advantage of the technological advancements made over the last 20 years that have significantly increased the ability of mass spectrometry to identify membrane proteins (82). This approach is advantageous in that it makes no assumption as to the identity of the CCV Cl^- transporting protein, although several members of the ClC family are likely candidates. The ClC proteins are a family of Cl^- transporting proteins composed of two distinct subclasses: intracellular channels, localized to the plasma membrane, and $2Cl^-/H^+$ transporters that reside in specific organelles along the endocytic pathway (35).

ClC-3,-4, and -5, located in endosomes and transport vesicles, all contain sorting motifs that allow them to at least transiently associate with clathrin (83). ClC-5 is localized to early endosomes and has been shown to facilitate Cl- movement in endosomes to assist in acidification (51, 129). However, it has a restricted tissue distribution and is found primarily in epithelia, most prominently in kidney and intestine (52). ClC-4 is broadly expressed and also localized to endosomes, but details of ClC-4's physiology and mechanism remain unclear (1, 58). ClC-3 is reported to be present in synaptic vesicles of neurons, synaptic-like microvesicles of endocrine cells, and the endosomal compartments of most tissues, where it has been implicated to be important for acidification (1, 65, 130). However, no reports have directly suggested that a ClC is involved in facilitating CCV acidification. The cystic fibrosis transmembrane conductance regulator (CFTR), a cAMP-regulated Cl^- channel expressed primarily in epithelial cells, has also been suggested to be involved in facilitating endosomal pH, but recent studies indicate that it is unlikely to play a role in endosomal acidification (70).

Identifying a common CCV Cl^- transporting protein is made more complicated when considering that the composition and acidification of CCVs may be tissue dependent (21, 22, 24). While both liver and brain CCVs display Cl^- facilitated acidification, a majority of brain vesicles have been shown to be primarily composed of synaptic vesicles (SVs) on the basis of membrane protein content similarities (131). SVs, while also formed via clathrin-mediated endocytosis, do not traffic cargo like CCVs but instead store neurotransmitters for use in neuronal signaling. SVs also contain a Cl^- permeability, suggested to be mediated by either ClC-3 or the SV-specific glutamate transporter, vGLUT1 (62, 66, 67). However, recently vGLUT1 has been definitively

shown to conduct Cl^- and, if a large overlap exists between brain CCVs and SVs, could be contributing to the Cl^- dependent acidification observed in CCVs (66, 67). Still, because liver CCVs also exhibit Cl^- dependent acidification, a tissue with no notable vGLUT1 expression (132), the identity of the Cl^- transporter responsible for CCV acidification in brain and liver is still debatable.

We sought to reproduce the Cl^- dependent acidification results published by Xie et al. (24) and extend these studies by identifying the protein responsible. We successfully isolated brain CCVs and observed robust, Cl^--dependent acidification, but could not further characterize the protein due to technical difficulties. Instead, we sought to determine if our sample of brain CCVs contained SVs, as has been previously suggested (131), by probing for and successfully detecting two synaptic proteins. We employed both immunoprecipitation and density gradient based approaches to isolate a population of acidifying CCVs that contained no SV proteins, but could not obtain a subpopulation that satisfied those conditions. Thus, using a different, functionally-based approach, we too conclude that a majority of CCVs are SVs, confirming conclusions made by Maycox and colleagues (131). Mass spectroscopy of CCVs reveal substantial levels of vGLUT1, strongly suggesting that this protein contributes to the CCV Cl^- dependence observed in brain. However, the Cl^- permeable protein in liver remains undetermined.

Methods and Materials:

Materials:

Fresh bovine brains were obtained from J.W. Treuth & Sons (Baltimore, MD, USA). All chemicals were purchased from Sigma, unless designated otherwise. Leupeptin hemisulfate and pepstatin A were from MP Biomedicals. Tubes and rotors were from Beckman-Coulter. Dounce homogenizers were from Wheaton. Detergents were purchased from Avanti or Anatrace. Lipids were purchased from Avanti. NuPage novex 4-12% Bis-Tris protein gels (NP0322BOX), PageRuler Plus prestained protein ladder (10-250 kDa) (26619), Pierce BCA protein assay kit (23225), and Protein G Dynabeads (10003D) were purchased from Thermo Scientific.

Antibodies:

Antibodies, with the dilution used for western blots in parenthesis:
Santa Cruz: clathrin heavy chain, sc-12734 (1:2000); clathrin light chain, sc-12735 (1:1000); Lamp1, sc-17768 (1:3333); synaptophysin 1, sc-55507 (1:3333). From Thermo: HRP goat α-mouse, #32430 (1:10000); HRP goat α-rabbit, #32460 (1:100000). BD transduction labs: Hsp60, #611562 (1:10000). Aves labs: synaptotagmin1, STG (1:3000); HRP goat α-chicken, H-1004 (1:10000). For westerns, PDVF blots were blocked with 5% milk and primary/secondary blocking steps were performed with 2.5-5% milk (Carnation).

Clathrin-coated vesicle isolation:

Clathrin-coated vesicles (CCVs) were isolated based on the methods of Nandi, et al. (133). Fresh bovine brains were obtained from a local slaughterhouse and placed on ice upon arrival (all solutions and brains were kept at 4°C or on ice, unless otherwise specified). 4-5 bovine brains were defatted and the meninges were removed. Brains were placed in a sieve and washed with 3.5 L of PBS (pH 7.0). Total brain mass was typically 800-1000 g. Brains were roughly minced and the sample homogenized with an equal volume of Buffer A (ex: 900 g of brain requires 900 mL of buffer) in a Waring blender with three 10-sec bursts at maximum speed. Buffer A was composed of 100 mM MES, 1 mM EGTA, 0.5 mM $MgCl_2$, pH 6.75, and contained protease inhibitors added right before using the buffer: AEBSF (0.02 mg/ml), leupeptin (0.0005 mg/ml), and pepstatin (0.001 mg/ml). The homogenate was centrifuged for 57 min at 22,000 x g. Avoiding the pellet, the supernatant was collected and filtered through gauze/cheesecloth to remove particulates and then spun at 100,000 x g for 1 hr to obtain a crude vesicle pellet. Pellets were resuspended in Buffer A with a Dounce homogenizer (size 'A' dounce). The suspension was centrifuged at 10,000 x g for 10 min to eliminate aggregated material. The high-speed spin (using 140,000 x g), resuspension, and low speed spin sequence was repeated 2 additional times. The resulting supernatant was then layered over a single step gradient of an 8% sucrose-deuterium buffer (containing buffer A salts) and centrifuged at 80,000 x g for 2 hrs at 17°C on a swinging bucket rotor (Beckman SW28). The pellet was washed and resuspended in buffer A. The solution was spun at 10,000 x g for 10 min to clear aggregate material and the supernatant was collected. This CCV sample was either stored at 4°C for several days or supplemented with 200 mM of sucrose, aliquoted, flash-frozen, and stored at -80°C for a minimum of 3 months with no loss of function. To scale

up the protocol, 12-15 brains were processed, stored sample overnight at 4°C after resuspending the pellet from the first 100,000 x g spin, and finished the protocol following day.

Thin section electron microscopy

250 µg of CCVs were pelleted by centrifuging for 30 minutes at 60,000 x g. Supernatant was removed and the sample was fixed with 4% glutaraldehyde in a 0.1 N sodium cacodylate buffer. After adding the buffer, one drop of albumin was added to the samples and they sat at room temperature for 1 hour. Samples were stored overnight at 4°C or until processed and mounted by the NINDS EM facility and imaged on an electron microscope.

Monitoring CCV acidification:

CCV total protein concentration was determined using a BCA assay (Thermo). CCV acidification experiments were performed in a FluoroMax-3 spectrophotometer. 75-90 ug of CCVs were added to a buffer containing 10 mM Hepes (pH 7.0 with NaOH), 10 mM $MgSO_4$, 100 mM cation/anion salt (ex: KCl), 200 mM sucrose, and 8 µM acridine orange. Similar to methods in (24), acridine orange fluorescence was excited at 492 nm and emission measured at 540 nm. Reactions were initiated with 1 mM Mg-ATP (pH 7.0) and 1 µM FCCP, 2 µM bafilomycin, and 1 µM valinomycin (all final concentrations) were added where indicated. Results were normalized to the first value measured after ATP addition and, because of slight variation in the activity of different CCV preps, only normalized to equivalent experiments performed on the same day.

To evaluate acidification of CCVs using synaptic vesicles acidification conditions, vesicles were added to either a sucrose buffer (10 μM acridine orange, 320 mM sucrose, 4 mM KCl, 4 mM $MgSO_4$, and 10 mM Hepes-KOH, pH 7.4) or a KCl buffer (10 μM acridine orange, 150 mM KCl, 4 mM $MgSO_4$, and 10 mM Hepes-KOH, pH 7.4). 1.5 mM Mg-ATP, 150 mM KCl, 1 mM Kglutamate, and 1 μM FCCP (all final concentrations) were added when indicated.

CCV partial reconstitution:

Solubilization and reconstitution methods were modified from Xie *et al*. (80). 1mL of concentrated CCVs (10-15 mg/ml) were combined with 0.34mL of 3M Tris-Cl (pH 8.5) and incubated on ice for 30 min. Sample was diluted with 1.68 mL of H_2O and centrifuged at 65,000 rpm for 1 hr (Beckman TLA 100.3 rotor). Pellets were dounce homogenized in 1.3 mLs of ice-cold 4% sodium cholate with 5 mM DTT and incubated on ice for 15 min to remove contaminants. 1.7 mLs of ice-cold H_2O was added to the sample, incubated for 15 min, and spun for 1hr. Pellets were washed with 3.2 mLs of 5 mM DTT and repelleted. Pellets were dounce homogenized in 1.5 mls of detergent (concentrations listed at end of paragraph), 10 mM DTT, 30mM Tris-Cl (pH 7.5), and 0.5 mM EDTA and incubated on ice for 45 min. 0.3 mLs of glycerol was added, sample was mixed well, and then centrifuged for 50 min. Solubilized proteins were in the supernatant. Stock solutions of detergents were added to the vesicles, with a final concentration selected based on the CMC. Listed are the final concentrations of all detergents screened. 1%: C_9G, $C_{10}G$, LDAO, cymal-6, cymal-7, cyclofos-7, and fos-choline-12. 1.8%: Deoxycholate. 3%: C_8G, C_8M, 0.5%: $C_{12}E_9$. Optimized solubility was test using 2% and

6% C_9G, 2% cyclofos-6, 1% and 2.5% cyclofos-7, 1% and 4% fos-choline-12, 1% and 4% LDAO, and 1.8% and 4% deoxcholate.

Reconstitution of the transporter was performed by combining 104 µl of buffer B (5.6% sodium cholate, 28% glycerol, 430 mM potassium gluconate), 20 µl of Buffer C (0.6 M DTT, 66 mM magnesium gluconate), and 120 µl of lipids (phosphatidylcholine, phosphatidylethanolamine, phosphatidylserine, & cholesterol at a mass ratio of 4.34: 2.76: 0.2: 2.7 and used at concentrations ranging from 12.5-25 µg/µl; lipids were suspended in 1% sodium cholate, 1 mM DTT, 10 mM Tris-Mes (pH 7.0)). Samples were incubated at room temperature for 5 minutes, frozen in dry ice-ethanol, thawed, and incubated at room temperature for 45 min. Samples were diluted with 40 mLs of room temperature dilution buffer (150 mM KCl, 50 mM Tris-Mes (pH 7.0), 3 mM magnesium gluconate), and centrifuged at 200,000 x g for 1 hr at 17°C.

Proteoliposome acidification was evaluated using the methods described in 'monitoring CCV acidification'. Cl^- movement across the proteoliposome membrane was assessed by monitoring fluorescence changes in the Cl^- sensitive dye 6-Methoxy-N-(3-Sulfopropyl)Quinolinium (SPQ). Proteolipsomes were diluted into inside buffer (300 µM SPQ, 225 mM KCl, 20 mM Tris-Mes (pH 7.0), and 3 mM Mg gluconate), freeze-thawed 3x, and sonicated to change the internal buffer. Proteoliposomes were pelleted and resuspended twice to remove external dye and resuspended in inside buffer without SPQ. At the start of the experiment, proteoliposomes were added to outside buffer (25 mM Kgluconate, 2 mM Tris-Mes, 3 mM MgGluconate, and sucrose to match osmolarity of inside buffer) and the experiment initiated with 2 µM valinomycin.

Immunoprecipitation with dynabeads:

50 µl of protein-G dynabeads of magnetically pelleted beads were resuspended in an antibody solution consisting of 9 µg of Clathrin X-22 (Thermo, MA1-065) in 200 µl of PBS + 0.02% Tween20 (PBS+T) and incubated for 15 minutes with rotation at room temperature. Antibody solution was removed from pelleted beads, which were then rinsed once with PBS+T. Beads were resuspended in 250 µl of 6 µg/µl CCVs in buffer A and incubated for 1 hr at room temperature (rotating). Beads were pelleted, supernatant removed, and resuspended in PBS. The wash step was repeated 2 additional times. Beads were moved to a fresh tube and sample was eluted by adding 26 µl of 50 mM glycine (pH 2.8) and rotating for 2 min. Once eluted, sample pH was neutralized with addition of 3 µl of 2 M Tris (pH 7.0).

Density Centrifugation Gradients:

Nycodenz step gradient: gradient solutions, solubilized in either D_2O or H_2O, contained 1x buffer A, 8% sucrose, and 23%, 26%, 30%, or 34% nycodenz (w/v). Each layer contained 2.2 mLs per step, bottom-loaded by adding steps of increasing density. 1 part CCVs in 1x buffer A and 250 mM sucrose were mixed with 2 parts of a 45% nycodenz solution and layered underneath the gradient. The gradient was spun on a swinging bucket rotor (Beckman SW41) for 2 hrs at 95000 x g at 4°C

8-26% sucrose step gradient: gradient solutions consisted of buffer A, solubilized in D_2O, and one of the following concentrations of sucrose: 8%, 10%, 14%, 18%, 22%, and 26% (w/v). Each layer contained 2 mLs, top loaded by adding steps of decreasing

density, except the top 8% layer contained 0.5 mL. CCVs were layered on top and the gradient was spun for 2 hrs at 21600 rpm at 17°C with no brake (Beckman SW41).

0.5 M and 0.7 M sucrose step gradient: CCVs were diluted to a total of 3 mLs with a solution of 320 mM sucrose and 4 mM Hepes and layered onto a 0.5 M and 0.7 M sucrose step gradient (both layers contained 10 mM Hepes (pH 7.0); 3 mLs per step). Gradient was spun for 1 hr on a Ti70.1 rotor (Beckman) for 38000 rpm at 4°C.

Iodoxinal step gradient: Gradient solutions contained 1x buffer A, 0.24 M sucrose, and 20%, 24%, 28%, or 32% optiprep (company; 50% w/v stock solution). The gradient contained 2.5 mLs/step, layered by adding decreasingly density solutions with CCVs applied to the top. The gradient was spun for 100 min at 25300 x g at 4°C (Beckman SW41).

1 mL samples were fractionated either from the bottom with a peristaltic pump or manually with a pipette from the top of the gradient (pipetting from the top only performed when a loose pellet was present at the bottom of the gradient).

Mass spectrometry of CCV sample:

In-gel samples were digested with trypsin at 37°C for 18 hr. Tryptic peptides were extracted then desalted before injected into a nano-LC/MS/MS system where an Ultimate 3000 HPLC (Thermo-Dionex) was coupled to an Orbitrap Elite mass spectrometer (Thermo Scientific) via an Easy-Spray ion source (Thermo Scientific). Peptides were separated on a ES800 Easy-Spray column (75 μm inner diameter, 15 cm length, 3 μm C18 beads; Thermo Scientific) with a 25 min linear gradient of 2–27% mobile phase B (mobile phase A: 2% acetonitrile, 0.1% formic acid; mobile phase B: 98% acetonitrile,

0.1% formic acid). The HPLC flow rate was 300 nl/min. Thermo Scientific Orbitrap Elite mass spectrometer was operated in positive data-dependent LC-MS/MS mode. The resolution of the survey scan was set at 60k at m/z 400. The m/z range for MS scans was 300–2000. For MS/MS data acquisition, the minimum signal intensity required was 3e4, the top two most abundant ions were selected for product ion analysis, the isolation width was 1.9 m/z, and the dynamic exclusion window was 7 sec. Xcalibur RAW files were converted to peak list files in mgf format using Mascot Distiller (version 2.4.3.3). Database search was performed using Mascot Daemon (2.4.0) against NCBInr_Bovine database.

RESULTS:

Clathrin-coated vesicle isolation and characterization

We isolated bovine brain CCVs using a previously described method (133). A western blot containing samples extracted at the beginning and end of the preparation indicates that the clathrin heavy chain was highly enriched in the final sample when compared to the initial brain supernatant (Fig 1), suggesting successful CCV isolation. Comparing immunoblotted CCVs to identical SDS-PAGE samples shows that the clathrin heavy chain clearly corresponds to a band near 180 kDa, the known molecular weight for the heavy chain (Fig 1). Thin section electron microscopy (EM) images show frequent vesicles surrounded by a rod-like lattice with a diameter between 50-80 nm, characteristic of vesicles coated with clathrin (Fig. 2A and 2B) (134). In addition to coated vesicles, the sample also contained some large, non-coated vesicles (Fig. 2B), whose diameters ranged between 60-250 nm. While the extent of this contamination is difficult to quantitatively assess with EM, some contamination in a CCV prep is common (22, 135). Likely contaminants of an organelle prep are other organelles due to their similar sizes and densities. Using western blots to evaluate sample purity, we found that CCVs were highly enriched in clathrin and showed no detectable signal for markers of lysosomes and mitochondria (Fig. 1). Based on these data, we successfully isolated a highly enriched sample of CCVs with minimal contamination.

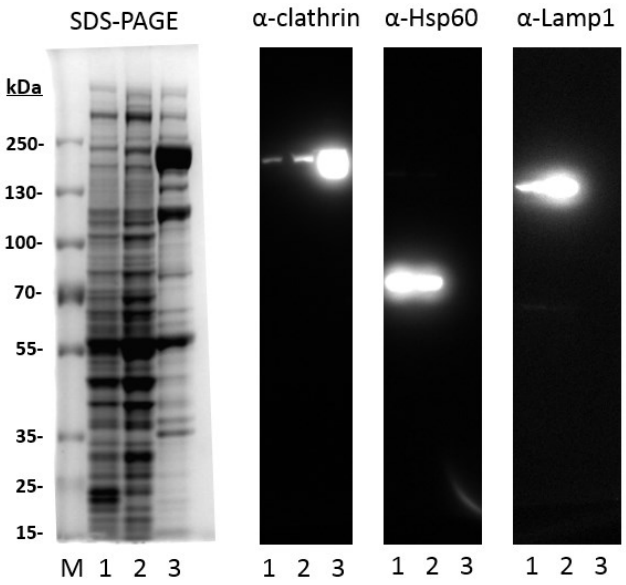

Figure 1: The isolated CCV sample is highly enriched in clathrin and is not contaminated by lysosomes or mitochondria.
Identical PDVF western blots contain whole brain lysate (lane 1), clarified brain lysate (supernatant from whole brain lysate after 22000g spin) (lane 2), and the final CCV sample (lane 3). Westerns were probed with antibodies against clathrin, Hsp60, and Lamp1, proteins typically found in CCVs, mitochondria, and lysosomes (respectively). Blots were overexposed to ensure purity. Included is the commassie-stained protein gel with a molecular weight ladder (M) included.

CCVs acidify in a Cl^--dependent manner

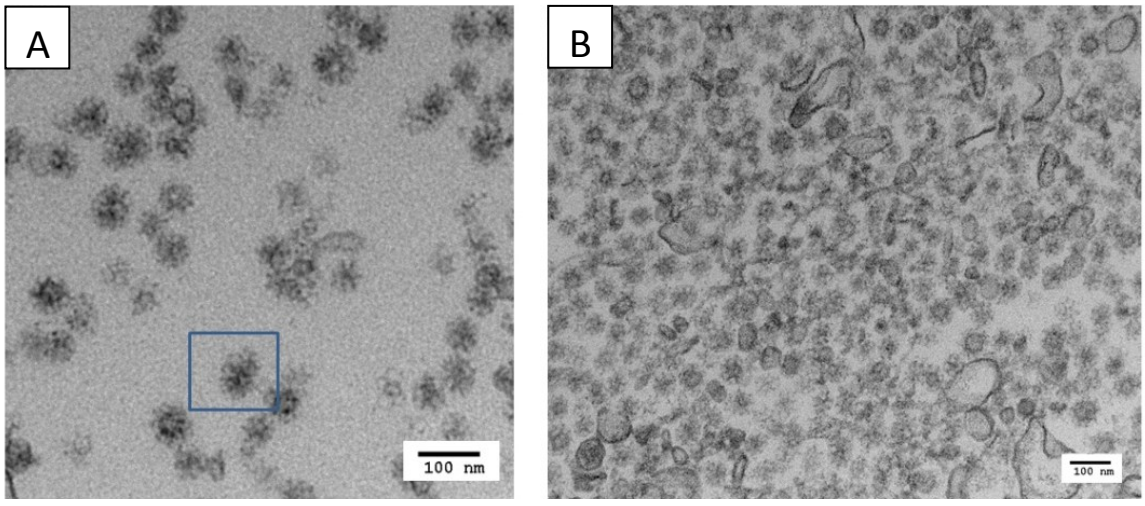

Figure 2: Thin section electron microscopy images show the CCV sample is enriched in CCVs.

(A) The image depicts CCVs with their typical lattice structure. An individual vesicle is shown in the blue box. (B) The image displays the typical distribution of the sample, showing an enrichment of CCVs and some smooth vesicular contamination. Both scale bars measure 100 nm.

We characterized the Cl^--dependent acidification properties of the CCV sample using the membrane permeable, pH sensitive dye acridine orange. The dye is thought to become protonated and subsequently membrane-impermeable when in an acidic compartment, self-quenching as it accumulates, which then qualitatively indicates vesicular acidification (136). Upon addition of ATP, CCVs in a bathing buffer with 100mM KCl rapidly acidified to a stable level within 2-3 minutes (Fig 3A). Addition of FCCP, a proton ionophore, returned fluorescence back to its initial intensity, demonstrating that fluorescence loss is reversible and the result of a change in the H^+ gradient. Acidification was inhibited when CCVs were incubated with bafilomycin, an inhibitor of the V-ATPase, indicating that the V-ATPase is responsible for generating the pH gradient. CCV acidification was stable, robust, and consistent, with very little variation between different CCV brain preparations. The CCV sample acidified to the same extent after being stored for more than 3 months at -80°C and retained at least 50% acidification after being stored at 4°C for 7 days (Data not shown).

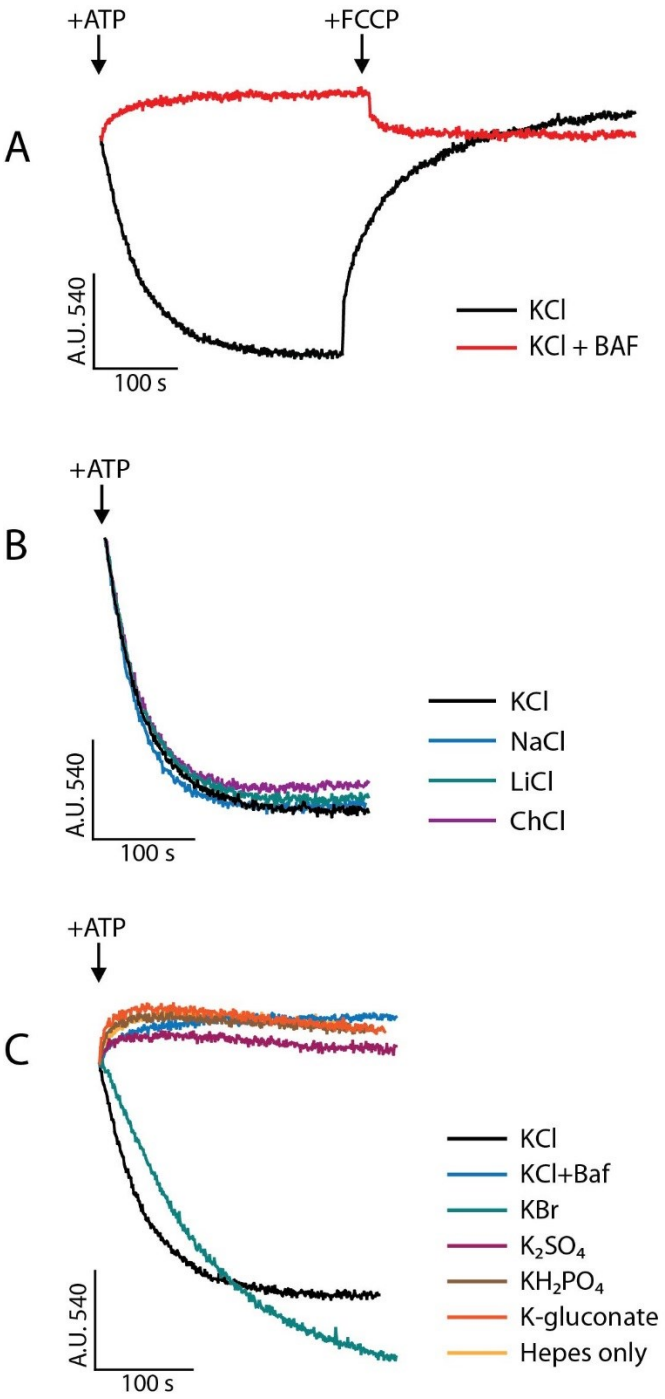

Figure 3: Acidification of CCVs in the presence of various inhibitors and ions indicates acidification requires the presence of Cl^-

(A) A representative trace is shown where CCVs were added to a 10mM Hepes buffer (pH 7.0) that contained 100mM KCl and 8 uM acridine orange. The experiment was initiated with 1mM ATP and a decrease in fluorescence emission indicates acidification. Identical experiments were performed in the presence or absence of 2uM bafilomycin, an inhibitor of the V-type ATPase. 1uM FCCP is a proton ionophore, was added where indicated. The spike seen when FCCP is added is a machine artifact due to pausing the fluorometer. The vertical axis depicts arbitrary fluorescent units measuring emission at 540 nm (A.U. 540) and the horizontal axis represents time in seconds.
(B) CCV acidification was tested in buffers where K^+ is substituted for sodium, choline or lithium, but chloride remains in the buffer.
(C) CCV acidification tested in buffers were K^+ constantly remains in the external buffer but chloride is substituted for Br^-, SO_4^-, or gluconate, A Hepes buffer only control is included.

While CCVs in a KCl buffer acidify, vesicles in a salt-free buffer display no measurable acidification (Fig. 3C). To determine the ionic requirements of CCV acidification, we tested the relative contributions of K^+ and Cl^- by measuring activity in their absence. Acidification appeared unchanged when K^+ was substituted with choline, sodium or lithium (Fig. 3B), indicating that acidification does not depend on the cation. In contrast to the robust acidification in KCl, no acidification was observed when Cl^- was substituted with gluconate, phosphate, or sulfate, results very similar to the salt-free and +bafilomycin controls (Fig 3C). Substituting Cl^- with Br^- slightly enhanced the rate of acidification and, while the increase was not anticipated, it is unsurprising that Br^- can substitute for Cl^- considering most Cl^- channels/transporters tend to discriminate poorly between the two anions (44, 57, 137). Therefore, we have confirmed the previous findings that brain CCV acidification requires external Cl^- and appears to be cation independent.

CCVs are not amenable to internal buffer exchange via freeze-thaw sonication methods

Given the robust CCV acidification, we sought to characterize these results in a more quantitative fashion. Acridine orange cannot indicate the magnitude of the pH change, nor can it indicate initial or final pH values. The ability to control CCV internal buffer composition and load a membrane impermeable dye would allow for such measurements, and could potentially designate if Cl^- is moved across the membrane via a channel or a couple transporter. A typical method for modifying internal buffer composition is to freeze-thaw (FT) vesicles several times and then sonicate, which produces unilamellar vesicles that should contain the bathing buffer (44). We performed a 3x freeze-thaw and subsequent sonication (FTS) cycle on CCVs, finding they acidified

to the same extent as unmodified vesicles when measured by acridine orange (data not shown). However, we detected no fluorescent signal when CCVs were FTS in a solution containing the membrane impermeable dye fluorescein, indicating no dye incorporation. We hypothesized that the clathrin coat was preventing the CCVs from breaking open and fusing during the freeze-thaw step and removed the coating protein by incubating vesicles in 0.5M Tris (138). SDS-PAGE shows that Tris-treatment freed a substantial portion of the clathrin from pelleted vesicles, implying that many vesicles no longer retained their clathrin coat (Fig 4A). We used electron microscopy (EM) to evaluate the preparation and ensure the vesicular structure was being modified by the FTS cycle. Consistent with the SDS-PAGE results, many vesicles lost their coat after Tris incubation (Supplemental 1A-B). The freeze-thaw sample contained large, multilamellar vesicles and subsequent sonication reduced vesicular size and yielded smaller, unilamellar vesicles (Supplemental 1C-D). These data indicate the amenability of uncoated vesicles to structural modifications and therefore internal buffer modification may be possible. We evaluated the functional effects of Tris, Tris-FT, and Tris-FTS treatments on vesicles by measuring acidification in acridine orange. We found that increased modifications progressively decreased the vesicles' ability to acidify (Fig 4B) and, while this loss of function was substantial, enough activity remained to attempt internal dye incorporation. Unfortunately, no measurable dye incorporation occurred even after a wide range of dyes, buffers, and loading conditions were tested. The absence of dye may be attributed to a lack of tightly resealed vesicles, possibly due to a high concentration of membrane proteins, too little internal dye incorporation, or the inability of the Cl^- transporter to withstand the FTS conditions. The remaining acidification we observed after FTS may be

those residual uncoated vesicles that were protected from the harsh FTS step. Ultimately, we were unable to modify the internal buffer solution of the CCVs while retaining acidification activity.

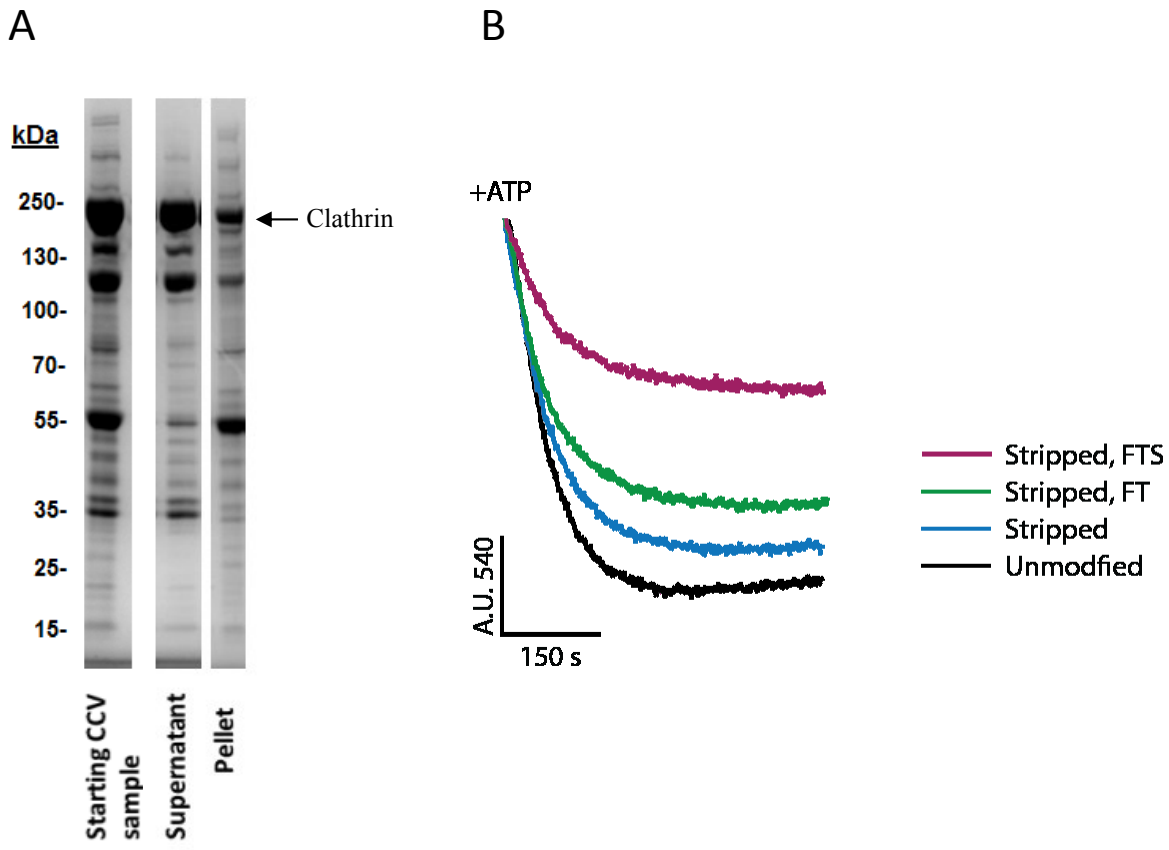

Figure 4: Incubation with Tris partially removes the clathrin coat and further structural modification affects vesicular acidification
(A) CCVs were treated with 0.5M Tris for one hour at 4°C to remove their clathrin coat, pelleted at high speed, and the supernatant and pellet were compared. Shown is an SDS-PAGE with standard molecular weights marked. The second lane shows the starting CCV sample, the third lane is the CCV supernatant, and the fourth lane are pelleted vesicles. (B) The acidification of untreated CCV is compared to vesicles stripped of clathrin using 0.5M Tris, stripped and freeze-thawed 3x, or stripped, freeze-thawed 3x, and sonicated. Acidification conditions are the same as those described in Fig. 3

Partial reconstitution of CCVs using various detergents

An alternative approach to studying the properties of the Cl^- transporting protein is to solubilize, isolate, and reconstitute the protein into proteoliposomes. Previously Xie, et al. solubilized uncoated vesicles in $C_{12}E_9$ and successfully reconstituted a partially purified Cl^- transporting fraction into proteoliposomes, but did not identify the protein (80). As a first step toward identification, we omitted the purification step and directly reconstituted solubilized uncoated vesicle proteins into liposomes, a method previously used to reconstitute the V-ATPase from CCVs (139, 140). We evaluated successful incorporation by assaying ATP-initiated acidification, which would only occur if both the V-ATPase and the Cl^- transporting protein were properly reconstituted into proteoliposomes. Additionally, we monitored the functionality of the Cl^- transporting protein by loaded the proteolipsomes with 225mM KCl and the Cl^- sensitive dye 6-Methoxy-N-(3-Sulfopropyl)Quinolinium (SPQ), whose fluorescence decreases in the presence of Cl^-. These vesicles were placed in an external buffer without Cl^- and we initiated the experiment with the addition of Valinomycin, an ionophore that allows K^+ to freely cross the membrane to act as a counterion. If a Cl^- transporter is present, K^+ acts as a counterion to allow movement of the anion out of the lumen, resulting in an increase in the fluorescent signal. Unfortunately, no fluorescent changes were observed in either assay and we hypothesized this may be due to a low concentration of reconstituted protein. Indeed, an SDS-PAGE of the proteoliposomes indicates little protein incorporation. To optimize reconstitution, we solubilized uncoated vesicles in various detergents and compared levels of solubilized protein on an SDS-PAGE (Fig 5). Cyclofos-6, cyclofos-7, fos-cholate-12, deoxycholate, LDAO, and C_9G all appeared to

solubilize protein than $C_{12}E_9$, the starting detergent (Fig 5, cyclofos-6 not shown but was very similar to cyclofos-7). After optimizing different concentrations of these selected detergents, we determined that cyclofos-6, fos-cholate-12, and deoxycholate allowed for the most reconstituted protein again using SDS-PAGE. However, no SPQ fluorescence changes were detected after assaying for Cl^- transporting activity in these optimized proteoliposomes, again preventing us from characterizing/identifying the Cl^- transporting protein.

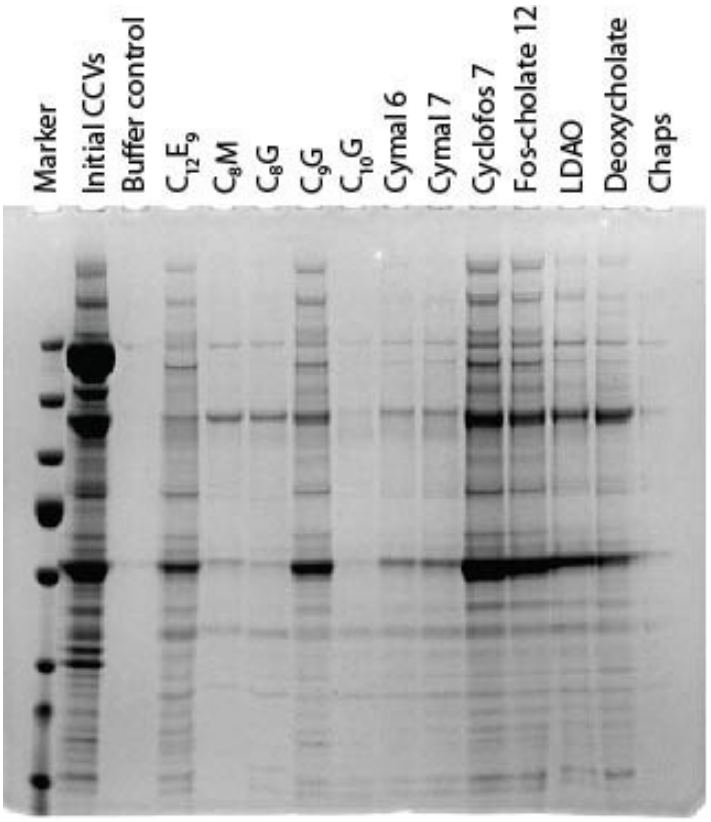

Figure 5: CCV solubilization in various detergents

Uncoated CCVs were treated with various detergents, spun at high speed, and supernatants were run on an SDS-PAGE. The first lane contains a molecular weight marker, the second contains starting CCVs, and the third contains proteins solubilized in buffer A. The rest of the samples are solubilized with the indicated detergents.

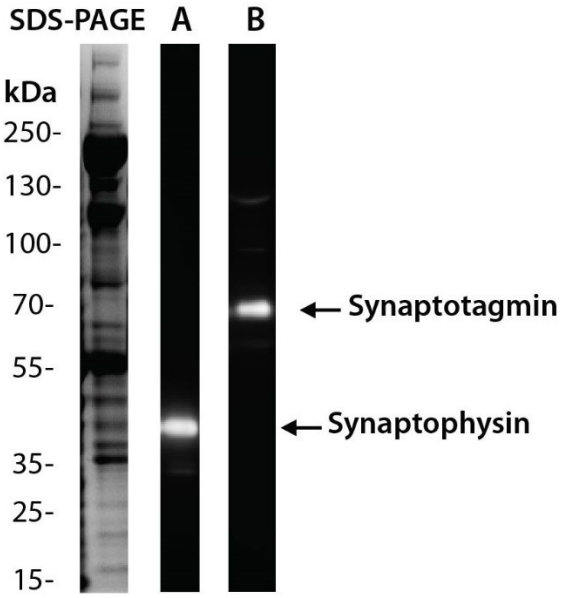

Figure 6: Immunoblotted CCV samples probed with antibodies against either synaptophysin-1 or synaptotagmin-1.

The SDS-PAGE on the right shows a protein ladder, with standard molecular weights marked, and a lane containing isolated CCVs. 'A' is a PDVF membrane with the CCV sample probed with a-synaptophysin; 'B' is the identical sample probed against synaptotagmin.

Examining CCV acidification using synaptic vesicle acidification conditions

Both brain and liver CCVs acidify in the presence of Cl^- (21, 22, 24), suggesting a general mechanism of CCV, and perhaps early endosome, acidification. However, experiments published by Maycox et al. show that brain CCVs are primarily composed of SVs on the basis of extremely similar membrane protein content in both populations (131). Their conclusions, while convincing, contain no functional comparisons of the two populations; nor did their work exclude the possibility of a small sub-population of non-SV CCVs. Our CCV sample, isolated using a somewhat different protocol than Maycox et al., appears to have a different protein distribution upon comparison of our SDS-PAGE results. Therefore, we investigated if our brain CCV sample also contained SVs by immunoblotting against two characteristic SV proteins, synaptophysin-1 and synaptotagmin-1 (Fig 6). We detected a substantial signal for each protein, suggesting that a significant portion of the sample could be SVs. Since SVs contain a V-ATPase and

acidify in the presence of glutamate and low concentrations of Cl^-, we further explored the overlap of the two vesicle populations by tested CCV acidification employing the same experimental parameters previously used to test SV acidification (141). The addition of 1mM glutamate to CCVs in 4mM KCl caused a small increase in the magnitude and rate of acidification, while addition of 150mM KCl greatly enhanced both rate and magnitude (Fig 7A). These results were extremely similar to those observed for SVs under identical conditions (141), suggest that CCVs could use glutamate as a counterion. We then tested if, like SVs, CCVs require a small concentration of Cl^- to utilize glutamate for acidification, finding that glutamate was unable to induce acidification when 0mM KCl was present, but similarly increased the rate of acidification in the presence of either 2mM or 4 mM KCl (Fig 7B). Again, CCVs and SVs have very similar acidification profiles (141). However, these results also show that glutamate either only acts like a counterion when Cl^- is present or its presence somehow changes the activity of the transporter. The striking similarities between SVs and brain CCVs acidification properties prompted the following questions: was the Cl^--dependent acidification from CCVs, SVs, or some combination of both? What percentage of the CCV sample was SVs? Could CCVs be separated from SVs and still retain acidification?

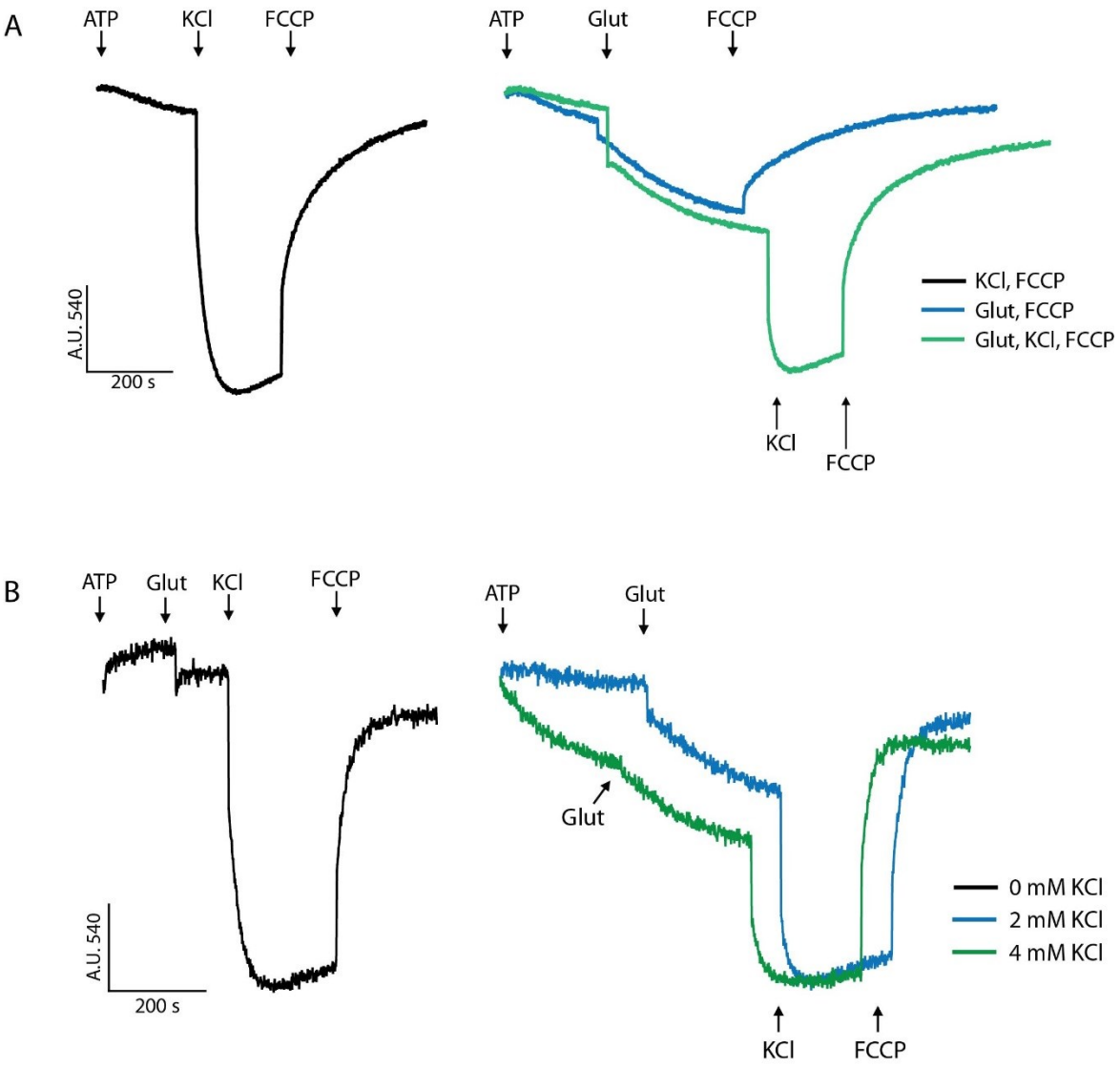

Figure 7: CCVs can partially acidify in the presence of glutamate and varying KCl concentrations.

(A) CCV acidification was measured with acridine orange, as in Fig.3, but the starting buffer contained 4 mM KCl buffer. Marked are additions of 1mM ATP, 1 mM glutamate (glut), 150 mM KCl, and 1µM FCCP. Two of the traces are overlaid to allow a better comparison. The label shows the addition order of KCl, glutamate, and/or FCCP.
(B) CCV acidification using the same conditions as (A) except the buffer contained 0, 2, or 4 mM KCl. The points where ATP, KCl, glutamate, and FCCP were added are marked. Sample addition order for all was: ATP, glutamate, KCl, FCCP.

Attempts to separate CCVs and SVs using immunoprecipitation and density gradients

To determine if Cl^--dependent acidification is a property of brain CCVs and/or SVs, we attempted to isolate a subpopulation of acidifying vesicles from CCVs that did not contain SVs. We employed immunoprecipitation, a technique that precipitates a protein or protein complex out of solution using an antibody that binds specifically its target, to isolate a subpopulation of CCVs. Using a clathrin antibody as the bait, we evaluated if SVs were also extracted by monitoring the presence of synaptophysin. Western blot analysis indicates we successfully immunoprecipitated a small amount of a clathrin labeled sample, but synaptophysin was also present (Fig 8). We were unable to confirm the functionality of the isolated sample because neither the bead-bound sample nor glycine-eluted samples acidified when tested with the acridine orange assay, although the harshness of the acidic glycine likely explains the lack of activity in the latter. To explore if targeting different locations of the clathrin lattice or SVs themselves would pull-down a unique vesicle population, we performed immunoprecipitation with two additional clathrin antibodies and the synaptophysin antibody, but SDS-PAGE showed no protein was pulled-down from the overall CCV sample. Thus, immunoprecipitation did not separate out a distinct subpopulation of non-SV vesicles from the overall CCV pool.

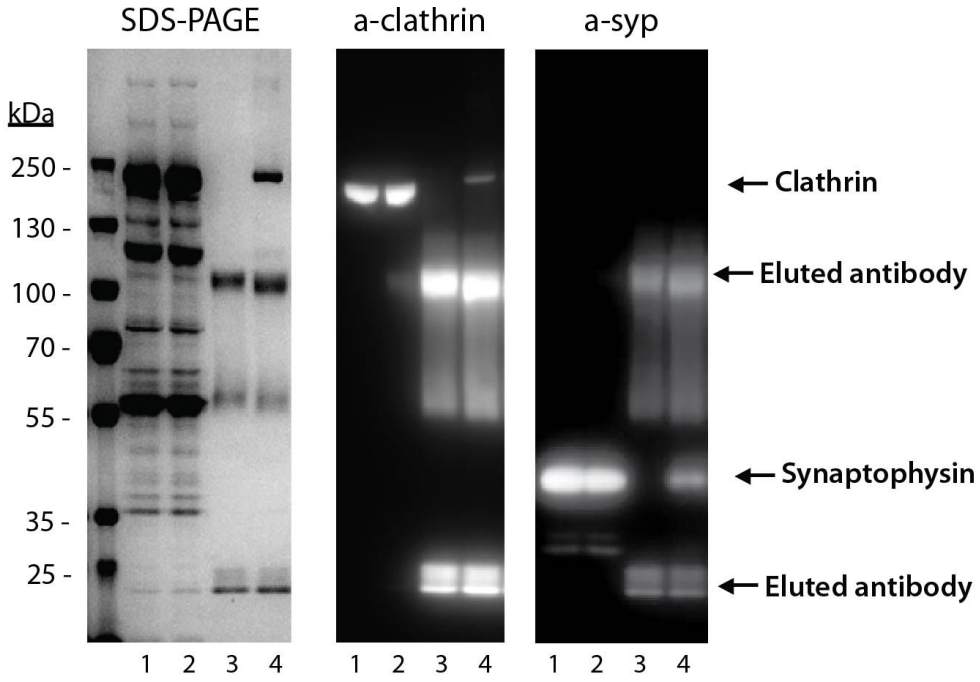

Figure 8: Immunoprecipitation of CCVs using a clathrin antibody attached to protein G dynabeads.
SDS-PAGE and westerns show CCVs incubated with either a clathrin or synaptophysin antibody attached to magnetic dynabeads. Lane 1 contained the starting CCVs sample, lane 2 contained the CCV supernatant after dynabead incubation, lane 3 contained the antibody attached to the dynabeads, and lane 4 contained the sample eluted off the beads (including the clathrin antibody).

If SVs and CCVs are different populations of vesicles, then it is possible they might have different physical properties, like density. We employed density gradient centrifugation, a technique that separates heterogeneous samples based on the physical properties of mass, size, and/or density, to seek a difference between SVs and CCVs. We designed gradient compositions based on previous protocols used to isolate CCVs, SVs, or other similar organelles, selecting sucrose, iodixonal, and/or nycodenz as the gradient materials. After fractionating samples of a spun gradient, we evaluated the protein

distribution of the samples using SDS-PAGE, monitored the presence of synaptophysin with westerns, and measured their acidification with the acridine orange assay. Gradients typically yielded three outcomes. The first, and most frequent, was no apparent separation of proteins across the gradient (Supplemental figure 2), indicating that the CCVs and SVs are not separated. The second was an asymmetrical distribution of several CCV proteins, implying a separation of the sample into subsets, but synaptophysin was evenly distributed throughout the gradient (Fig 9A-B), indicating that no subset of CCVs was separated from SVs. The third was an asymmetrical distribution of synaptophysin, but the no/low synaptophysin samples tended to have very little protein and did not acidify (Fig 10A-B). Because of the reduction in the number of proteins, the non-acidifying CCVs may be empty baskets, spontaneously formed clathrin coats that lack an internal membrane (138). Therefore, we were unable to separate acidifying CCVs from SV markers, likely because that population is very small or too physically like SVs to extract. Our results agree with previous work from Maycox et al. arguing that CCVs are primarily composed of SVs (131).

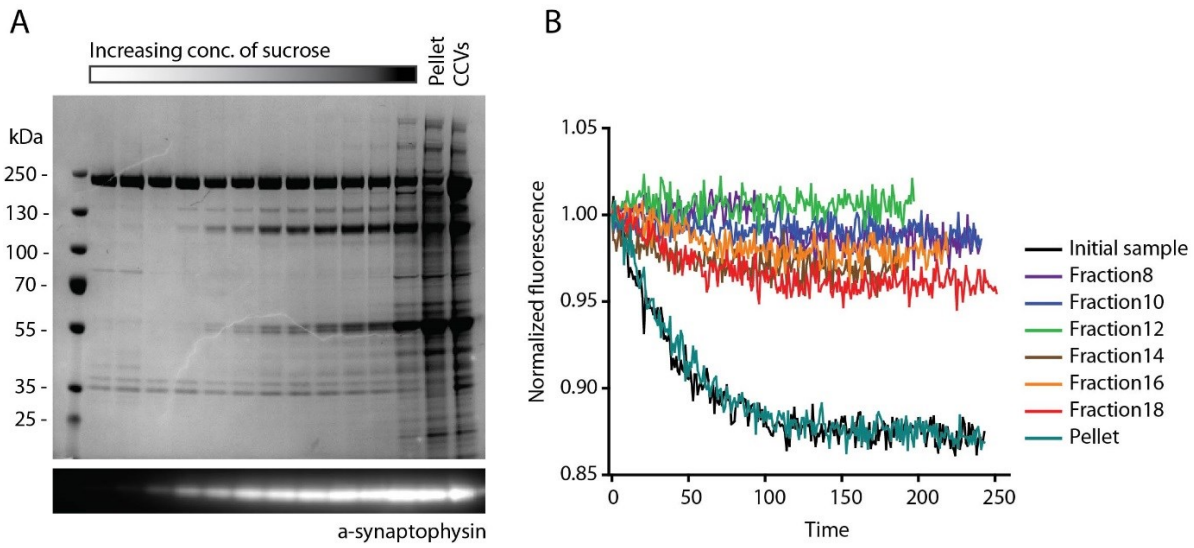

Figure 9: Sucrose gradient to separate CCV marker and SV markers.

(A) CCVs layered on top of a 0.5M and 0.7M sucrose step gradient were spun and fractionated. The SDS-PAGE gel, with labeled molecular weight markers, contains fractions of CCVs, ordered by increasingly high concentrations of sucrose. The final 2 samples are the resuspended gradient pellet and the starting CCVs. Below the SDS-PAGE is a western blot of the same samples probed with an antibody against synaptophysin. (B) Acidification of representative fractions from the gradient were tested under the same conditions described in Fig 3.

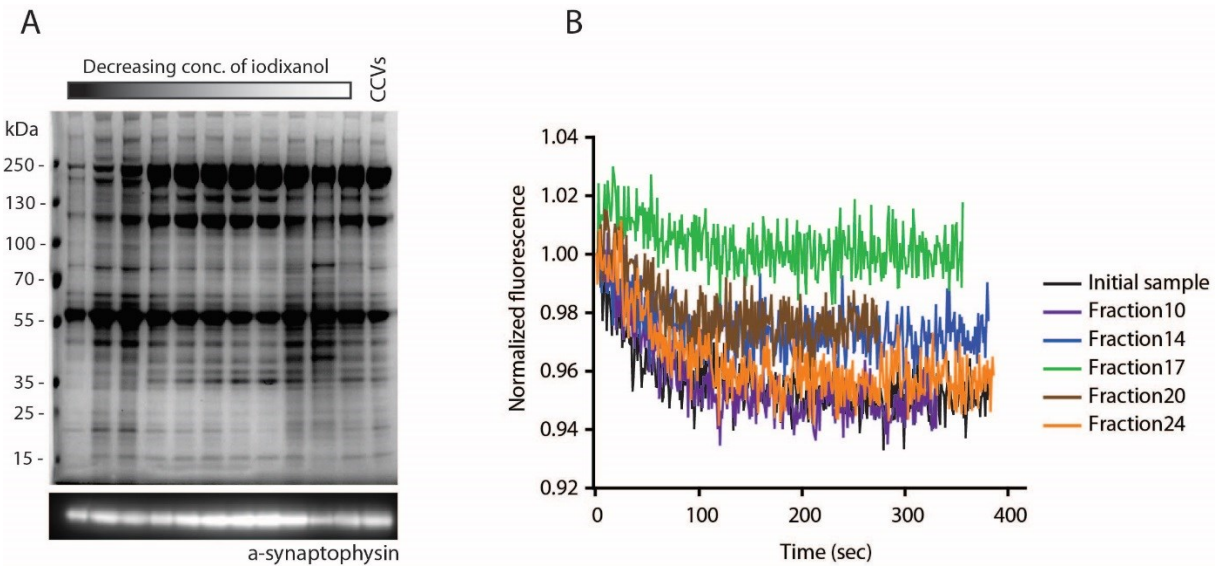

Figure 10: Iodixanol gradient to separate CCV marker and SV markers and acidification.

(A) CCVs layered on top of a 0.5M and 0.7M sucrose step gradient were spun and fractionated. The SDS-PAGE gel, with labeled molecular weight markers, contains fractions of CCVs, ordered by decreasing concentration of iodixanol. The starting CCVs are the last sample. The initial sample was so dilute it was not properly normalized. Below the SDS-PAGE is a western blot of the same samples probed with an antibody against synaptophysin. (B) Acidification of representative fractions from the gradient were tested under the same conditions described in Fig 3.

Mass spectrometry reveals CCV- and SV-specific proteins

We attempted to identify a possible Cl^--transporting protein using mass spectrometry (MS) analysis. Because clathrin and its related adaptor proteins are such substantial portions of the protein sample, we uncoated the vesicles using Tris to increase the percentage of membrane proteins in the sample. We split the initial vesicle sample in half and evaluated it two different ways. We analyzed half of the sample to evaluate the overall levels of protein in the vesicles. We ran the other half on SDS-PAGE to separate the sample based on mass, split it into different 8 samples, and analyzed them

individually to increase the likelihood of detecting low abundance proteins (supplemental graph 1). In both the individual and total protein samples, we found many of the expected structural components of CCVs, including the clathrin heavy and light chains, adaptor proteins, coating and uncoating proteins, components of the V-type ATPase, and proteins relating to microtubules. Additionally, we identified many neuronal specific proteins such as neurofilaments, synaptosomal associated proteins, and SV-specific SNAREs. Similar to the SV westerns, we also detected synaptophysin-1 and synaptotagmin-1 (Fig 6). We examined the samples for Cl^- transporting proteins, finding vGLUT-1 in both the individual and overall samples. One individual sample contained ClC-4, a 2 Cl^-/H^+ transporter that may have some importance in endosomal acidification (58), but that remains unclear. One individual sample contained the Na^+-driven Cl^-/bicarbonate exchanger, although it is unlikely to influence CCV acidification given that there is neither Na^+ nor bicarbonate in most of our experiments. Interestingly, we did not detect ClC-3, a protein known to be present in SVs but rarely identified using MS, implying that even though MS methods for detecting membrane proteins is improving, they remain challenging to identify (82).

Discussion:

A consistent, highly regulated internal pH is vital to the function of many organelles. Endosomal organelles are acidified by the V-ATPase, a membrane protein that pumps H^+ into the lumen. H^+ movement across the membrane is an electrogenic action that requires an ionic shunt or counterion to dissipate and prevent voltage accumulation. In this study, we examined the ions required to facilitate acidification in brain CCVs and explored their similarity to SVs. While Cl^- appears to function as the counterion in CCV acidification, the identity of the Cl^- transporting protein remains unclear (21, 22, 24). Our data are consistent with a previously proposed model showing that brain CCVs are primarily composed of SVs and thus the Cl^- transporting protein is most likely vGLUT1, a SV-specific glutamate transporter (67, 131). However, similar Cl^--dependent acidification has been observed in liver CCVs, and the identity/function of that Cl^- transporting protein remains unknown.

Cl^- has long been implicated as a counterion in endosomal acidification and we sought to investigate its role by characterizing isolated CCVs in a well-defined ionic environment. Our sample of highly enriched CCVs relies on the V-ATPase to acidify the vesicular lumen, without any observable contribution from potentially contaminating mitochondrial or plasma membrane ATPases (Fig 3A). We showed that external Cl^- was necessary for CCV acidification and substituting Cl^- with gluconate, phosphate, or sulfate yields no acidification, similar to the salt-free and +bafilomycin controls (Fig 3B). We also found that Br^- could substitute for Cl^- and facilitated acidification to an even greater extent. While the enhancement of acidification was surprising, that Br^- can substitute for Cl^- was not since many Cl^- transporting proteins are typically unable to discriminate

between the two ions (44, 137). These data agree nicely with the results from previous brain CCV experiments (22, 24), except the enhancement of acidification from Br^- was only seen by our group and by Van Dyke et al. when testing uncoated brain vesicles (22). However, since Br^- is present in cells at such a low concentration, its effects on CCV acidification in vivo are likely negligible.

We also explored the role of cations in CCV acidification by pairing Cl^- with K^+, Na^+, Li^+, or choline, demonstrating that none of these cations are required for the acidification of CCVs (Fig 3B). Our results are similar to those previously observed in brain CCVs, where another group observed no substantial change when K^+ was substitute for Na^+ (22). However, they found that the substitution of Li^+ or choline for K^+ caused a decreased rate of acidification whereas our results are much cleaner and show no acidification reliance on the cation. We are unsure what caused this difference because our isolation protocols and SDS-PAGE results are very similar. However, while acknowledging that electron microscopy images are not quantitative, their sample appears to have more of the large, uncoated vesicle contaminants than ours, which may have contributed to the discrepancy. Thus, we have presented evidence that even more clearly highlights that brain CCV acidification appears to be independent of the external cation and requires Cl^-.

To further characterize the properties of the Cl^- transporting protein, we used two separate approaches. First, we attempted to modify the internal buffer composition of uncoated vesicles using freeze-thaw sonication, which yielded structurally altered vesicles but no internal dye incorporation occurred (Supplemental figure 1). Second, we attempted a partial isolation and reconstitution of the Cl^- transporting protein, which led

us to optimize and improve existing reconstitution conditions, but no Cl^- movement across the proteoliposome membrane was detected (Fig 5). The lack of transporter function was surprising, given the robust CCV acidification and that reconstitution success reported by others (80, 139, 140). Potentially a step in our solubilization/reconstitution conditions prevented the Cl^- transporting protein from functioning or the final concentration of the transporter was too small to yield detectable Cl^- movement. Therefore, additional properties of the transporter remain uncharacterized.

While CCVs in both brain and liver exhibit Cl^- dependent acidification, Maycox et al. showed that brain CCVs are primarily composed of recycling SVs based on membrane protein content similarities. However, they provided no functional data to support this overlap, nor did they exclude the possibility of a small sub-fraction of non-SV CCVs existing in the sample. Our CCV sample was isolated using a slightly different protocol than Maycox et al. and appeared to have a somewhat different SDS-PAGE protein pattern, which led us to question if our acidification was from CCVs, SVs or both (131). We found our CCV sample positively tested for synaptic vesicle proteins when evaluated with immunoblotting and mass spectroscopy (Fig 6, supplemental graph 1). Further, when evaluated with conditions mimicking those used to examine glutamate-induced acidification in SVs, CCVs produced remarkably similar results (Fig 7) (141), again indicating that these two populations are alike. To investigate the overlap between CCVs and SVs, we tried to isolate a sub-population of acidifying CCVs that contained no SV markers using immunoprecipitation and density-gradient based approaches. Immunoprecipitating a subpopulation of CCVs was unsuccessful because the isolated sample contained both clathrin and synaptophysin (Fig 8). The results from separating

CCVs from SVs using density gradients were slightly more informative and yielded one of two general outcomes (Fig 9). The first was an asymmetric separation of CCVs proteins, indicating some separation into subsets, but synaptophysin remained evenly distributed throughout the gradient. The second was an asymmetric distribution of CCV proteins in addition to a gradient of synaptophysin concentration, with the no/low synaptophysin samples containing very little protein and no observable acidification. This result suggests two possibilities, either all acidifying vesicles contain synaptophysin or the low protein samples are empty clathrin baskets, a spontaneously formed clathrin coat without a lipid membrane (138). Because empty baskets can be common in clathrin preps, the latter option is quite likely, but this does not exclude the possibility that the former is also correct. Thus, by taking a functional approach and using a different set of criteria and experiments than Maycox and colleagues, we too have shown that CCVs and SVs have a remarkably similar composition based on the similar acidification pattern of CCVs and SVs, the presence of synaptophysin in most CCV samples, and mass spectroscopy results showing the presence of many SV-specific proteins.

The prevalence of SVs in our CCV sample argues that the protein facilitating the observed Cl^- dependent acidification is likely to be vGLUT1. This transporter contains a Cl^- permeability and requires a small concentration of Cl^- to facilitate glutamate uptake, similar to the acidification properties that we observed in CCVs (Fig 7) (67, 141). However, vGLUT1 is a neuronally expressed protein and CCVs are ubiquitously present through the body. If both liver and brain CCVs need Cl^- to acidify, do they use the same protein or are the Cl^- proteins/counterion requirements organ specific? It is also possible we were unable to isolate the subset of non-SV brain CCVs that use a different Cl^-

transporting protein, potentially because of its extreme similarities to coated SVs or because they are a very small portion of the overall vesicle pool. Besides vGLUT1, our mass spectroscopy results suggested one additional Cl- transporting protein, ClC-4. However, the protein was in low abundance and its role in endosomal acidification remains unclear. One possibility is that a potential small subset of CCVs that are not SVs may employ ClC-4 to acidification, but that would require further testing. Liver CCVs have a slightly different counterion requirement profile in that they do not require Cl^- for acidification, but its presence greatly enhances the extent of acidification (21). If the anion/cation utilization is tissue-dependent, then is Cl^- facilitated acidification necessary or just useful based on specific situations/cell type? Historically, CCVs have been isolated from liver and brain due to the ease of obtaining these larger organs. Exploration into the CCVs from other organs could provide insight into the role of Cl^- and counterions in these early endosomes.

Chapter 2: Supplemental figures

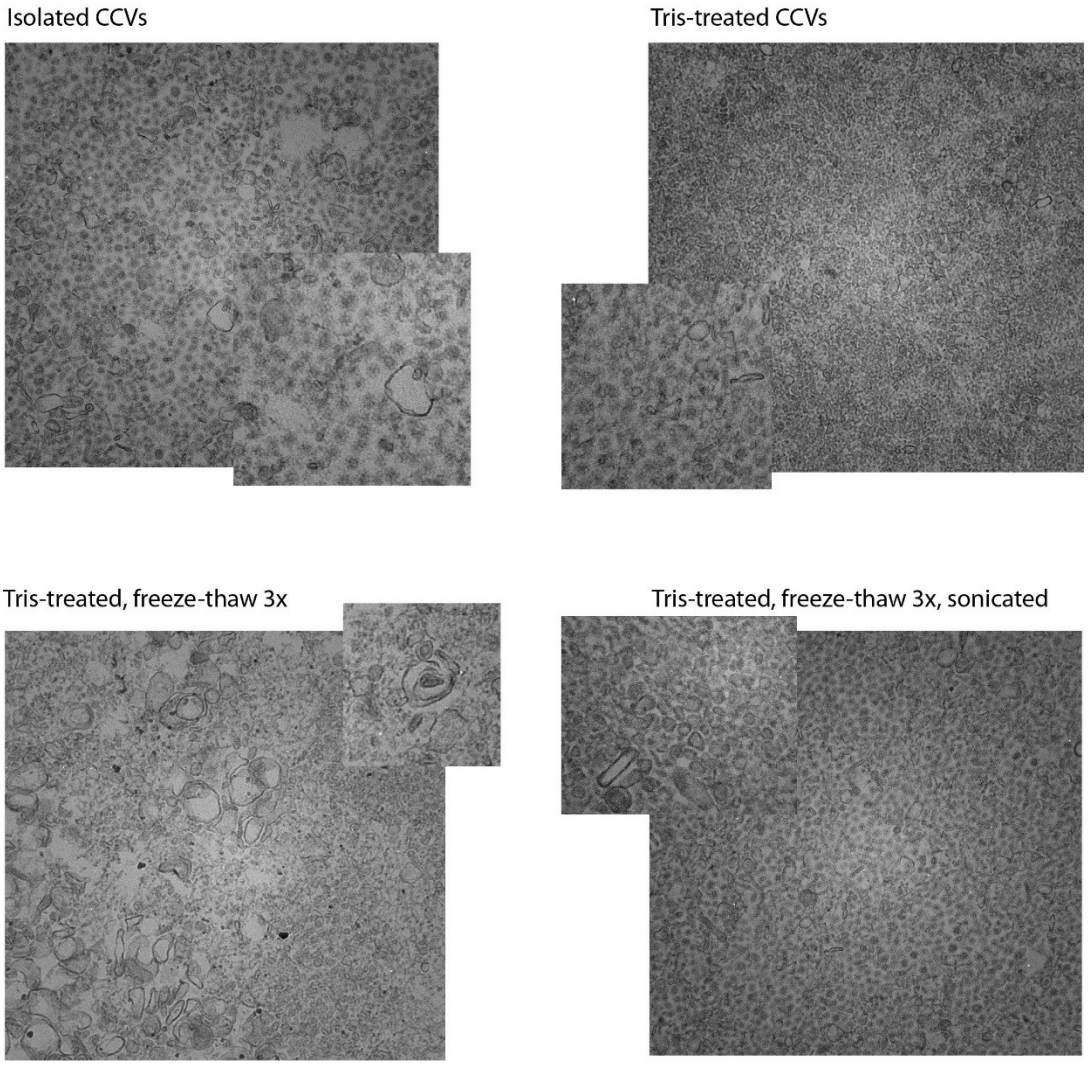

Supplemental Figure 1: Electron microscopy images of CCVs treated in various ways

Shown are representative EM images of CCVs treated in different ways. All CCV samples originated from the same stock and sample removed at the mentioned intervals. CCVs were were stripped of clathrin; stripped and freeze-thawed 3x; or stripped, freeze-thawed 3x, and sonicated. Included for each condition is a magnified image of the vesicles.

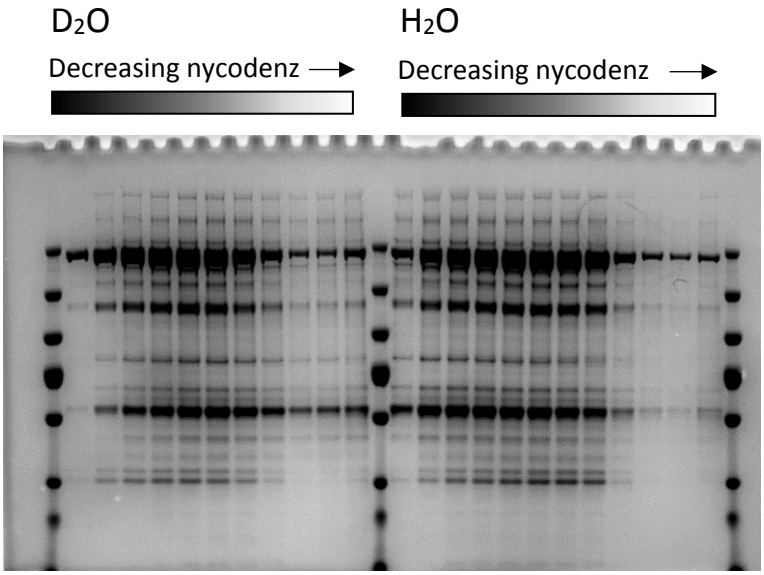

Supplemental Figure 2: Nycodenz step gradients of CCVs

CCVs were spun on a 23-34% sucrose step gradient solubilized in either D_20 (left) or H_20 (right) and alternating fractionated samples were run on an SDS-PAGE gel in order of decreasing density.
The rightmost fractions with little protein are most likely empty baskets.

Supplemental graph 1

This is a microsoft excel file with the mass spectrometry sequencing of the entire CCV sample (total sample) and of the individual CCV fractions from the same CCV starting material (fractions 1-8).

CHAPTER 3:

Probing the role of ClC-7 in hepatocyte lysosomal pH maintenance

Contributing authors: Mary R. Weston, Anorawul Amin, and Joseph A. Mindell

ABSTRACT

Lysosomes, the terminal organelles of the endocytic pathway, maintain a characteristic internal pH essential for their function. This acidic luminal pH is generated and maintained by the V-type ATPase, a membrane protein that pumps protons into the organelle against their electrochemical gradient using energy provided from ATP hydrolysis. H^+-pumping generates a voltage across the membrane; an additional ion, known as a counterion, must move to dissipate this charge buildup and allow bulk acidification. Given that lysosomal acidification is Cl^- dependent, and that the lysosomal protein ClC-7, a Cl^-/H^+ antiporter, moves Cl^- into lysosomes, this protein has been suggested to mediate such counterion movement. In this context, it is surprising that ClC-7 knockout (KO) mouse lysosomes in primary cultures seem to acidify to the same extent as wild type (WT), even though the mice have osteopetrosis and massive lysosomal storage defects. We generated mice with a liver-specific ClC-7 KO to test these results in isolated lysosomes and live cells in parallel. Isolated WT lysosomes relied on Cl^- for acidification and KO displayed little to no acidification. We employed a robust, quantitative method to measure lysosomal pH in live cells using the ratiometric dye Oregon Green 488 covalently linked to dextran. We measured a similar lysosomal pH both WT and ClC-7 KO hepatocytes that was unaffected by the length of culturing time

(3-72 hrs). To evaluate if increasing metabolic demand on the lysosomes asymmetrically affected WT and KO pH by inducing autophagy, a catabolic mechanism used to degrade dysfunctional or unnecessary cellular components. Both WT and KO hepatocytes experience a similar, small increase in lysosomal pH upon amino acid starvation. Alkalinizing lysosomes with NH_4Cl and monitoring reacidification did not reveal a difference in WT and KO lysosomes, as both reacidified to initial levels faster than we could monitor. Thus, while ClC-7 obviously affects the state of lysosomes, we were unable to detect a pH change in KO lysosomes in living cells when exposed to metabolically challenging conditions.

INTRODUCTION

Lysosomes, the terminal organelles of the endocytic pathway, are responsible for breaking down macromolecules and resupplying the cell with basic metabolites. These specialized organelles, the most acidic in the cell, contain various hydrolyases which function at a pH optima between 4.0-5.0. This acidic luminal pH is generated and maintained by the V-type ATPase, a membrane protein that harnesses the energy of ATP hydrolysis to unidirectionally pump protons into the organelle against their electrochemical gradient (4). An accumulation of protons generates a voltage across the membrane unless an additional ion, known as a counterion, simultaneously moves to dissipate charge buildup and allow bulk acidification. The counterion could be a cytoplasmic anion entering the organelle, a luminal cation exiting the organelle, or a combination of both. The identity of the counterion(s) responsible for lysosomal acidification is debated (26, 93), but Cl^- appears to be important based on functional studies in isolated lysosomes (20, 23, 44, 92, 94). In one such study, Okhuma et al. used isolated lysosomes containing the pH sensitive FITC-dextran dye to explore the effects different ions had on acidification (20). In these experiments, removing external Cl^- from the bathing media substantially slowed and reduced acidification, but exchanging the cation had little effect, arguing that anions function as counterions. Later Graves et al. established that the primary pathway for Cl^- flux in the lysosome is from a transporter exchanging two Cl^- ions for one proton moving the opposite direction (44). The lysosomal-specific chloride transporter was demonstrated to be ClC-7, a $2Cl^-/H^+$ antiporter, knocking down (KD) its expression in HeLa cells yielded lysosomes that appeared to have a more basic pH when assessed with a non-quantitative, pH-sensitive

dye. Together, these experiments argue that ClC-7 mediates counterion movement in lysosomes. However, quantitative measurements from several different studies evaluating the lysosomal pH of ClC-7 knock out (KO) primary cells reveal no significant pH change compared to wild-type (WT), even though the mice themselves have severe osteopetrosis, lysosomal storage defects, and only live 3-5 weeks (94, 99, 100, 102, 116).

Several possibilities may explain this discrepancy. First, the ClC-7 KD experiments were performed using only one siRNA and measured with a non-quantitative dye, casting doubt on the results (44). However, unpublished data from our lab indicates this result is reproducible when performed with a pool of siRNAs and measured with a quantitative, pH-sensitive dye (S.B. Lioi and J.A. Mindell, unpublished results). Secondly, knockout mice may have various mechanisms that compensate for the loss of ClC-7 and allow for proper lysosomal acidification. For example, the ClC-7 KO mouse has been shown to retarget other members of the ClC family, ClC-3 and ClC-6, to lysosomes (120). Third, the mechanism by which various tissues and cell types compensate for the loss of ClC-7 is unknown. Perhaps tissues most affected by a loss of ClC-7, such as brain and bone, either compensate differently or place a higher demand on their lysosomes then macrophages and fibroblasts, where KO lysosomal pH has primarily been evaluated.

To determine the effects of ClC-7 on lysosomal acidification, we created a liver-specific ClC-7 KO mouse. This approach allowed us to evaluate the acidification of isolated lysosomes in parallel to measuring lysosomal pH in primary hepatocytes, a cell type where ClC-7 KO pH has not been previously characterized. KO mice had a similar life span and were visually similar to WT, but both the entire body weight and the liver

weight of the KO were about 25-30% heavier than WT. Similar to published results, we observed that isolated lysosomes exhibited Cl^--dependent acidification that was absent in KO lysosomes. However, like published literature, the lysosomal pH in live WT and KO hepatocytes were very similar. We postulated that the role ClC-7 plays in lysosomal pH maintenance could become apparent when the workload demand on lysosomes is increased. To test this, we stressed lysosomes by inducing autophagy, a catabolic mechanism used to degrade dysfunctional or unnecessary cellular components, to increase the volume of material targeted to the lysosome (89). Additionally, we tested the ability of ClC-7 KO hepatocytes to regenerate an acidic pH after alkalization by a weak base. Yet, in all metabolic conditions tested, the lysosomal pH of KO primary hepatocytes matched that of the WT. Thus, while ClC-7 is clearly important in lysosomal physiology, its exact effects remain undetermined.

METHODS AND MATERIALS

All chemicals were purchased from sigma unless other designated.

ClC-7 liver specific KO mouse generation

Wild-type C57BL/6 and homozygous Alb-Cre^{+} transgenic mice were obtained from Jackson Laboratory. The lox-ClC-7 mice were developed by Xenogen technologies. Several crossings of the Alb-Cre^{+} and lox-ClC-7 generated homozygous Alb-Cre$^{+/}$lox-ClC-7 mice (confirmed via genotyping). RNA was isolated from fresh livers using the RNA PureLink kit (ThermoFischer Scientific). RNA was converted to cDNA (iScript; Biorad) and amplified with the SsoAdvance kit (Biorad) on a C1000 thermal cycler (Biorad, CFX96 RealTime). ClC-7 primers used were: forward (5'-CGCCAGTCTCATTCTGCACT-3') and reverse (5'-GCTTCTCGTTGTGTGGAATCT-3'). 18s rRNA control primers used were: (F: 5'-TGTGCCGCTAGAGGTGAAATT-3', R: 5'-TGGCAAATGCTTTCGCTTT-3').

Liver/kidney lysosomal preparation from rat or liver

Fluorescein isothiocyanate-dextran (70 kDa FITC-dextran (Sigma) in 1X PBS) was injected into a rat or mouse (10 mg/100 g of body weight of rat; and 10 mg/mouse) intraperitoneally and subsequently starved overnight (~12-14 hours). The isolated liver or kidney obtained from the euthanized rat or mouse was minced and then homogenized (Homogenizer Motor Drives, Glas-Col) with HM buffer (ice cold 10 mM HEPES, 1 mM K_2-EDTA, 0.25 M sucrose, pH 7.0) at 4°C. As in (20), the homogenate was centrifuged

at 800 xg for 10min. The supernatant was collected and centrifuged again for 10 min at 20,000 xg to isolate the light mitochondrial fraction (LMF). A percoll:LMF mixture (4:5 ratio) was centrifuged at 35,000 x g for 90 min (without break) at 4°C. The gradient was fractionated (0.8 mL for rat liver; 0.4 mL and 0.2 mL of mouse liver and kidney, respectively) from the bottom using an Econo pump (Biorad). Collected fractions were spun at 100,000 X g for 60 m, at 4°C to remove the percoll from lysosomes. Protein concentration was determined using a BCA colorimetric assay kit (ThermoFisher Scientific). Lysosome-rich fractions were confirmed by fluorescence spectroscopy (excitation 490 nm; emission 520 nm) (Jobin Yvon FluoroMax-3 spectrofluorimeter).

Proton-driven $^{36}Cl^-$ uptake:

Protocols were followed as in (44). 100 μg the lysosome-rich fraction was freeze thawed 3x and sonicated with internal buffer (5 mM NaCl, 10 mM KCH_3SO_3, 20 mM citrate; pH 4.0). The external solution was exchanged using a sephadex G-50 column equilibrated with external buffer (5 mM $Na^{36}Cl$, 10 mM KCH_3SO_3, 1 mM $NaVO_3$, and 20 mM HEPES at pH 7.0). H^+-driven $^{36}Cl^-$ uptake was initiated by addition of 1 μM valinomycin. At indicated times, the reaction was terminated by addition of a 20x volume of ice cold quench buffer (5 mM NaCl, 10 mM KCH_3SO_3, 1 mM $NaVO_3$, and 20 mM HEPES at pH 7.0) and rapid filtration through a 200-nm nitrocellulose filter (Millipore). The filter was washed 2x with quench buffer, the filter was dissolved in FilterCount liquid scintillation cocktail (PerkinElmer) and the $^{36}Cl^-$ internalized by the proteoliposomes was counted with a Beckman LS6500 scintillation counter.

Lysosomal acidification

100 µg of the lysosome-rich fraction was suspended in 1.25 mL of buffer (100 mM of KCL/K_2SO4/ChCl/K-Gluconate, 10 mM $MgSO_4$, 250 mM sucrose and 10 mM HEPES/KOH, pH 7.0) in a glass cuvette at room temperature. FITC-dextran emission (excitation 490 nm; emission 520 nm) was monitored as a function of time and 1 mM *Mg^{2+}-ATP and* 1 µM FCCP were designated. Fluorescence intensity was normalized to the value measured right after addition of *Mg^{2+}-ATP*.

Hepatocyte isolation

A 24G catheter was injected into the IVC vein of the liver of an CO_2 sacrificed mouse and ~35 mLs of hepatocyte wash media with 1x penicillin/streptomycin (Gibco 17704024, ThermoFisher 15140122) was perfused into the liver. The SVC vein was cleaved to increase the flow of media. After losing its color, ~30 mLs of EGTA buffer was perfused until the liver turned white, then wash media with 0.1% collagenase (Type IV; Gibco 17104019) was perfused until the liver because mushy (25-35 mLs). The liver was moved to a sterile hood (where all experiments occur henceforth), finely chopped, and suspended in 21 mLs of 0.067% collagenase in wash media. The liver solution was incubated at 37°C for 10-15 minute (with gentle inversion every couple minutes) and then filtered through a 70 µM cell strainer. 20 mLs of wash buffer was added to the cell solution and centrifuged for 5 min at 65xg. The supernatant was discarded, the cell pellet gently resuspended in 50 mLs of wash media, and then spun at 65xg for 5 min. This wash step was repeated an additional time and the final cell pellet was resuspended in 11 mLs of wash media. 10 mLs of a percoll solution (9 mLs percoll + 1 mL 10x PBS) was added

to the cell solution and spun at 200 g for 10 min with low acceleration and low brake. The supernatant was removed and the pellet resuspended in 25 mLs of wash media. After a final 65xg for 5 min, the supernatant was discarded and cells were resuspended in wash media (3-4 mLs). Cells were plated onto collagen-coated plates or slides (Collagen: corning 354249 with final concentration of 5.77 μg/mL; Nunc Lab-Tek II slides 155382) in 2% FBS DMEM (Gibco 17104019) and maintained in at 37°C with 5% CO_2.

Measuring the lysosomal pH of live cells

Confocal images of Oregon Green 488 loaded cells were collected using a FITC filter on a Ziess AIRY and deconvolved at something using X camera.

To evaluate lysosomal pH, cells were incubated overnight in DMEM containing 4 mg/mL Oregon green 488 10,000 MW dextran (ThermoFisher Scientific D7170). Upon dextran removal, cells were rinsed 3x with PBS, and chased in dye-free media for 4 hours. Ratiometric, fluorescent images were collected using a Ziess widefield microscope and a CCD camera (Photometrics CoolSNAP HQ2). Excitation bandpass filters 440/40 and 485/20 were used to excite the Oregon Green 488 fluorophore, and a 506nm dichroic filter with a bandpass filter 534/42 were used to collect the emission from both excitation wavelengths. Cells were imaged in medium 2 (in mM: 150 NaCl, 5 KCl, 1 $CaCl_2$, 1 $MgCl_2$, 20 hepes, 10 glucose, 30 sucrose; pH 7.4 with HCl) (142). Greater than 15 cells/experimental condition were imaged. Hepatocytes were incubated for 15-20 min in 32 nM bafilomycin in imaging media (Sigma B1793) where noted. An Oregon Green calibration curve was determined by incubating cells with buffers titrated at half pH unit increments, from pH 4.0-7.0 +/- 0.01, and 10 μM each of Monensin and Nigericin (Sigma

M5273, N7143). The calibration buffers contained imaging media and a designated buffer (for pH 4.0-5.5, 50 mM Tris-maleate; for pH 6.0, 25 mM Na_2HPO_4 and 25 mM Tris-maleate; for pH 6.5-7.0, 50 mM Tris-maleate). Cells were incubated for five minutes prior to imaging to allow for pH equilibration across all membranes. The well was rinsed thoroughly after each pH measurement before the next pH buffer was added.

For starvation-induced autophagy, Oregon green 488 loaded cells were incubated in EBSS (Sigma E2888) for 2-3 hrs prior to imaging. For chemically induced autophagy, cells in growth media were incubated for 1-2.5 hr with either 2.2-4.4 μM rapamycin or 250-500 nM Torin-1 (Tocris 4247). Lysosomes were alkalized by adding either 5 or 10 mM NH_4Cl in imaging media and incubating with cells for 2-3 min. Cells were rinsed 3-4x with imaging media to removed NH_4Cl.

Image analysis

Images were analyzed using either MetaMorph Imaging software or Slicer2D, a Matlab-based program created for lysosomal analysis by the CIT group under the direction of Huey Cheung at NIH. In short, after applying a wavelet filter and thresholding for spots whose intensities were in the top 80%, lysosomes were identified as individual objects in each 440 and 490 image. Identified objects from each image were reconciled with the other image to ensure the same objects were being evaluated in both images. The original images were background subtracted (using average intensity of the lowest 5% of intensities) and then the average and total intensity for each object was measured. The fluorescence ratio (490/440) was calculated using the total fluorescent intensity of each object. The lysosomal pH was calculated using cells with greater than

10 lysosomes. To convert ratio to pH, lysosomal values from each individual pH calibration tested were averaged and the data fit to a four-parameter sigmoidal equation. The pH values for individual cells were interpolated using the sigmodal equation values obtained from fitting to the pH calibration curve.

Westerns and Immunofluorescence:

Cells were solubilized in RIPA buffer (Sigma R0278) with protease inhibitors. For westerns, PVDF membranes were blocked in 5% BSA. Primary antibodies were used at 1:1000 (Cell Signaling Technology; p70-S6K (#9202) and P-p70-S6K (#9205)) and a goat α-rabbit secondary at 1:7500 (ThermoScientific; 32460).

For immunofluorescence, cells were fixed for 10 min in 3% PFA, permeabilized in 0.2% trition for 5 min, and quenched with 0.1 M glycine. Blocking steps were performed with 3% BSA. 1:200 Albumin (Bethyl Laboratories; A90-134A-16) and 1:1000 donkey α-goat alexa fluor 488 (ThermoFisher; A-11055) were used for primary and secondary steps, respectively.

RESULTS

Characterizing the ClC-7 liver specific knockout mouse

We investigated the effects of ClC-7 on lysosomal acidification by crossing a *loxP*-flanked ClC-7 mouse with a mouse expressing Cre recombinase under the liver-specific albumin promoter, creating a liver-specific ClC-7 KO mouse (Fig 1A). The partial knockout strategy yields mice without osteopetrosis and other detrimental phenotypes associated with the full body ClC-7 knockout (99, 100, 102), while allowing us to investigate the impact of ClC-7 using both isolated lysosomes and primary cells from the same organ. Due to the lack of commercially available, reliable ClC-7 antibodies, we used RT-PCR to measure the efficiency of knockout. After normalizing WT expression to 100%, the KO mouse had undetectable expression of ClC-7 (Fig 2). The liver-specific KO and WT mice are visually similar with a comparable life span (Fig 1B). However, KO mice have a shifted weight distribution, weighing 25-35% more than WT littermates (Fig 1B, 1D). Upon opening the chest cavity, the KO mice frequently had more fat lining the gut and a larger, fattier liver (Fig 1C). Although individual livers varied, the average KO liver weighed ~25% more than WT (Fig 1C-D).

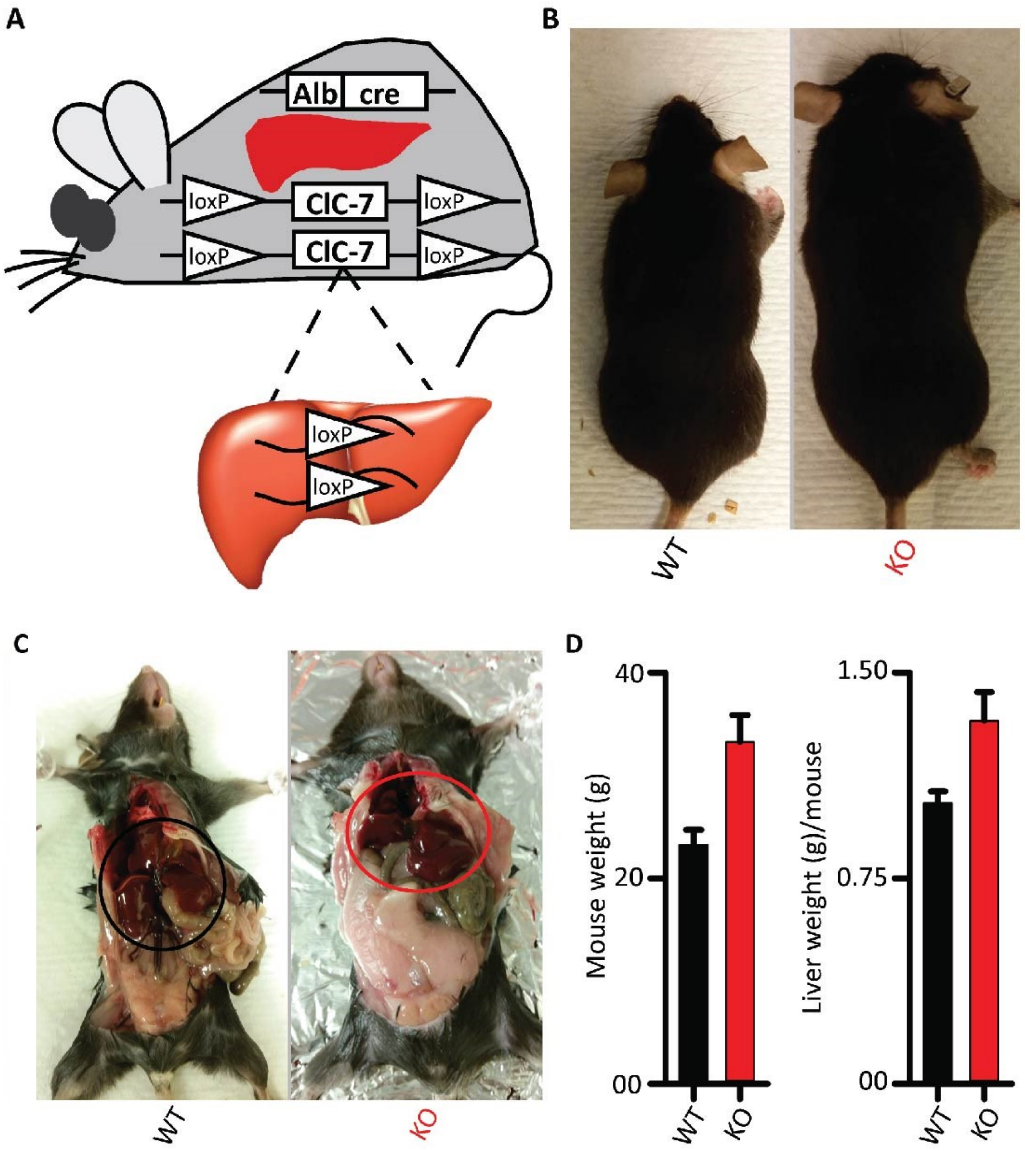

Figure 1: Characterization of the ClC-7 liver-specific KO mice.
Data and figure by Anowarul Amin
(A) Schematic of ClC-7 liver-specific knockout shows loxP-flanked ClC-7 was combined with a cre-lox expressed under the liver specific promoter albumin. (B) Images depict the sizes of WT and KO mice. (C) Images show the relative sizes of WT and KO livers (circled). (D) Quantitative measures of (B) and (C) showing the average and standard deviation of the body weight and liver weight of WT and KO mouse, indicating a 30% and 25% increase in size, respectively.

Previous work established that ClC-7 is the primary pathway for Cl^- flux in the lysosome (44). To further confirm that KO lysosomes contained no ClC-7, we evaluated the ability of WT and KO lysosomes to move Cl^- across their membrane using a H^+-driven Cl^--uptake assay (Fig 3). In these experiments, lysosomes are exposed to an outwardly directed H^+ gradient (pH 4.0 inside; pH 7.0 outside) and symmetrical Cl^- on both sides of the membrane. If a H^+-driven Cl^- transporter was present, the H^+ gradient would drive the uptake of outside $^{36}Cl^-$ into the lysosomal lumen. The transport assays show that isolated WT lysosomes were capable of H^+ driven $^{36}Cl^-$-uptake, but KO lysosomes accumulated no measurable level of labeled substrate, demonstrating that ClC-7 is knocked out. Additionally, previous ClC-7 KO models showed some retargeting of ClC-3 or -6 from the late endosome to the lysosome, suggesting a potential mechanism cells employ to compensate for loss of ClC-7 (120). The lack of Cl^- uptake indicates that no compensatory Cl^- transporting pathway is present in our KO lysosomes.

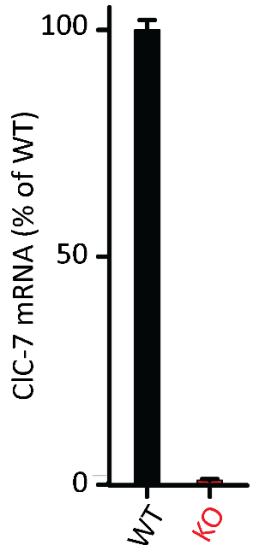

Figure 2: ClC-7 KO mice do not express measurable ClC-7 mRNA

Data and figure by Anowarul Amin.

mRNA was extracted from WT and KO isolated livers and relative expression of WT and KO ClC-7 was measured using qRT-PCR. WT expression was normalized to 100% and KO mice express ~0% mRNA when compared to WT (n>3 livers for WT and KO each).

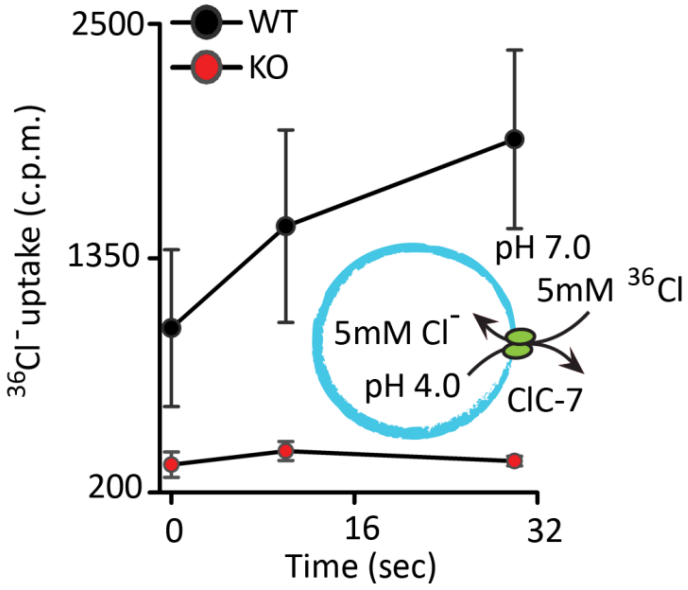

Figure 3: Proton-driven $^{36}Cl^-$ flux is abolished in isolated KO hepatocytes

Data and figure by Anowarul Amin

Lysosomes containing 5 mM Cl^-, pH 4.0 were added to a buffer with 5 mM $^{36}Cl^-$, pH 7.0. Data are shown for WT (black) or ClC-7 KO (red) lysosomes measured after 1, 10, and 30 seconds. Expression was normalized to 100% and KO mice express ~0% mRNA when compared to WT (n>3 livers for WT and KO each).

Isolated lysosomes rely on Cl^- to facilitate acidification

After comparing the physical features of the WT and ClC-7 KO mice, we studied the acidification properties of isolated liver lysosomes. We used freshly isolated organelles loaded with FITC-dextran, a pH sensitive dye that decreases when exposed to acidic conditions. Upon addition of ATP, WT lysosomes in a KCl buffer showed a loss of fluorescence, indicating a more acidic luminal pH (Fig 4A). The subsequent addition of FCCP, a H^+ ionophore that allows the free movement of H^+ across the membrane, increased fluorescence and confirmed that the signal loss upon ATP addition was due to an acidic shift in luminal pH. Lysosomes incubated with bafilomycin, an inhibitor of the V-ATPase, displayed no acidification, showing that the V-ATPase is primarily responsible for acidification. To determine the ionic requirements of acidification, Cl^- was substituted for gluconate and SO_4^{2-}, resulting in a ~50% and ~80% reduction of acidification, respectively. These results indicate that Cl^- plays an important role in facilitating acidification. When K^+ was substituted for choline, acidification was slightly enhanced, indicating that the cation is not essential for acidification. In contrast, KO mice lysosomes displayed little acidification upon addition of ATP, with the rate and magnitude of acidification being similar in KCl, ChCl, Kgluconate, and K_2SO_4 (Fig 4B). We evaluated the rate of acidification during the first 30 seconds after ATP was added, observing that while WT relies primarily on the anion to acidify, KO lysosomes experience little acidification in all buffers (Fig 4C). Thus, we find that WT utilizes Cl^- to acidify while KO lysosomes have little to no acidification activity. Together, the experiments in isolated lysosomes strongly argue that ClC-7 is knocked out in the liver,

isolated lysosomes rely on Cl^- to acidify via ClC-7, and no additional ClC transporters are functionally active in isolated KO lysosomes.

Isolating and characterizing primary hepatocytes

After establishing that ClC-7 clearly plays a role in the acidification of isolated liver lysosomes, we evaluated the effects of ClC-7 on lysosomal pH in hepatoctyes to provide as equivalent of a comparison as possible. We devised a hepatocyte isolation protocol, incorporating previously published methods, that consists of the perfusing of liver with collagenase, filtering out contaminates with a percoll gradient, and plating cells on collagen-coated plates/slides. The percoll gradient was necessary to obtain consistent, non-contaminated cells. Cultured hepatocytes were a largely homogenous population based on shape and size (Fig 5A). Our isolated cells appeared similar to cultured hepatocytes reported in literature based on cell appearance and the expected binucleated/quadnucleated cells were seen 24-48 hrs post-isolation (143). We tested the identity of the cells by immunostaining fixed cells for albumin, a hepatocyte-specific protein, and found positive expression in most cells (Fig 5B). Visually, there were no obvious differences between WT and KO hepatocytes.

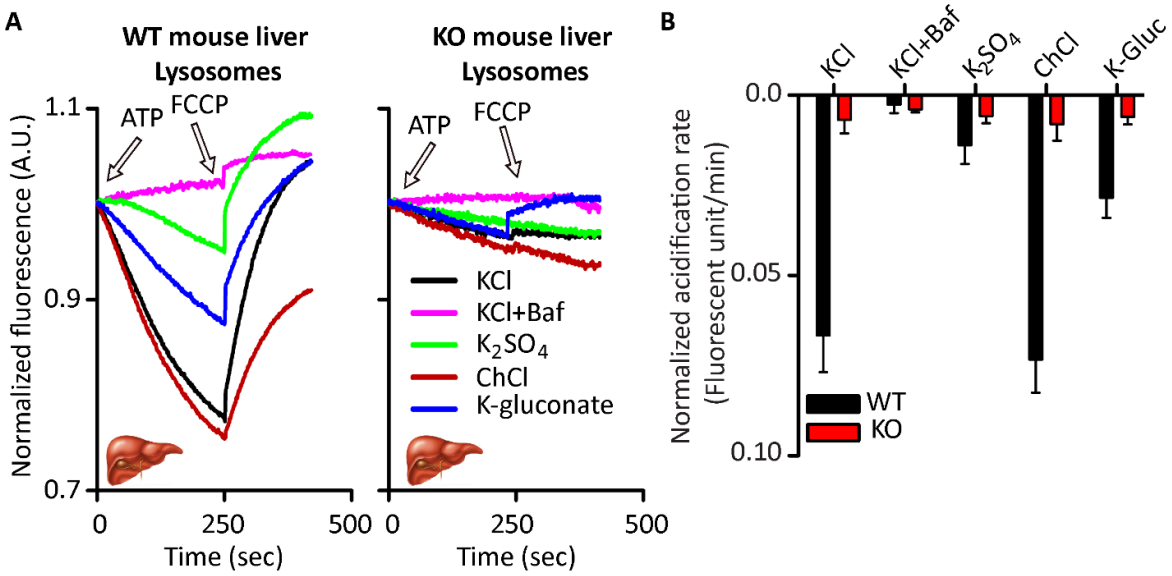

Figure 4: Isolated WT lysosomes utilize external Cl^- to facilitate acidification but KO organelles display severely reduced acidification and no reliance on Cl^-

Data and figure by Anowarul Amin

(A) Representative acidification traces of isolated lysosomes loaded with FITC-dextran in a 10mM Hepes buffer (pH 7.0) with 100 mM of KCl (black), K_2SO_4 (green), choline-Cl (ChCl) (red), or K-gluconate (blue). Reactions were initiated with 1 mM ATP and a decrease in fluorescence indicates acidification. Reactions were normalized to the first time point after ATP addition. Where noted, lysosomes were incubated with 2 µM bafilomycin, a V-ATPase inhibitor, for 15 min prior to addition of ATP (pink trace). 1 µM FCCP, a proton ionophore, was added where indicated. (B) Quantification of isolated lysosomal acidification data for WT (black) and KO (red) are expressed as the rate of normalized fluorescence over the first 30 seconds after ATP addition.

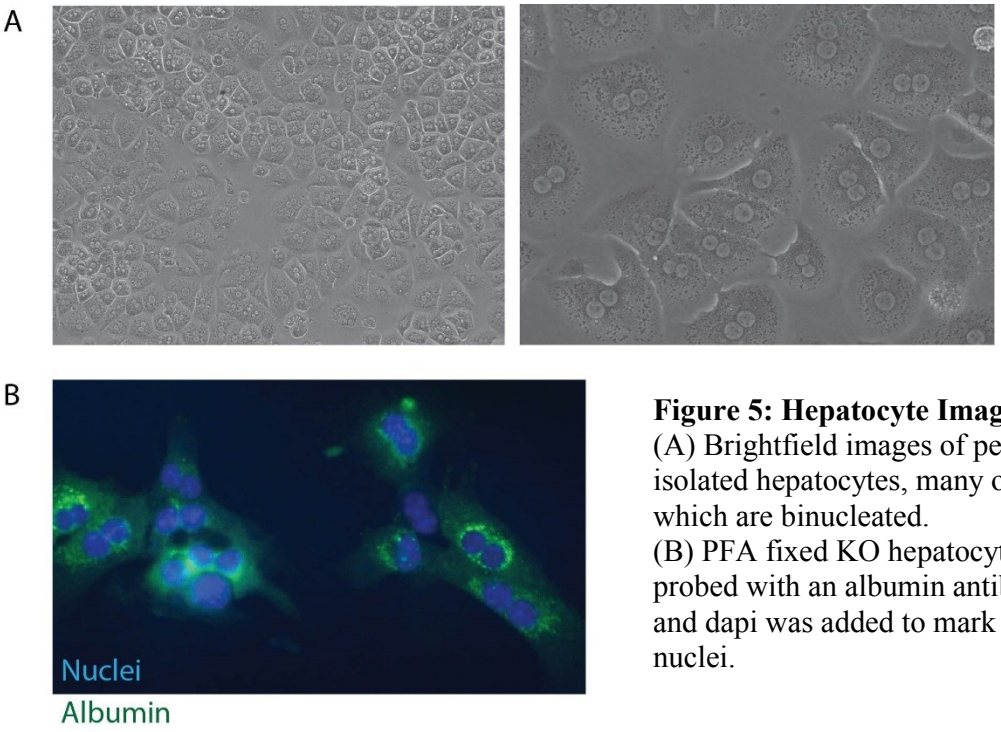

Figure 5: Hepatocyte Images
(A) Brightfield images of percoll isolated hepatocytes, many of which are binucleated.
(B) PFA fixed KO hepatocytes probed with an albumin antibody and dapi was added to mark the nuclei.

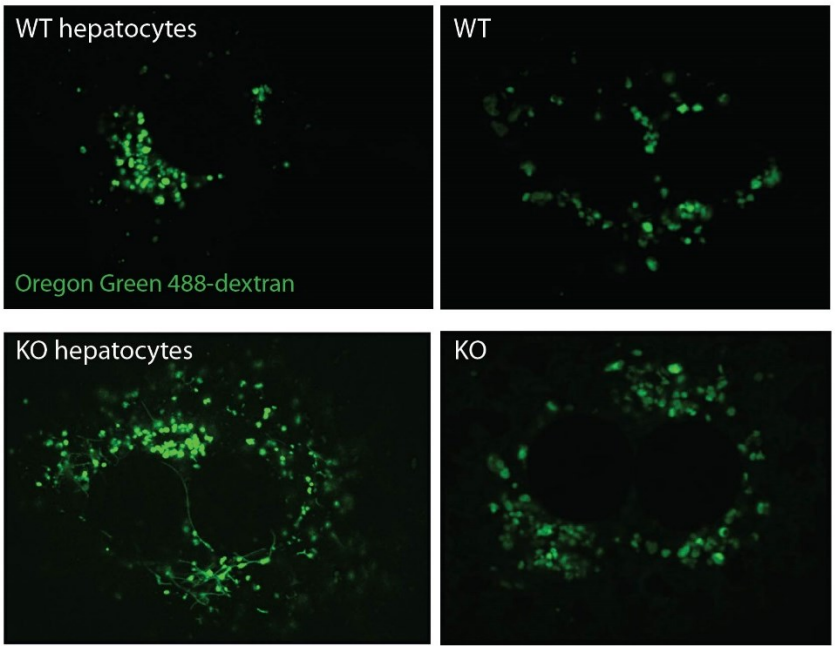

Figure 6: WT and KO hepatocytes uptake Oregon Green 488 and have similar lysosomal distributions
Deconvolved AIRY scan confocal images of live WT and KO hepatocytes incubated with Oregon Green 488-dextran overnight.

Measuring lysosomal pH in primary hepatocytes

After successfully isolating primary cells from the liver, we explored if ClC-7 was important for their steady state lysosomal pH. We employed a robust and quantitative method for pH measurement in live cells using the fluorescent, ratiometric dye Oregon Green 488 covalently attached to dextran. When incubated with cells, the dye is transported into the cell via endocytosis and subsequently trafficked through the endosomal pathway to the lysosome. We imaged WT and KO hepatocytes loaded with dye, observing a similar lysosomal distribution pattern (Fig 6). Oregon Green 488 emits a pH independent (excitation 440 nm) and pH dependent (excitation 490 nm) fluorescent value, the ratio of which can be correlated to a specific pH using an experimentally derived calibration curve (Fig 7A-B). We found that the steady-state lysosomal pH of the WT and KO was not significantly different, with respective values of 5.1 +/- 0.1 and 5.2 +/- 0.1 (Fig 7C). Thus, like previously reported results, knocking out ClC-7 did not modify lysosomal pH. To ensure that increased hepatocyte culturing time did not affect lysosomal pH, we compared the effects of increasing culturing time to 72 hrs compared to the typical 48 hr time point. We found WT and KO lysosomal ratios were not only similar to each other, but comparable to the 48 hr time point as well (Fig 7D). These results demonstrate that ClC-7 KO lysosomes maintain the same pH as WT in cultured hepatocytes.

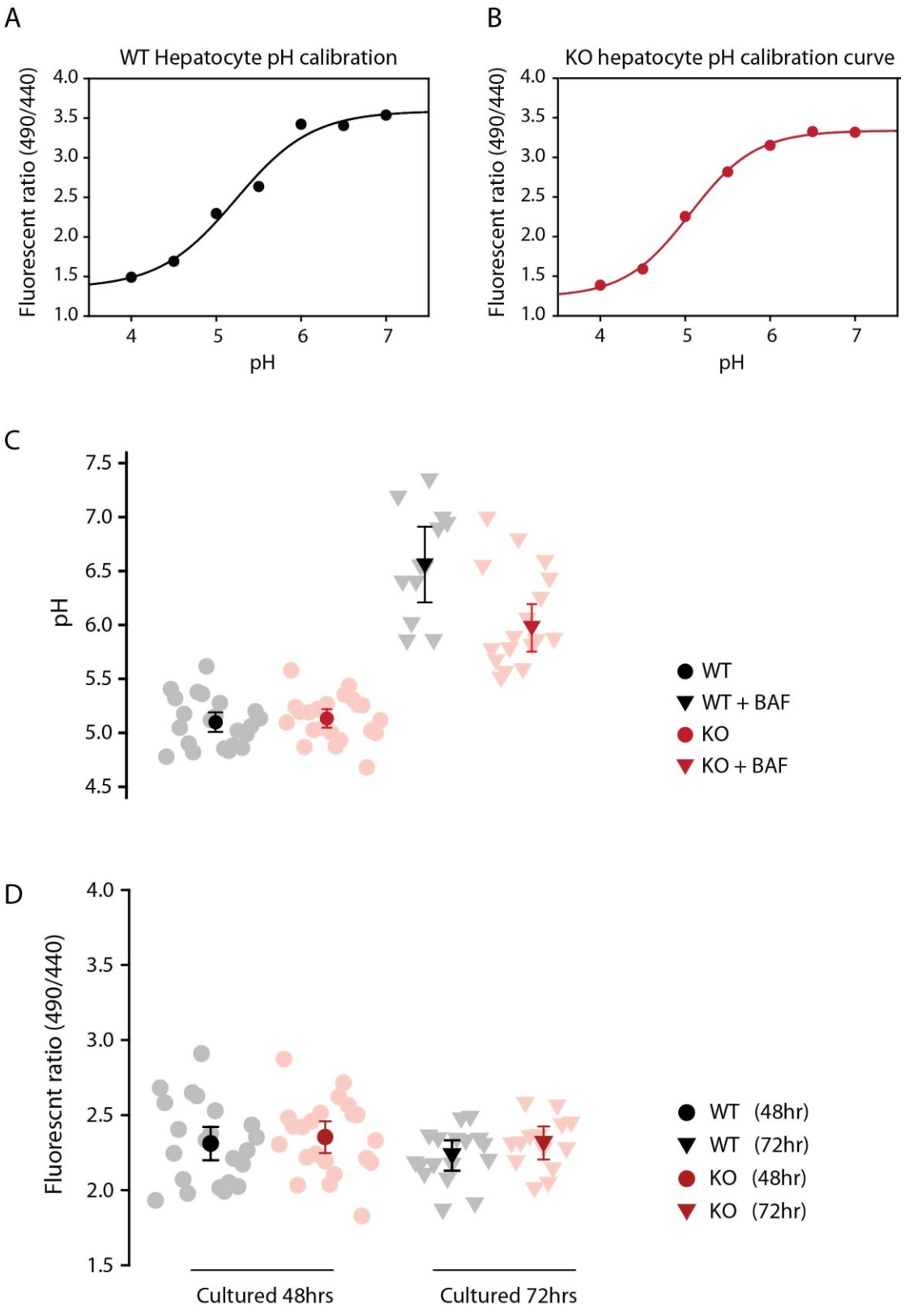
A
WT Hepatocyte pH calibration
Fluorescent ratio (490/440)
4.0
3.5
3.0
2.5
2.0
1.5
1.0
4
5
6
7
pH
B
KO hepatocyte pH calibration curve
Fluorescent ratio (490/440)
4.0
3.5
3.0
2.5
2.0
1.5
1.0
4
5
6
7
pH
C
pH
7.5
7.0
6.5
6.0
5.5
5.0
4.5
WT
WT + BAF
KO
KO + BAF
D
Fluorescnt ratio (490/440)
4.0
3.5
3.0
2.5
2.0
1.5
Cultured 48hrs
Cultured 72hrs
WT (48hr)
WT (72hr)
KO (48hr)
KO (72hr)

Figure 7: WT and ClC-7 KO hepatocytes have similar steady-state lysosomal pH. Lysosomes loaded with Oregon green 488 dextran from WT and ClC-7 KO hepatocytes were imaged at two excitation wavelengths and the resulting values are a fluorescent ratio (analyzed with slicer2D) of the pH dependent value/pH independent value. (A)-(B) To convert fluorescent ratio to pH, hepatocytes were incubated with buffers every 0.5 pH units from 4.0-7.0. Calibration curves for WT (A) and ClC-7 KO (B) are shown. (C) Steady-state lysosomal pH of WT (black) and KO-ClC-7 (red) hepatocytes loaded with Oregon green 488 were imaged and the ratio converted to pH using the values from (A) and (B). Lightly shaded points represent the average lysosomal pH for one cell (>12 lysosomes/cell). The average and SEM for each condition are shown as the darkly shaded points. Hepatocytes incubated with 32 nM bafilomycin were imaged as a control. Cells had been isolated from the mouse approx. 48 hrs prior to being imaged. (D) Cells isolated at the same time as (C) were left for an additional 24 hrs before loading with dye and identically imaged the following day. The data are expressed in fluorescent ratio because no pH calibration curve was conducted on the 72 hr time points.

Given that the whole-body ClC-7 KO mouse displays symptoms of lysosomal storage disease, that ClC-7 is a lysosomal membrane protein responsible for moving ions related to pH, and that isolated lysosomes rely on Cl^- for acidification, the lack of a lysosomal pH change in cultured cells is surprising. We investigated if the similarity between WT and KO lysosomal pH is explained by a potential reduction in metabolic demand due to a change in the cellular environment. In our experiments, hepatocytes are transitioned from an organ to a cultured media, an environment that likely places less metabolic demand on the cells than tissue. If ClC-7 affects the rate of acidification, then plating KO hepatocytes in culturing media for more than 24 hrs may be enough time for the lysosomes to gradually attain a pH value similar to the WT. We investigated the effect of plating time by examining lysosomal pH after hepatocytes had been plated for only 3 or 6hrs (Fig 8). Because hepatocytes need an overnight incubation with Oregon Green 488 to accumulate enough dye to provide a reliable signal, we evaluated lysosomal

pH using the pH-sensitive dye FITC-dextran intraperitoneally injected into the mice the night prior to hepatocyte harvest. After 3 hrs of plating, the majority of hepatocytes remained fairly spherical, not unexpected given the short plating time. The lysosomal ratios of both cell types were high, representative of a more alkaline pH, potentially induced by the stress of removal from the liver. After 6 hours of plating, hepatocytes become flatter and the lysosomal ratio settled to a level similar to the ratio measured after 24-30 hours of plating. Therefore, if length of time in culturing media does influence lysosomal pH, it is difficult to detect while cells are simultaneously adjusting to a new environment.

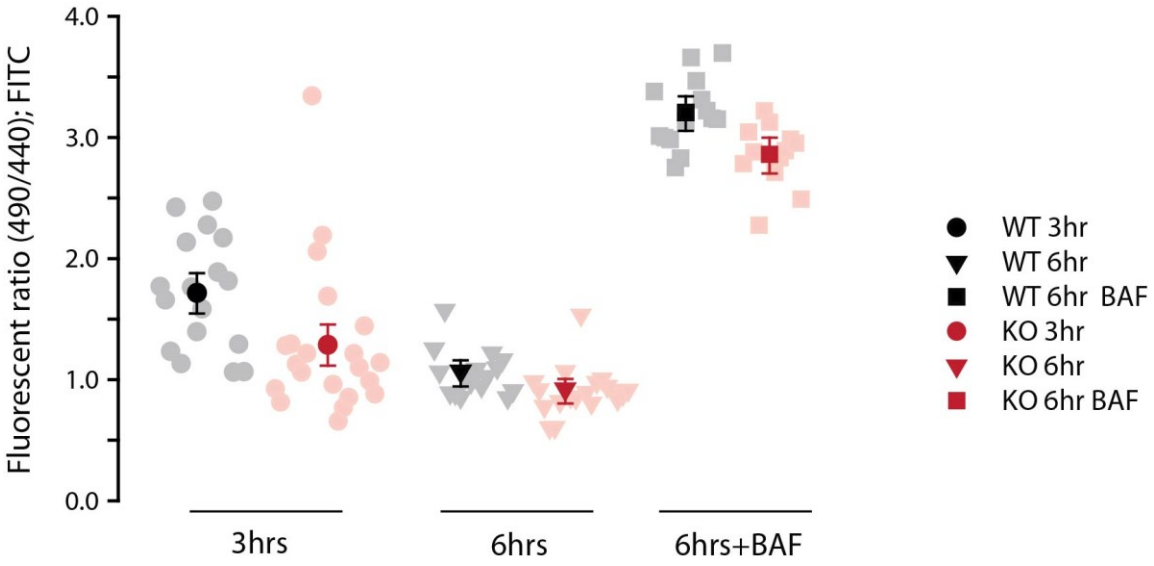

Figure 8: WT and KO hepatocytes imaged after short plating times have similar fluorescent ratios.
The night prior to hepatocyte isolation, WT and KO mice were injected with 10 mg of FITC-dextran. Hepatocytes were harvested, plated for either 3 or 6 hrs, and ratiometric imaging was performed to derive a fluorescent ratio (analyzed with Slicer2D) based on FITC fluorescence, similar to Fig 7. WT data are in black, KO are in red.

Evaluating the impact of various metabolic challenges on KO hepatocytic pH

A possible explanation for the discrepancy in ClC-7's lysosomal role of ClC-7 is that KO lysosomes can acidify under quiescent conditions (like cell culture) using alternative pathways, but are unable to maintain proper pH under 'stressful' conditions, where protons are rapidly utilized and must be swiftly replenished to maintain internal pH. If true, then exposing cells to a taxing condition may asymmetrically affect WT and KO lysosomal pH and reveal a role for ClC-7. To test this hypothesis, we stressed lysosomes using autophagy, a catabolic mechanism that degrades dysfunctional or unnecessary cellular components. Autophagy is primarily regulated by mTOR, the mechanistic target of rapamycin, an evolutionarily conserved serine/threonine kinase that regulates cell growth and division in response to energy levels, growth signals, and nutrients (particularly amino acids) (121, 122). mTOR is found in the mTORC1 complex, where it resides in its inactivated form on the lysosomal membrane. In response to starvation, mTORC1 disassociates from the membrane, triggering a cascade of signals resulting in changes in enzyme phosphorylation status, protein localization, and mRNA translation (123). By inducing a large influx of cytosolic material into lysosomes using autophagy induction, we can then assess whether they maintain steady state lysosomal pH. We employed both starvation and chemical means to induce autophagy and evaluated activation by monitoring the phosphorylated form of p70-S6K (S6K). Using an antibody specific for general S6K as a control, we found that both media starvation and chemical inhibitors of mTOR caused a drastic reduction in phosphorylated p70-S6K, indicating induction of autophagy (Fig 9A). We tested the effects of autophagy on hepatocyte lysosomal pH, finding that WT and KO began at a ratio of 2.17 and 2.19 +/-

0.1 and shifted to a higher ratio of 2.50 and 2.45 +/- 0.1, respectively. Thus, we see a general trend where starvation-induced autophagy shifted the pH of the lysosomes to a higher ratio (Fig 9B), but there was no difference in the effect on WT and KO hepatocytes, signifying that absence of ClC-7 does not appear to influence lysosomal pH during autophagy.

We investigated whether ClC-7 influences the rate at which lysosomes can establish their pH by comparing the reacidification of alkalized WT lysosomes to KO. After imaging hepatocytes preloaded with FITC-dextran, we alkalized lysosomes using the membrane permeable, weak base ammonium chloride (NH_4Cl) and imaged the same well again. After rinsing out the base, we imaged the cells an additional time to determine the extent of reacidification. Figure 10A shows an overlay of the ratios of WT and KO lysosomes when hepatocytes were treated with 5 mM NH_4Cl. Both cell types rapidly reestablish their internal pH within 2 minutes, a rate faster than the parameters of the experiment could measure. Figure 10B shows the pre-, during, and post-NH_4Cl treatment averages for multiple experiments. These data imply that ClC-7 is not required to reestablish proper lysosomal pH after alkalization within these time constraints (2-3 min).

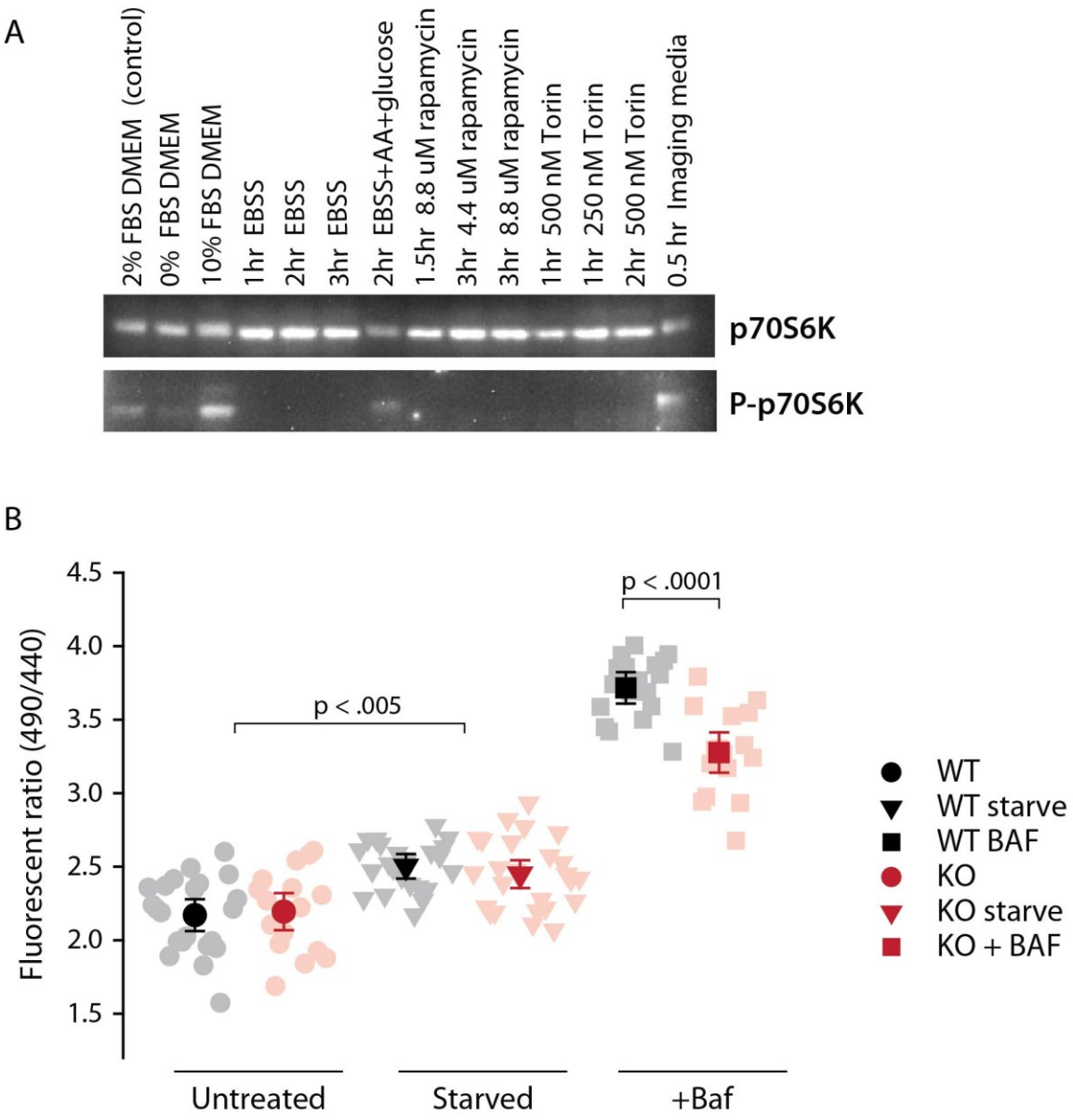

Figure 9: Buffer induced starvation of WT and KO hepatocytes causes an increase in the lysosomal ratio.

(A) KO hepatocyte lysates subjected to various autophagy-inducing conditions were immunoblotted against p70-S6K. Total p70-S6K expression serves as the control and autophagy induction is shown by the reduction/loss of phospho-p70-S6K. (B) WT (black) or KO (red) hepatocytes, containing lysosomal Oregon green 488, were imaged and processed as in Fig 7. Hepatocytes were incubated for 2 hrs in EBSS prior to imaging to induce autophagy. The untreated and starved hepatocytes were significantly different, as were the two bafilomycin samples, when compared using a student's t-test.

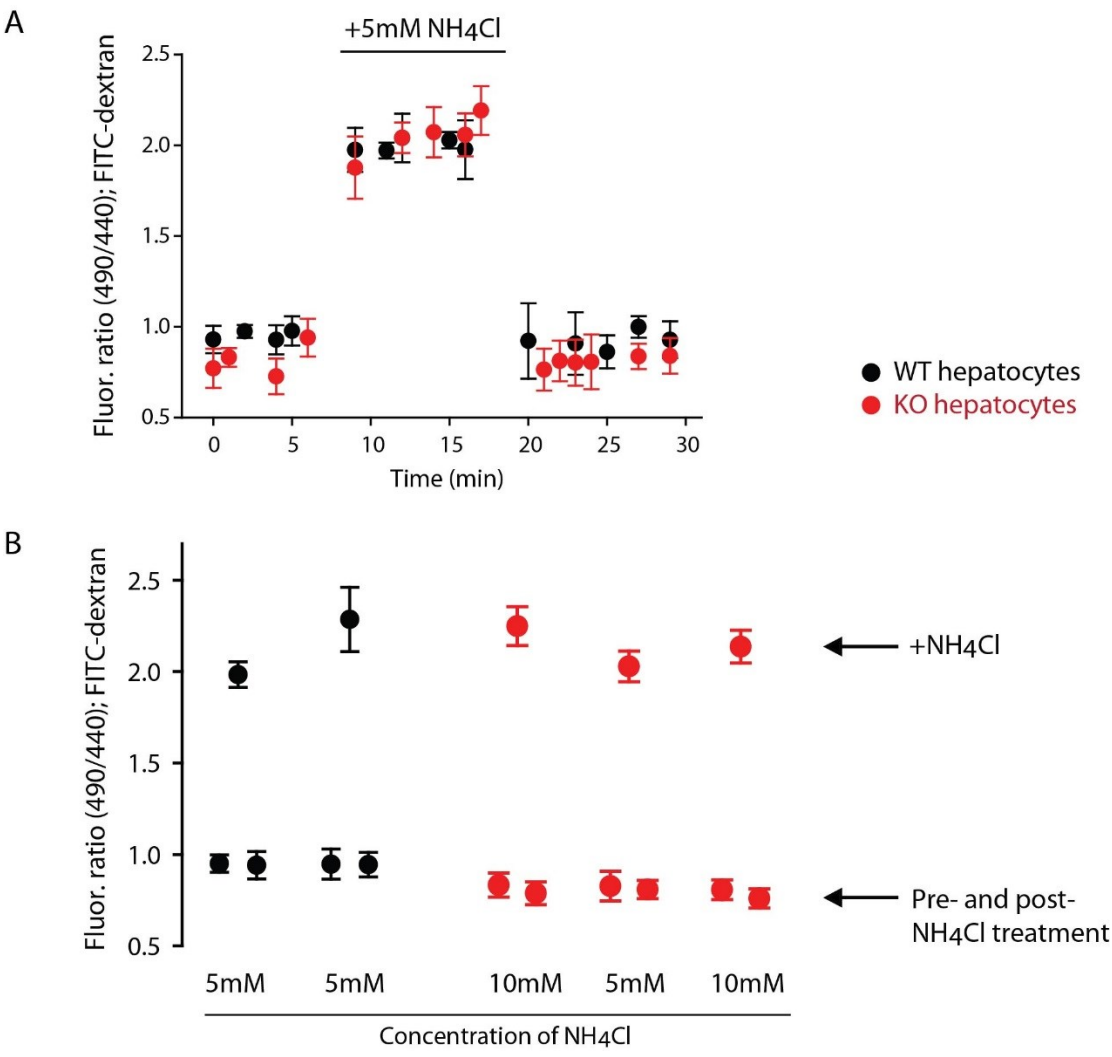

Figure 10: Alkalized WT and KO lysosomes rapidly reestablish lysosomal pH. WT (black) or KO (red) hepatocytes, pre-loaded with FITC-dextran (as in Fig. 8), were imaged prior to NH_4Cl addition, in the presence of either 5 or 10 mM NH_4Cl, and after NH_4Cl had been removed and the cells rinsed 3x. (A) An overlay of hepatocytic lysosomal ratios from WT and KO hepatocytes prior to, during, and after a 5 mM NH_4Cl incubation. Each point is the average lysosomal ratio and SEM of the cells imaged at the labeled time (2-4 cells/time point). (B) Cumulative results from several NH_4Cl experiments conducted in WT and KO hepatocytes. Within each group of experiments (>14 cells/condition), the first point is the average lysosomal ratio of all cells imaged prior to NH_4Cl addition, the center point is average ratio in the presence of NH_4Cl, and the last point is the average ratio once NH_4Cl was washed out. The concentration of NH_4Cl used to alkalize each group of hepatocytes is labeled at the bottom of the graph.

Discussion:

The role that counterions play in maintaining lysosomal pH is crucial, but poorly understood. Given that acidification in isolated lysosomes has been shown to be Cl^--dependent, and that the lysosomal transporter ClC-7 facilitates the movement of Cl^- into lysosomes, this protein has been suggested to mediate such counterion movement. However, the role of ClC-7 in lysosomal homeostasis has been highly debated, with some groups finding that ClC-7 influences organelle pH, while others observe no change (44, 94, 100, 102, 115). We bred a mouse containing a liver specific knockout of ClC-7 to investigate these claims, an approach that facilitates the testing of both isolated lysosomes and primary cells from the same tissue while avoiding the gravely ill phenotype accompanying the full body knockout. We reproduced the same conflicting results in our system; isolated lysosomes had no significant acidification upon loss of ClC-7, while primary KO hepatocyte lysosomes appeared to have the same pH as WT. We explored alternative roles ClC-7 may play on lysosomal pH maintenance during metabolically demanding conditions, finding that KO lysosomal pH matched WT pH regardless of the stress imposed on the hepatocytes.

After obtaining the liver specific knockout of ClC-7, we evaluated any phenotypical changes compared to WT littermates. The KO mice had a similar appearance and lifespan as WT, but both the liver and the whole-body weight of the KO mice were an average of 25-35% heavier than WT (Fig 1B-D) with visible excess fat lining the inside of the gut. While the reason for this is unknown, it is possible the removal of ClC-7 somehow affects the metabolic status the liver. Mice with a deletion in Tsc-1, a negative regulator of the mTORC1 complex that regulates metabolic growth in

response to nutrient levels and other signals, also have a similar increase in liver size (144). Additionally, mice expressing a non-conducting mutation in ClC-7 exhibit increased autophagy markers, although the cellular basis and subsequent effects of this increase are unknown (116). Therefore, ClC-7 may be involved in some sort of response to autophagy, although this mechanism is unclear.

We isolated lysosomes and examined the importance of external ions in facilitating acidification. In WT and KO lysosomes, no acidification was observed when lysosomes were incubated with bafilomycin, an inhibitor of the V-ATPase, indicating that the rotary protein was responsible for acidification (Fig 4). In WT, we observed acidification in the presence of KCl that was unchanged when K^+ was substituted with choline, indicating that anions act as counterions to facilitate proton pumping. Conversely, keeping K^+ in the system but replacing Cl^- with sulfate or gluconate greatly reduced acidification ~80% and ~50%, respectively. In KO lysosomes, ChCl, KCl, and Kgluconate all facilitated a similar level of acidification that only reached, at most, 40% of the level of WT in the presence of Cl^-. When evaluating the rate of acidification during the first 30sec, KO lysosomes experienced a similar level of acidification in all ionic buffers tested, indicating a baseline acidification that was not reliant on the presence of Cl^-. Thus, WT lysosomes depend primarily on Cl^- for acidification and KO lysosomes lose the ability to robustly acidify.

After evaluating acidification in isolated lysosomes, we harvested primary cells from the liver to directly compare acidification properties between organelles in live cells and those that have been isolated. Given that we observe no $^{36}Cl^-$ uptake in isolated KO lysosomes, we deduced that there must be little expression of functional, compensating

ClCs in the liver lysosomes, unlike a previously characterized ClC-7 KO model (Fig 3) (120). We evaluated the steady state lysosomal pH of hepatocytes, a cell type where the absence of ClC-7 has not been previously characterized, finding that ClC-7 KO hepatocyte lysosomes acidified to the same extent as WT when evaluated with the pH sensitive dye Oregon Green 488 (Fig 7C). These perplexing results do not match those observed in isolated lysosomes, but are similar to have previously published results from live cells (fibroblasts and macrophages) (47, 100, 102).

We explored the possibility that ClC-7 affects the rate of lysosomal acidification, hypothesizing that a cultured media environment may be less metabolically demanding than the liver. Since the 24-48 hrs of plating could allow KO lysosomes to gradually reach a pH value similar to the WT, we varied the length of time WT and KO hepatocytes were plated from 3 hrs to 72 hrs (Fig 3D, Fig 4). While the fluorescent ratio of both cells types was increased at the 3hr time point, corresponding to a more basic pH, we continually observed similar pH values for WT and KO lysosomes at all time points. Given the more basic pH of the early time points, it is difficult to detect a difference between WT and KO cells that are simultaneously adjusting to a culturing media environment. Therefore, no discernible impact of ClC-7 on lysosomal pH was detected when examining different lengths of plating time.

We investigated other situations where ClC-7 may be important for lysosomal pH. One possibility is that ClC-7 knockout lysosomes can acidify under quiescent conditions, like cell culture, but are unable to maintain the appropriate acidic pH in an environment where a high demand is placed on the lysosomes. We used starvation induced autophagy to direct a large influx of macromolecules to the lysosome, increasing the metabolic

demand placed on the organelle. While the lysosomal pH of both WT and KO become slightly more basic during autophagy, the shifts were similar in both cell types. Although this experiment did not reveal a role of ClC-7, expanding these studies by varying the length of starvation and induction method of autophagy may yield additional findings. Further, the pH lysosomes maintain during autophagy is not well characterized, but the only experiments of this nature were described from three different groups using various cells types and starvation induction methods. In contrast to our observation of more basic pH, they report that lysosomal pH was either unchanged or became more acidic (110, 121, 124), indicating that characterizing pH in various cell types could provide valuable in future work.

Finally, we examined if ClC-7 assists in lysosomal pH maintenance when pH is increased by an abnormal amount. We used the weak base NH_4Cl to alkalize lysosomes and assessed if the KO organelles could reacidify at the same rate, or to the same extent, as WT. We found that even after alkalization of lysosomes to a quite basic pH, both WT and KO rapidly reacidified to initial levels within two minutes (Fig 10A). Resolving acidification activity faster than two minutes was not possible due to technical difficulties, but monitoring lysosomal pH as NH_4Cl is being removed could yield different results. Yet, if ClC-7 is playing a role in reacidifying lysosomes, the cell can compensate for its loss effectively and reacidify quickly.

Although both WT and KO lysosomes alkalized to a similar pH value during treatment with NH_4Cl, treatment with bafilomycin, an inhibitor of the V-ATPase, yields a different result. We consistently observed that WT hepatocytes treated with bafilomycin become more alkalized than KO lysosomes (Figs 7C, 8, 9B). While the reason for this

differential shift is unknown, this effect may suggest something about the method cells use to compensate for a loss of ClC-7. Perhaps some sort of mechanism exists that clamps the lysosomal pH to a low value, resulting in a pH maintenance system that is less flexible/responsive, but keeps the lysosome at a sufficiently lower pH. If this system were to exist, that could explain the lower pH levels of hepatocyte KO lysosomes incubated with bafilomycin. Treating hepatocytes with nM concentrations of NH_4Cl that only slightly adjust the pH may expose a difference in the lysosomal state of WT and KO cells.

What is the role of ClC-7 in lysosomes? The Jentsch lab created mice containing an uncoupled ClC-7 (Unc), a point mutation that changes it from a transporter to a channel, and observed the animals have a normal coat color and more mild osteopetrosis, but still have severe lysosomal storage disease (LSD) symptoms like the KO (102). Assuming that the single point mutation does not substantially modify ClC-7's architecture, a reasonable assumption based on ClC crystal structures (3), these results argue that the transporter activity of the protein is essential and a Cl^- channel cannot substitute. The Jentsch lab has postulated that a specific concentration of Cl^- is required for proper lysosomal function, pointing out that two hydrolyses have been shown to display $[Cl^-]$-dependent activity (103-105, 107). Results from a mathematical model of lysosomal acidification indicate that a ClC-7 transporter generates higher lysosomal luminal $[Cl^-]$ than a channel (106) and, when combined with a recent paper arguing that high luminal Cl^- is necessary for proper lysosomal function, suggests an important function for the transporter function of ClC-7.

However, ClC-7 still seems to be important for acidification, at least in some situations. Experiments performed by Maxfield et al. indicate that ClC-7 is important for lysosomal acidification in primary microglia and its knockdown yields more basic lysosomes (115). This could indicate a cell type dependent response where either the requirement for ClC-7 or the ability to compensate for a lack of ClC-7 varies between tissues. Interestingly, the times when ClC-7 has been observed to modify lysosomal pH in live cells are when the protein was knocked down, not completely removed, as shown by the Maxfield lab, the Graves et al. paper, and additional unpublished observations using U2OS cells from our lab (S.B. Lioi and J.A. Mindell). Perhaps knocking down ClC-7 partially affects the cell but its complete removal somehow triggers an unknown compensatory mechanism.

ClC-7 is likely important in protein-protein interactions as well. The Jentsch lab generated a transport-deficient (Td) ClC-7 mouse, which expresses a ClC-7 with mutation that completely prevents ion conductance (116). The Td mouse had the same osteopetrosis and neurodegeneration defects as the KO, but had a normal coat color, indicating a signaling based role for ClC-7 (102, 116). A potential new role of ClC-7 in lysosomal physiology has been hinted at in a paper studying the effects of a drug that inhibits the endolysosomal lipid kinase PIKfyve (phosphatidylinositol-3-phosphate 5-kinase) (117). Gayle et al. found that the PIKfyve inhibitor Apilimod has selective cytotoxic activity in B-cell non-Hodgkin lymphoma (B-NHL) compared to normal cells (117), but a CRISPR knockout of ClC-7 or Ostm1 prevented the phenotypical formation of cytosolic vacuoles and abolished the killing effect. Although the signaling pathway

and mechanism by which PIKfyve interacts with these proteins is unknown, it hints at a potential role for ClC-7 in kinase signaling and/or protein-protein interactions.

CHAPTER 4:

A de novo *CLCN7* mutation decreases intralysosomal pH and leads to a novel disorder of cutaneous albinism, lysosomal storage and neurodegeneration

Raluca-Elena Nicoli[1]*, Mary R. Weston[2]*, Mary Hackbarth[1]*, Alissa Becerril[2], Austin Larson[4], Wadih Zein[3], Peter R. Baker[4], John Douglas Burke[5], Heidi Dorward[5], Mariska Davids[1], Yan Huang[1], David R. Adams[1,6], Patricia Zerfas[7], Dong Chen[8], Thomas C. Markello[1,6], Camilo Toro[1,6], Gene Elliott[9], Lisa Garett[9], Wei Zheng[10], Wei Student[10], Cynthia J. Tifft[1,6], William A. Gahl[1,5,6], Debra Day-Salvatore[11], Joseph A. Mindell[2], May Christine V. Malicdan[1,6]

1. NIH Undiagnosed Diseases Program, Common Fund, Office of the Director, NIH and National Human Genome Research Institute, NIH, Bethesda, Maryland, USA
2. Membrane Transport Biophysics Section, National Institute of Neurological Disorders and Stroke/NIH, Bethesda, MD, USA
3. Ophthalmic Clinical Genetics Section, National Eye Institute, National Institutes of Health, Bethesda, Maryland, USA
4. Department of Pediatrics, Section of Genetics, University of Colorado School of Medicine, Aurora, CO
5. Human Biochemical Genetics Section, National Human Genome Research Institute, National Institutes of Health, Bethesda, MD
6. Office of the Clinical Director, National Human Genome Research Institute/NIH, Bethesda, Maryland, USA
7. Embryonic Stem Cell and Transgenic Mouse Core, National Human Genome Research Institute, NIH, Bethesda, Maryland USA
8. Division of Hemapathology, Mayo Clinic, Rochester, Minnesota USA
9. Diagnostic and Research Services Branch, Office of Research Services, National Institutes of Health, Bethesda, Maryland, USA
10. National Center for Translational Science, National Institutes of Health, Bethesda, Maryland, USA
11. Department of Medical Genetics and Genomic Medicine, Saint Peter's University Hospital, New Brunswick, New Jersey, USA

*Contributed equally
**Contributed equally

ABSTRACT

Lysosomes, the most acidic organelles in the endocytic pathway, are responsible for macromolecule degradation. The acidic pH is created and maintained by the V-ATPase, a rotary pump that uses ATP hydrolysis to pump protons into the organelle lumen. Proton pumping is electrogenic and movement of a neutralizing current (known as a counterion) must occur simultaneously to allow proper acidification. ClC-7, a $2Cl^-/H^+$ antiporter located in the lysosomal membrane, is the primary pathway of Cl^- into the organelle and is thought to provide an anion as a neutralizing counterion to assist in acidification, although this role has been highly debated. In this paper, we present two patients with an identical pathogenic *de novo* variant in *CLCN7*, a single missense mutation of Y715C, as revealed by whole exome and genome sequencing. The patients display hypopigmentation, a delay in gross and fine motor skills, abnormal liver/spleen/kidneys, and failure to thrive. However, unlike every other reported ClC-7 mutation in humans, they display no osteopetrosis. Fibroblasts isolated from both patients contain large vacuoles scattered through the cytoplasm, but they do not stain for lysosomal markers. However, patients possess a vast increase in the number of lysosomal-like compartments that do stain for Lamp1. Lysosomal pH in cultured patient fibroblasts are more acidic than the neonatal controls and heterologous expression of the mutant ClC-7 in *Xenopus* oocytes revealed substantial increases in transport activity. These results suggest a gain-of-function of this Cl^-/H^+ antiporter, causing dysregulation of the acidification of lysosomes and lysosome-related organelles.

INTRODUCTION

Lysosomes are the terminal organelles of the endocytic pathway that are responsible for macromolecule degradation. They rely on a precise, acidic luminal pH for optimal function, including enzymatic activity and the coupled transport of intracellular catabolites. Defects in lysosomal channels or transporters can lead to a variety of physiological disruptions, including neurodegeneration and lysosomal storage disease (99, 100, 125, 126). Lysosomal acidification is maintained by various ion channels and transporters that control movement of H^+, Cl^-, and possibly other ions across the lysosomal membrane (26, 27, 44, 145). The rotary pump V-ATPase is responsible for the active accumulation of H^+ to maintain acidic pH, but luminal acidification also requires a neutralizing current, referred to as the counterion pathway (4, 26, 91). This may be in the form of a cation exiting the lysosome or an anion entering the lumen.

CLCN7, encoding ClC-7, is a member of the ClC gene family of Cl^- channels and Cl^-/H^+ exchangers (146, 147). Four of the nine mammalian ClC proteins are plasma membrane Cl^- channels (ClC-1, -2, -K_a, -K_b) (148-151), while the rest are antiporters (ClC-3, -4, -5, -6, -7), all of which are localized to various organelles along the endolysosomal pathway (58, 62, 99, 120, 147, 152, 153). Specifically, ClC-7 is found in late endosomes and lysosomes, where it provides the primary permeation pathway for Cl^- through the lysosomal membrane (44). Inactivating mutations in *CLCN7* and its β-subunit Ostm1 cause both autosomal dominant and recessive forms of osteopetrosis and neurodegeneration (47, 126). In humans, Albers-Schonberg disease, or autosomal dominant osteopetrosis type II, is the most common form of osteopetrosis caused by mutations in ClC-7 (127). Of the more than 40 different reported missense, disease-causing mutations in ClC-7, occurring in

various locations throughout the protein, all have resulted in osteopetrosis (to varying degrees of severity) (128) and no gain-of-function ClC-7 mutations have been described.

Here we describe two patients who presented with cutaneous albinism, global developmental delay, hepatosplenomegaly, and failure to thrive, but without osteopetrosis; one child also had gut dysmotility leading to total parenteral nutrition dependence. Electron microscopy of the gut, liver and skin tissue revealed accumulation of autophagic vacuoles and abnormal lysosomal morphology. Whole exome and genome sequencing revealed an identical pathogenic *de novo* variant in *CLCN7* in both patients. Similar phenotypical results are seen in a CRISPR mouse containing the same mutation. Measurement of lysosomal pH revealed increased acidity *in vivo* in fibroblasts cultured from the both patients compared to a neonatal control. Heterologous expression of the mutant ClC-7 in *Xenopus* oocytes revealed substantial increases in transport activity, suggesting a gain-of-function of this chloride/proton antiporter, causing rampant dysregulation of the acidification of lysosomes and lysosome-related organelles.

MATERIALS AND METHODS

Patients

Proband 1 was enrolled in the NIH Undiagnosed Diseases Program (154, 155) and admitted to the National Institutes of Health Clinical Center (NIH-CC) under clinical protocol 15-HG-0130, "Clinical and Genetic Evaluation of Patients with Undiagnosed Disorders Through the Undiagnosed Diseases Network", approved by the National Human Genome Research Institute (NHGRI) Institutional Review Board (IRB). Written informed consent

was obtained from the parents. Proband 2 was received and treated by Dr. Debra Day-Salvatore.

Genetic Analysis

For Proband 1 and her family, genomic DNA was extracted from whole blood using the Gentra Puregene Blood Kit (Qiagen, Valencia, CA). Whole Genome Sequencing was performed using the Illumina HiSeq X sequencing platform and aligned to human reference GRCh37. Variants were filtered based on allele frequencies in the UDP (156-158), cohort (<0.06) Sanger dideoxy sequencing was performed by Macrogen (Rockville, MD, USA); the sequences were analyzed with Sequencher v.5.0.1 (Gene Codesm Ann Arbor, MI, USA).

Tissue and Cell Studies

Standard procedures were used for light and electron microscopy. Primary dermal fibroblasts were cultured from forearm skin-punch biopsies as described (159). Melanocytes were derived from the same skin biopsy and processed as described in Supplemental Methods. Control fibroblasts and melanocytes were purchased from ATCC (PCS201-012) and Corriel (GM23972A). Fibroblasts from a patient with NPC were obtained from Dr. Forbes Porter (NIH) served as a positive control for acidification studies.

For Lysotracker studies, cultured fibroblasts were plated at 6,000 cells/well into 96-well cell-culture microplates [GBO #655090] and incubated with 83.3 nM LysoTracker Red DND-99 (Thermo Fisher Scientific, L7528) at 37°C for 1 hour. They were imaged on an

InCell Analyzer 2200, using the Dapi, Texas Red, and Brightfield channels, with intensity of LysoTracker per cell used as an outcome measure. Primary patient fibroblasts were compared to positive-staining NPC-25 fibroblasts and 3 negative control cell lines (Coriel GM23972A; ATCC PCS201-012; ATCC neonatal WT, etc). Immunofluorescent studies employed the following primary antibodies: Lamp1 (H4A3, DSHB), Lamp2 (DSHB, H4B4), and CD63 (DSHB, H5C6) for lysosomes. Alexa Fluors 488 and 594 (donkey-anti-mouse, ThermoFisher Scientific) were used as secondary antibodies. Hoescht 33342 (ThermoFisher Scientific) was used to visualize the nucleus.

To measure lysosomal pH, 50,000 cells were incubated with 3.5 mg/mL Oregon green 488 10,000 MW dextran (ThermoFisher Scientific D7170) overnight on chambered coverglass slides (Nunc Lab-Tek II; 155382PK) Upon dextran removal, cells were rinsed 3x with PBS, and chased in dye-free media for 4 hours. Ratiometric, fluorescent images were collected using a Ziess Observer Z.1 widefield microscope and a CCD camera (Photometrics CoolSNAP HQ2). Excitation bandpass filters 440/40 and 485/20 were used to excite the Oregon Green 488 fluorophore, and a 506nm dichroic filter with a bandpass filter 534/42 was used to collect the emission at both excitation wavelengths. Cells were imaged in medium 2 (in mM: 150 NaCl, 5 KCl, 1 $CaCl_2$, 1 $MgCl_2$, 20 hepes, 10 glucose, 30 sucrose; pH 7.4 with HCl) (142). Greater than 15 cells/experimental condition were imaged. An Oregon Green calibration curve was determined by incubating cells with buffers titrated at half pH unit increments, from pH 4.0-7.0 +/- 0.01, and 10μM each of Monensin and Nigericin (Sigma M5273, N7143). The calibration buffers contained imaging media and a designated buffer (for pH 4.0-5.5, 50mM Tris-

maleate; for pH 6.0, 25mM Na_2HPO_4 and 25mM Tris-maleate; for pH 6.5-7.0, 50mM Tris-maleate). Cells were incubated for five minutes prior to imaging to allow for pH equilibration across all membranes. The well was rinsed thoroughly after each pH measurement before the next pH buffer was added. Images were analyzed using the Matlab-based program Slicer2D, created for lysosomal analysis by the CIT group under the direction of Calvin Johnson and Huey Cheung at NIH (details in Chapter 3). To convert ratio to pH, lysosomes from each pH value were averaged and data fit to a four-parameter sigmoidal equation. The pH values for individual cells were interpolated using the sigmodal equation values. For chloroquine treatments, the designated concentration of drug (Sigma C6628) was incubated with the cells overnight.

Electrophysiology analysis

Expression constructs

c-Myc-tagged CLC-7 and c-myc-tagged OSTM1 constructs (RC203450 and RC209871, respectively, from ORIGENE) were subcloned into pGEM-HE2 vector for heterologous expression in *Xenopus laevis* oocytes. Y715C point mutation was made using the Quikchange II site directed mutagenesis kit (Agilent Technologies). All constructs were confirmed by sequencing the complete ORF.

Voltage-clamp Xenopus laevis oocytes

Xenopus laevis oocytes were injected with cRNA (23 ng for myc-tagged ClC-7 constructs and additional 23 ng for myc-tagged Ostm1) which was transcribed with the mMessage Machine kit (Ambion) from pGEM HE-2 vector. After a 5-day incubation at 17°C,

currents were measured using standard two-electrode voltage techniques (OC-725C; Warner Instruments) in ND96 (96 mM NaCl, 2 mM KCl, 5 mM HEPES, 1 mM MgCl2, and 1.8 mM CaCl2 at pH 7.6 with NaOH). Microelectrode resistances were 0.1–1 MΩ when filled with 3M KCl. All experiments were performed at room temperature (~22°C).

Detection of Surface Protein

Surface expression of protein was determined 6 days after cRNA injection by surface using the procedure of Silberberg et al (2005) with slight modifications (160). 5 d after injection of cRNA, oocytes were incubated for 30 min at room temperature with Sulfo-NHS-LC-Biotin (0.5 mg/ml; Pierce Chemical Co.) in ND96 buffer containing (in mM) 96 NaCl, 2 KCl, 1.8 $CaCl_2$, 1 $MgCl_2$, 5 HEPES, pH 7.6. After washing six times in ND96 buffer, oocytes were homogenized in 400 µl of buffer H containing (in mM) 100 NaCl, 20 Tris.Cl, pH 7.4, 1% Triton X-100, 5 µl/ml protease inhibitor cocktail (Roche). Homogenization and all subsequent steps were performed at 4°C. After centrifugation at 16,000 *g* for 2 min, a 20-µl aliquot of the supernatant (total protein) was mixed with equal volume of 2× LDS sample buffer plus reducing agent: 50% 4× LDS sample buffer (Invitrogen), 20% 2-mercaptoethanol, 100 mM DTT. The remaining supernatant was diluted 1:1 with buffer H plus 60 µl of nuetravidin agarose beads (Thermo Fisher) and then tumbled gently overnight at 4°C. The nuetravidin agarose beads were washed six times with buffer H with a 2-min centrifugation (16,000 *g*) between each wash. At the end of the final wash, 30 µl of 1× LDS sample buffer plus reducing agent was added to the beads and samples were heated at 95°C for 10 min. Following a 2-min centrifugation (16,000 *g*), the supernatant (surface protein) and total protein (collected earlier) were

separated in a 10% Nu-Page Bis-Tris gel (Invitrogen) using a Nupage MOPS SDS Running Buffer (Invitrogen). PageRuler Plus (Thermo Fisher) was used as the protein molecular weight marker. Protein in the gel was transferred to PVDF membrane (Life Technologies) where the NuPAGE transfer buffer (Life Technologies) with 20% methanol. The nitrocellulose membrane was probed with mouse anti-myc antibody (Santa Cruz Biotechnology) diluted 1:1000 in TBST containing (in mM) 150 NaCl, 25 mM Tris-base, 0.1% Tween-20, 5% milk (Carnation), and CLC-7 expression was detected using ECL Super Signal West Femto Western blotting detection reagents (Thermo Fisher). The mutant *Shaker* potassium channels was used as a control lacked residues 6–46 and contained c-myc epitopes inserted at both termini.

RESULTS

Clinical Characteristics

Proband 1 (Fig. 1A) was a 22-month-old white female with intrauterine growth retardation born at 36 weeks' gestation having white hair, eyebrows, and eyelashes but pigmented irides. At 2 months, total parenteral nutrition was instituted for poor weight gain, vomiting, and diarrhea, and hepatosplenomegaly was noted. Skeletal survey (9 months) showed right hip dislocation and segmentation abnormalities of T1 and T2 (not shown).

On admissions to the NIH Clinical Center at 18 and 22 months, weight, length, and head circumference were at the third percentile for age. The face was nondysmorphic (Fg. 1A). There were delays in gross and fine motor skills with poor head control, but social interactions were normal. Muscle mass was decreased in the lower extremities, with limited range of motion in the ankles, diffuse hypermobility of the upper extremities, and generalized hypotonia. Visual acuity was 1.3 cy/cm (Teller Acuity Cards) or 20/600 (Snellen), with an optokinetic nystagmus response; fixation was central, steady, and maintained. The eyelashes displayed poliosis and the pupils were responsive to light. Ocular motility, visual pursuit, and saccades were normal. The retinas had no cherry red spots, but an electroretinogram showed scotopic amplitudes 40% of normal and photopic response amplitudes 50% of normal. Auditory steady state response thresholds predicted a profound hearing loss at 2000 Hz and 4000 Hz in the right ear; the neurodiagnostic auditory brain response was effectively absent.

Ultrasound showed enlarged liver and spleen, increased liver echogenicity compatible with steatosis or glycogen storage, and poor cortical-medullary differentiation

in the kidneys (Fig. 1C). MRI showed delayed myelination similar to that at 5 months of age, a thin posterior corpus callosum, hyperintensity of the brainstem, particularly in the subthalamic nuclei, and atrophy of the cerebellar vermis and hemispheres (Fig. 1E). Skull, spine, long bone, hands and feet radiographs were normal, with no sign of osteopetrosis. Hemoglobin was 7.4 g/dL (normal, 10.2-12.7); serum sodium was 146 mmol/L (normal, 136-145), serum chloride was 114 mmol/L (normal, 98-107), and there was generalized aminoaciduria, but serum liver function tests were normal. Electron microscopy of liver, duodenal and skin biopsies showed cytoplasmic inclusions containing amorphous floccular material suggestive of storage (Fig. 1G).

Proband 2 (Fig. 1B) was a 14-month-old Ghanaian male born whose prenatal ultrasound revealed shortened long bones, prefrontal edema, and polyhydramnios. At birth after 37 weeks' gestation, weight and length were appropriate, skin and hair were hypopigmented, and ankyloglossia was present. Ophthalmological exam at 6 weeks was unremarkable. At 4 months, weight and length had fallen below the second percentile, with head circumference at the fifth to tenth percentile. Development was appropriate for age.

At 8 months, the anterior fontanelle measured 2x2 cm, and there was complete head lag. Posterior auricular papules, epicanthal folds, hypertelorism, thickened gingivae, short sternum, and single palmar creases were noted. The skin was decorated with nevi and café-au-lait macules. The liver was echogenic, suggesting steatosis. A polymorphic pericentric inversion was present on chromosome 9 (p11q13). SNP microarray and extensive genetic and biochemical studies were normal. Urine oligosaccharide analysis suggested a mucopolysaccharidosis or mucolipidosis, but urine free sialic acid and glycosaminoglycans were normal.

After 8 months of age, the infant had poor growth, diarrhea with hypoalbuminemia, fevers, dehydration, and metabolic acidosis; at 11 months, a gastrostomy tube was placed. At 12 months, the kidneys had doubled in size and showed poor corticomedullary differentiation (Fig. 1D); hepatomegaly was present but not splenomegaly. There was no radiographic evidence of dysostosis multiplex or osteopetrosis on skeletal survey. Brain MRI showed delayed myelination, prominent subarachnoid spaces and abnormal signal intensity in the cerebral peduncles, pons and brainstem, but no leukodystrophy (Fig. 1F). A renal biopsy revealed marked distention of the medullary interstitium by lipid-laden macrophages; electron microscopy showed lipid inclusions in mesangial cells, medial myocytes, and some tubular epithelial cells, with rare inclusions in podocytes and endothelial cells of small arteries (Fig. 1H). At 13 months, the boy had tachycardia, sustained clonus, and myoclonic jerks involving the lower extremities.

WES identifies a de novo mutation in *CLCN7*.

Whole exome sequencing (WES) of both patient cases identified a *de novo* variant in *CLCN7*, a single point mutation in one allele that mutates Tyr715 to cysteine (NM_001287.5: c.2144A>G, p.Tyr715Cys; RCV000412760.1) (Fig 2A). Dideoxynucelotide sequencing of whole blood DNA from the parents and unaffected sibling of Proband 1 confirmed the *de novo* pattern of variance (Fig. 2B). First pass analysis of the whole genome sequencing using Carpe Novo software revealed no additional clinically relevant variants. The heterozygous variant is located in a highly conserved amino acid portion within the C-terminal, cytoplasmic CBS domain and is distinct from any previously documented mutations (Fig. 2A and C). The Y715C

mutation is predicted to be pathogenic by various *in silico* analyses. Further confirming the sequencing results, a *CLCN7* Y713C heterozygous knock-in CRISPR mouse also manifests splenomegaly and hair hypopigmentation, but does not appear to have osteopetrosis (data not shown). Given that all previously known missense or loss of function mutations of ClC-7 lead to some form of osteopetrosis, which is absent from both patients, we hypothesized that the pathogenic effects of the heterozygous Y715C mutation might result from a gain-of-function mutation in the protein.

Figure 1: Clinical and histological features of Proband 1 and Proband 2
Figure from the UDP clinical group
(A) Proband 1 has cutaneous albinism with normally pigmented irides and no facial dysmorphisms. (B) Proband 2 has hypopigmentation compared to his African parents. (C) Abdominal ultrasound of the left (i) and right (ii) kidney of Proband 1, enlarged to over 10 cm in length. (D) Abdominal ultrasound the left (i) and right (ii) kidney of Proband 2, enlarged to over 10 cm in length. (E), (F) Brain MRIs of Proband 1 at 20 months (E) and Proband 2 (F) at 12 months. Both MRIs show delayed myelination, a thin posterior corpus callosum, hyperintensity of the subthalamic nuclei, and cerebellar atrophy. (G) Transmission electron micrographs showing abnormal cytoplasmic inclusions (arrowhead), sometimes containing amorphous floccular storage material (double arrowhead), in the macrophages of the liver and histiocytes of the duodenum. Similar cytoplasmic inclusions were found in the skin of Proband 1. Scale bar = 1μm. (H) Transmission electron micrograph showing storage in the kidney of Proband 2. There are numerous interstitial macrophages filled with abundant cytoplasmic inclusions (arrowhead). Scale bar = 5μm.

Figure 1

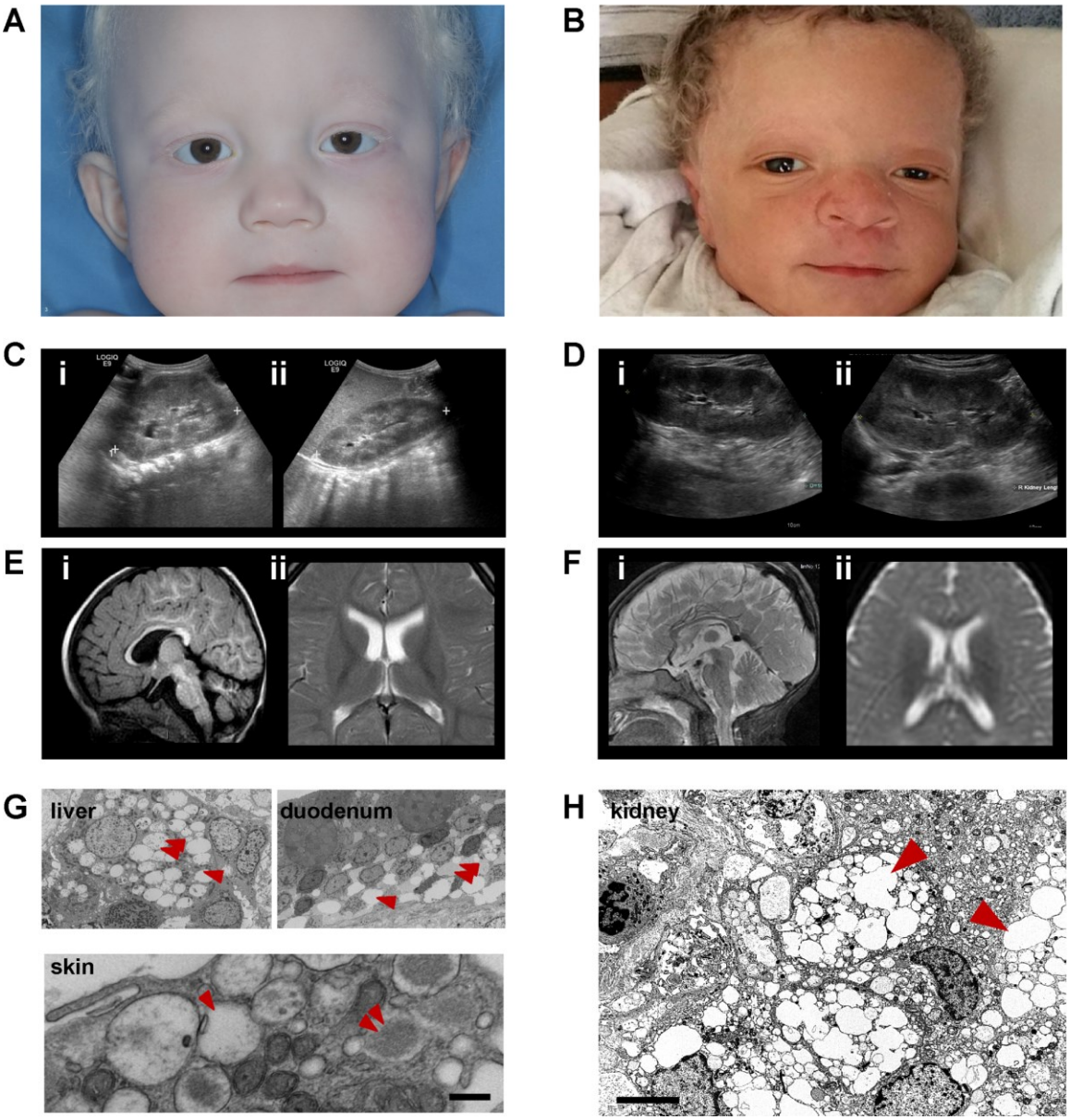

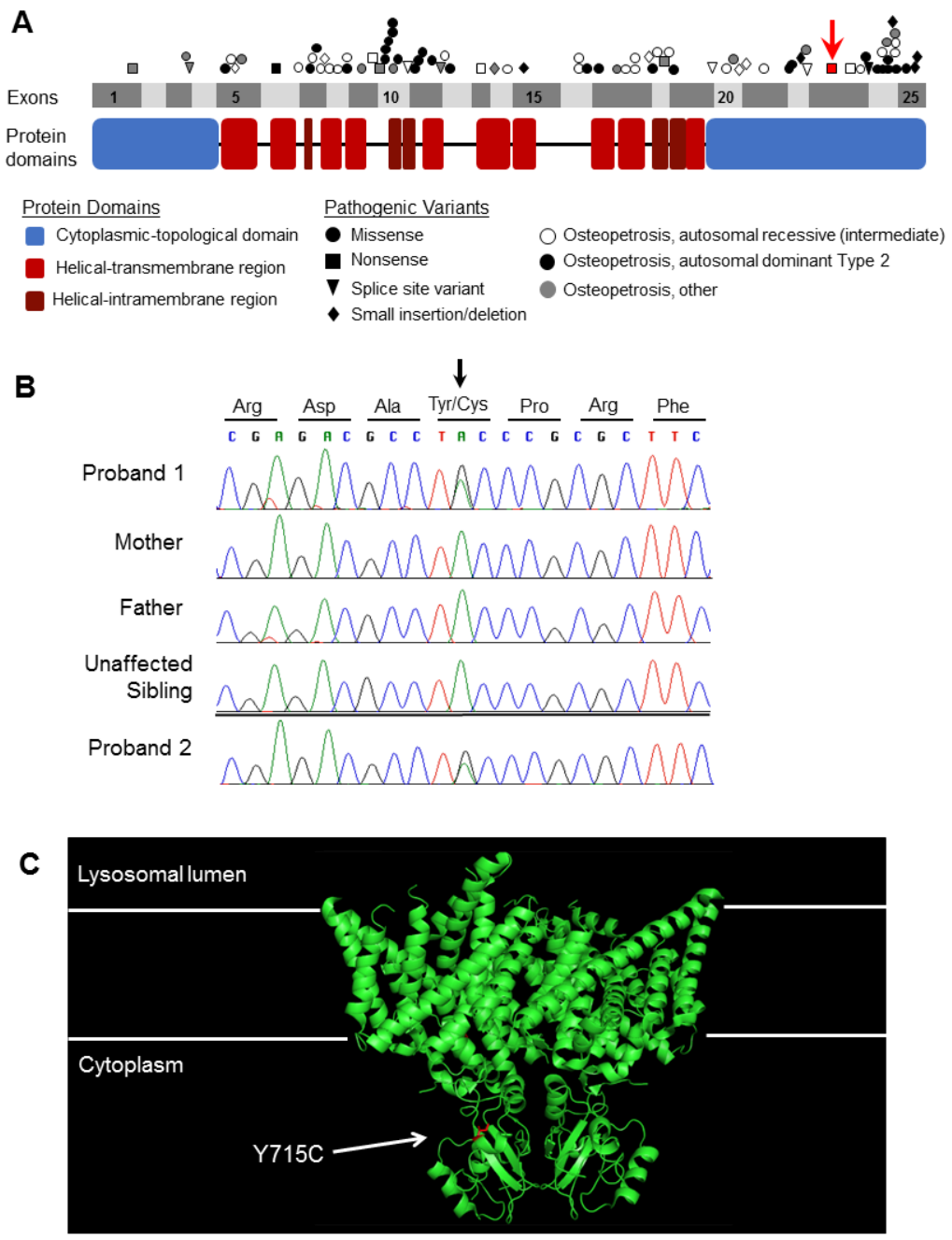

Figure 2: *de novo* mutation in *CLCN7* located in the CBS domain
Figure from the NIH sequencing group (A-B) and the Mindell lab (C)
(A) Figure shows the exons and protein domains of *ClCN7* with reside 715 highlighted below the red arrow and markings indicating pathogenic variants. (B) Sequence alignment of the small region flanking amino acid 715 comparing Proband 1 to her parents and unaffected sibling. Proband 2 is shown below with the same mutation as Proband 1. (C) Model of the eukaryotic cmClC homodimer with the crystal structure of ClC-7 with the mutated Y715C, located in the CBS domain of the protein, shown in red.

Patient fibroblasts contain vacuoles surrounded by lysosomal markers

Tissue biopsies from patients show lysosomal storage disease characterized by numerous large 'vacuoles'. Similarly, fibroblasts cultured from both patients contain a striking number of vacuoles scattered throughout the cytoplasm (Fig. 3A). The vacuoles are varied in size; some cells contain a multitude of tiny vacuoles, others contain a couple large vacuoles that fill most the cytoplasm, and other cells contain a mixture of vacuole sizes (Fig 3B). Additionally, some patient fibroblasts appear substantially larger than controls and they typically have tiny vacuoles. Electron micrographs show that the vacuoles appeared to be empty (data not shown) and we have not been able to determine their contents. The vacuoles did not stain for the lysosomal membrane marker Lamp1 (Fig 3C), nor for early or late endosomal markers (EEA1, Rab7) (data not shown). However, the vacuoles were surrounded by puncta of LAMP-1 staining, suggesting the presence of intact lysosomes. Similarly, Lysotracker red, a membrane permeable dye that accumulates in acidic compartments, appeared to primarily stain the areas around the vacuoles (Fig 5A).

Figure 3: Fibroblasts isolated from Proband 1 and Proband 2 have cytoplasms filled with vacuoles
Raluca-Elena Nicoli (A and C) and Mary Weston (B) contributed to this figure
(A) Brightfield images of Proband 1 and Proband 2 fibroblasts with extreme vacuolization. (B) Brightfield images of Proband 1 showing the variation in vacuole size in individual cells. (i) shows large vacuoles (white arrow) and tiny vacuoles (yellow arrow). (ii-iv) show examples of a small, a mixture of, and an extremely large vacuole, respectively. (C) Proband 1 and Proband 2 fibroblasts fixed and stained for Lamp1. The nucleus is showed in blue.

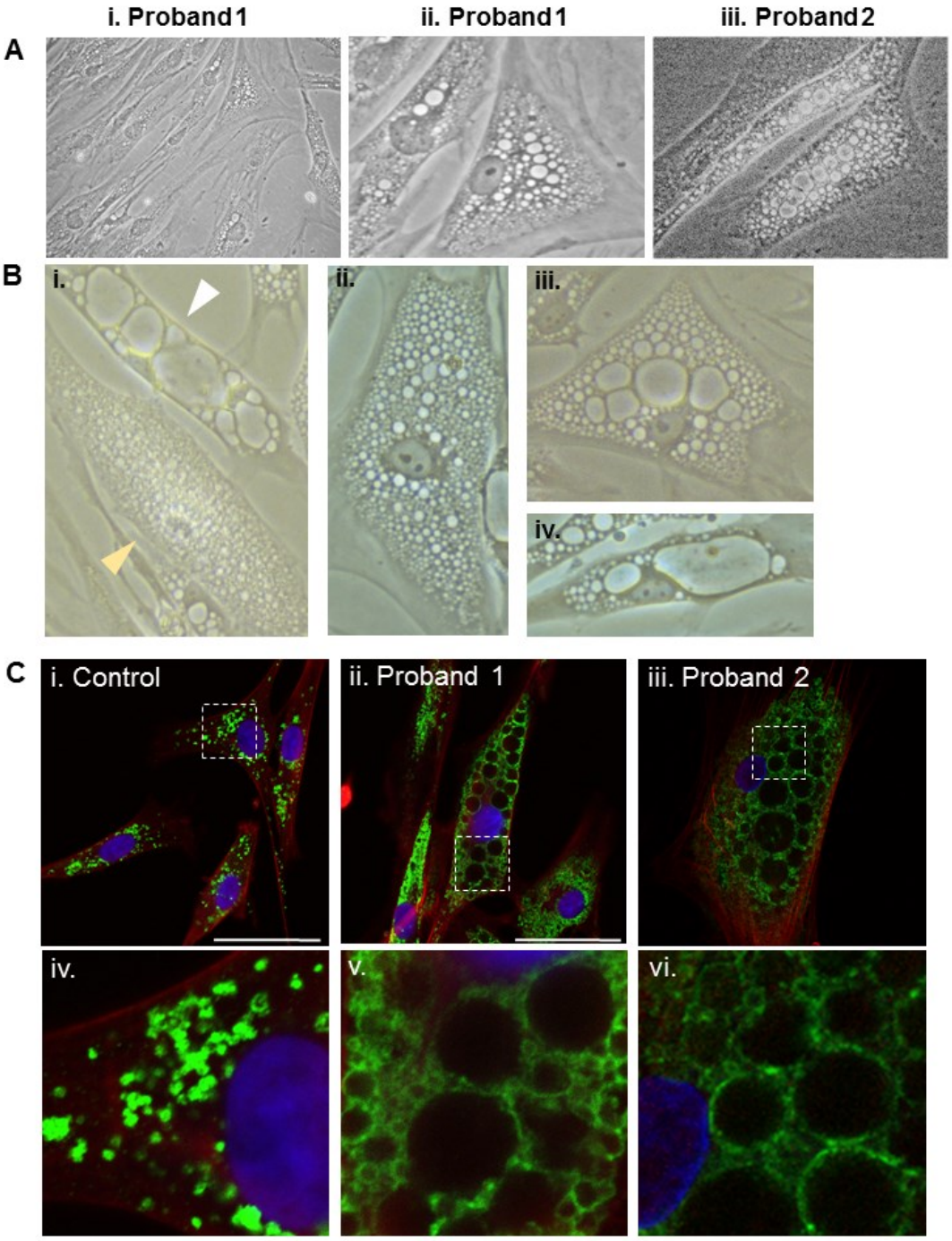
i. Proband 1
ii. Proband 1
iii. Proband 2
A
B
i.
ii.
iii.
iv.
C
i. Control
ii. Proband 1
iii. Proband 2
iv.
v.
vi.

Electrophysiological characterization of the T715C ClC-7 mutant

To assess if the disease-causing T715C mutation changed the transporting properties of the protein, we expressed human ClC-7 (along with its β-subunit Ostm1) with or without the T715C mutation in *Xenopus* oocytes after introducing additional mutations that redirect the transporter to the plasma membrane (128). Oocytes expressing WT ClC-7 had strongly outwardly rectifying currents that are activated ~+20 mV, similar to published results (128) (Fig 4A-B). The T715C mutant was also outwardly rectifying, but was activated closer to 0 mV and had a substantial (~3-fold) increase in the outward currents compared to WT (Fig. 4A-B), a highly reproducible result when measured on 3 separate batches of oocytes (Fig 4D). Surface biotinylation experiments indicated that similar amounts of WT and mutant protein are trafficked to the plasma membrane (Figure 4C), verifying that the increase in mutant current is not from a different levels of protein expression. We obtained the time constants of activation and deactivation from 0-80 mV, the potentials at which the protein is activated, by obtaining single-exponential fits of the rectifying current 15 ms after the voltage step to the respective voltage. These values, independent of the protein expression, fit to a single exponential and show that the mutant currents have a faster activation than WT and display larger and more slowly decaying tail currents at positive voltages (Figure 4E-D). Changing the external Cl^- concentration revealed similar shifts in reversal potential for WT and T715C currents (data not shown), suggesting that the 2:1 Cl-/H+ stoichiometry of the WT transporter is unchanged in the mutant protein (128). If ClC-7 is an important component of the lysosomal acidification mechanism, then the observed increase in Cl^- current in the mutant transporter could facilitate increased H^+ transport into lysosomes via the lysosomal V-type ATPase proton pump.

Figure 4: Electrophysiology of *ClCN7* Y715C Mutant
Alissa Becerril contributed this data.
(A) I-V plot of the mean ± SEM of currents from one experiment reached after 2s plotted as a function of voltage (Y715C, n=6; WT, n=8; uninjected, n=3 oocytes from 1 batch).
(B) Western blots of surface and total hClC-7 and Y715C expression. Total lysate (i) and neutravidin bead (ii) pulldown of +biotin/-biotin myc-tagged hCLC-7 WT, Y715C, and non-conducting Shaker K^+ channel (positive control). Each lane in (i) contains 30 μL of total cell lysate obtained from 20 oocytes either pretreated with biotin or not. Each lane in (ii) contains neutravidin bead pulldown of (i) pretreated with biotin (+) or not (-). Molecular weight markers are in kDa. Oocytes were injected at the same time as those from (A).
(C) Time constants of activation (τ) of hCLC-7 WT (blue) and Y715C (red) were obtained by single-exponential fits to the rectifying current from 15 ms after a voltage step to respective voltages. Shown are the mean ± SEM. Data obtained from the same oocytes as (A).
(D) Time constants of deactivation (τ) of hCLC-7 WT (blue) and Y715C (red) were obtained from single-exponentials fits to tail currents 15 ms after a voltage step to -80 mV, following a 2s pulse to respective voltages (mean ± SEM. Same oocytes as (A)).
(E) I-V plot of the mean ± SEM of currents from three separate experiments.

Figure 4: Electrophysiology of the *CLCN7* Y715C mutant

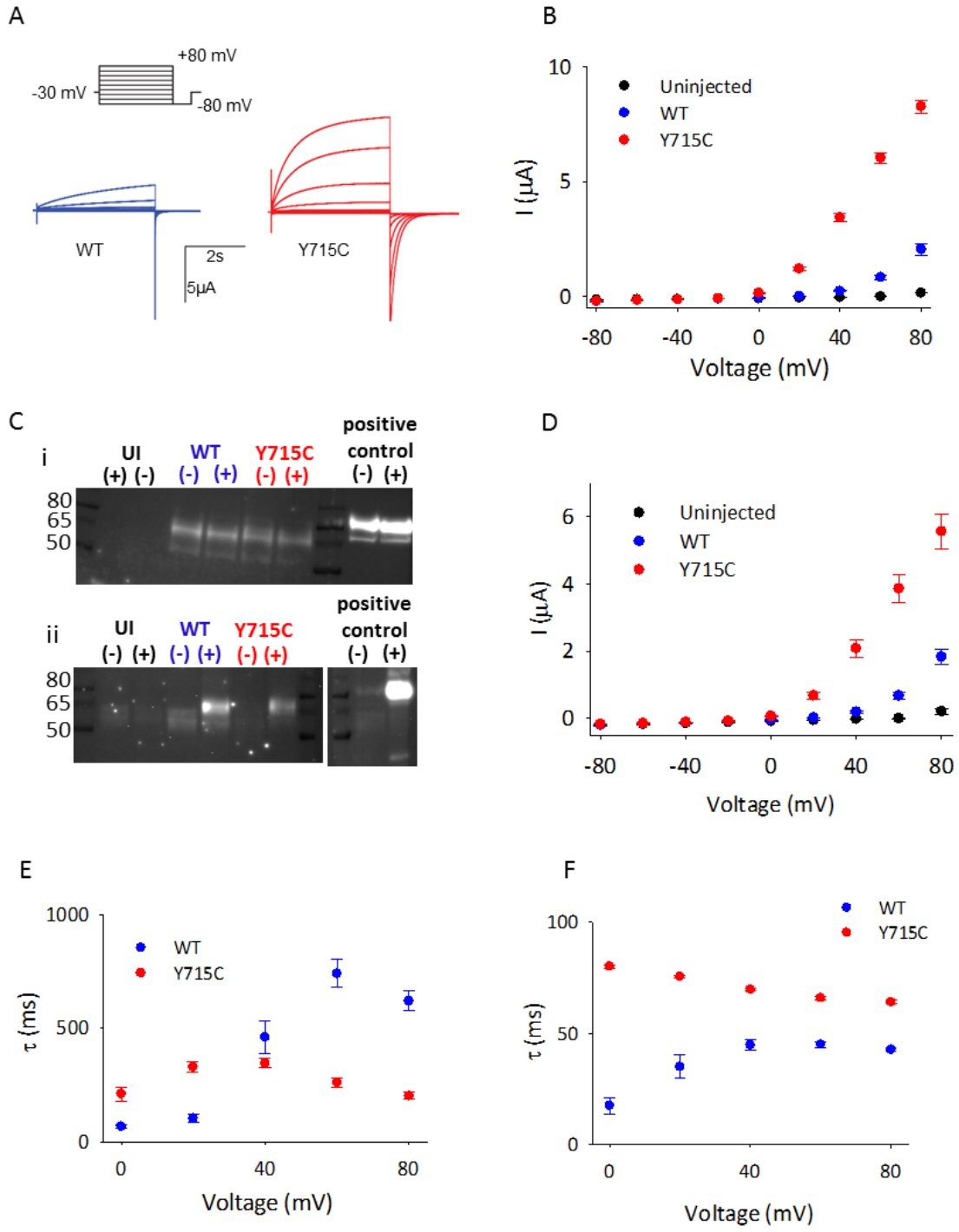

Lysosomal pH is decreased in fibroblasts with a Y715C mutation in *CLCN7* and treatment with chloroquine rescues the hyperacidity

If mutant *ClCN7* facilitates increased Cl^- movement into lysosomes, then the anion may act as a counterion and allow a greater number of H^+ to enter the lysosome, resulting in a more acidic luminal pH. We tested this prediction qualitatively with Lysotracker, a membrane permeable dye that accumulates in acidic compartments. While not quantitative, the more acidic the compartment, the greater the accumulation of dye and the more fluorescent the sample. We found that the fibroblasts of Proband 1 accumulated ~7-fold more lysotracker compared to wild-type controls, and ~3-fold more than our positive control, NPC25 cultured fibroblasts (Fig. 5A-B), highly indicative that lysosomal pH is more acidic in the Y715C patient cells.

We sought to confirm the change in a quantitative manner by measuring lysosomal pH in cultured fibroblasts from both patients and neonatal controls using the ratiometric dye Oregon Green 488-dextran (OGD). After incubating fibroblasts with the dextran overnight, the dye is endocytosed and trafficks to lysosomes (Fig 5D). In patient cells, the dextran accumulated only in small punctate compartments in the spaces between the large vacuoles and, like the Lamp1 staining pattern (Fig 3C), the large vacuoles failed to accumulate a substantial amount of dye (Fig 5C-D). This pattern is very different from the control, where dye is accumulated in a fewer number of distinct compartments. The fluorescent signal from the Proband 1 cells was ~4 times that of control fluorescence, indicating an increased amount of internalized dye (Fig 5C), as assessed after 4 and 16hrs of incubation with dye. Ratiometric imaging revealed that the lysosomes in cultured fibroblasts of both patients exhibited significantly lower luminal pH than those in control

cells (Fig 5E-F). These results show that a mutation in *ClCN7* affects lysosomal pH, a role that has previously been highly debated (26, 93), possibly caused by the increased transport capabilities of the mutant transporter.

Hyperacidic lysosomal pH may influence the enzymatic function of the lysosome and/or could be contributing to the accumulation of vacuoles. Thus, returning lysosomal pH back to normal levels is a potential therapeutic treatment. To achieve this, we tested the effects of the antimalaria drug chloroquine, a weak base that accumulates in acidic compartments and increases lysosomal pH (161), on the lysosomal pH of the fibroblasts. Patient cells incubated with chloroquine displayed reduced lysosomal pH in a dose-dependent fashion when evaluated with OGD or lysotracker over 24 or 72 hrs, respectively (Fig. 6). However, as far as we can tell, the size of the vesicles remained unchanged. In the future, we will explore if longer periods of treatment may assist in reducing vacuole number, but the chloroquine results point to a potential treatment that could be employed in patients.

Figure 5: Y715C patient fibroblasts have hyperacidic lysosomes
Raluca-Elena Nicoli (A and B) and Mary Weston (C-F) contributed to this figure.
(A) Fluorescent images of control and patient fibroblasts incubated with LysoTracker Red for one hour. (B) Quantitative data of the fluorescence from (A), expressed as intensity of lysotracker.(C) Representative brightfield images of identical exposure levels of control and Proband 1 fibroblasts incubated with FITC-dextran for 4 or 16hrs and fixed with PFA. (D) Representative confocal images of control and Proband 1 fibroblasts incubated with Oregon Green 488 overnight. (E) Representative data from one experiment measuring lysosomal pH of neonatal control, Proband 1, and Proband 2. Each dot represents the average lysosomal pH of a single cell. The black points are the average and SEM for each cell type. (F) The average and SEM of the lysosomal pH from multiple experiments for Proband 1, Proband 2, and control neonatal fibroblasts loaded with Oregon Green 488-dextran. A typical pH calibration curve used to convert ratio to pH is displayed in the corner.

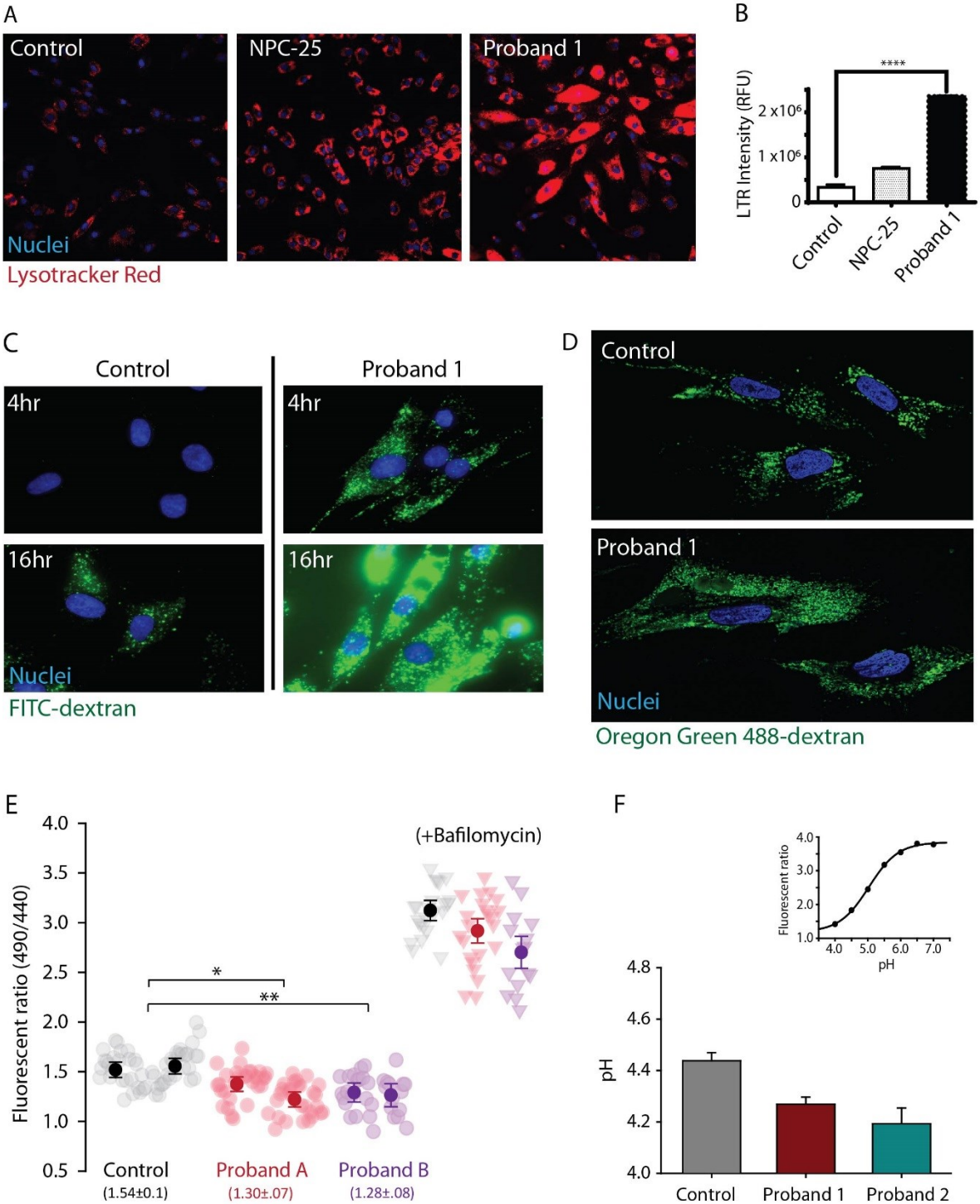
A
Control
NPC-25
Proband 1
Nuclei
Lysotracker Red
B
****
LTR Intensity (RFU)
2 x10⁶
1 x10⁶
0
Control
NPC-25
Proband 1
C
Control
Proband 1
4hr
4hr
16hr
16hr
Nuclei
FITC-dextran
D
Control
Proband 1
Nuclei
Oregon Green 488-dextran
E
(+Bafilomycin)
Fluorescent ratio (490/440)
4.0
3.5
3.0
2.5
2.0
1.5
1.0
0.5
*
**
Control
(1.54±0.1)
Proband A
(1.30±.07)
Proband B
(1.28±.08)
F
Fluorescent ratio
4.0
3.0
2.0
1.0
4.0
5.0
6.0
7.0
pH
pH
4.8
4.6
4.4
4.2
4.0
Control
Proband 1
Proband 2

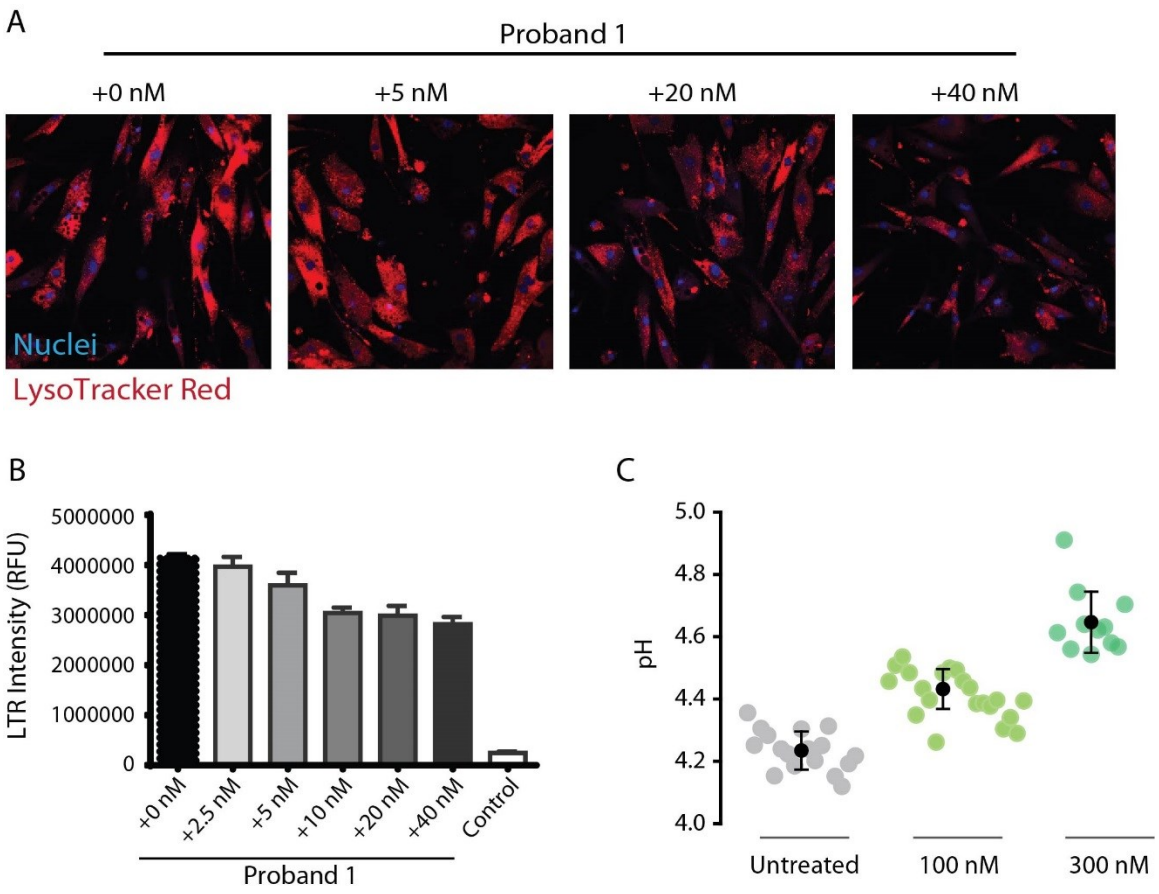

Figure 6: Lysosomal pH of Y715C fibroblasts and treatment with chloroquine
Raluca-Elena Nicoli (A and B) and Mary Weston (C) contributed to this figure.
(A) Fluorescent images of Proband 1 fibroblasts treated with 0-40 nM chloroquine for 72 hrs and incubated with LysoTracker Red for the final hour prior to imaging.
(B) Quantitative data of the fluorescence from (A), expressed as intensity of lysotracker.
(C) Proband 1 fibroblasts loaded with Oregon Green 488-dextran and incubated with the designated concentration of chloroquine for 18hrs and a non-drug control. Each dot represents the average lysosomal pH of one cell and the black points represent the average and SEM of each condition.

DISCUSSION

Loss-of-function and dominant negative mutations in *CLCN7* lead to osteopetrosis and lysosomal storage disease (LSD) in mice and humans, caused by a plethora of cellular defects that include delayed degradation of endocytosed proteins and reduced acidification of the resorption lacuna (99, 100, 103). In this paper, we presented two patients with an identical pathogenic *de novo* variant in *CLCN7*, who display hypopigmentation, a delay in gross and fine motor skills, abnormal liver/spleen/kidneys, and failure to thrive. However, unlike every previously reported *CLCN7* mutation, neither patient displays osteopetrosis. Lysosomal pH in cultured patient fibroblasts are more acidic than neonatal controls and electrophysiological measurements of the mutant transporter show altered gating and increased current, reflecting an increase in the turnover rate of transport. The simplest model to explain these results posits that increased turnover of lysosomal ClC-7 provides an increased counterion conductance which facilitates increased proton transport via the lysosomal V-ATPase and results in increased lysosomal acidity. These results clearly show that ClC-7 is involved in lysosomal pH, a role that is strongly debated (26, 93). We speculate that the numerous cellular and physiological defects observed in both patients result from the downstream sequalae of the hyperacidified lysosome, given the exquisitely tuned pH sensitivity of many lysosomal processes.

We presented two patients with an identical heterozygous point mutation of Y715C in *CLCN7*. This *de novo* mutation results in a striking cellular phenotype – the cytoplasm is filled with vacuole-like compartments that greatly vary in size (Fig 3). These vacuoles did not stain for various endosomal and lysosomal markers and their composition remains

unknown. Further, the origins of the vacuoles remain unknown as well – are they derived from lysosomes, a different organelle, or an accumulation of an inappropriately processed material?

Lysosomes, the most acidic compartment in the cell, creates and maintains its luminal pH via the proton pumping action of the V-ATPase. This is an electrogenic process and a neutralizing counterion, either a cation or anion, must also move across the membrane to dissipate any buildup in membrane potential. ClC-7 is the primary pathway for Cl^- into the lysosomes (44). Isolated lysosomes from ClC-7 KO animals display reduced acidification in comparison to WT, suggesting a role for Cl^- as a neutralizing counterion in lysosomal acidification (20, 23, 92). Furthermore, siRNA knockdown of ClC-7 has been shown to cause a decrease in lysosomal pH in HeLa cells and specialized glial macrophages (44, 115). However, the steady-state lysosomal pH in neurons, macrophages, and fibroblasts isolated from ClC-7 null mice is unaltered (94, 100, 102). Thus, the role of ClC-7 in lysosomal physiology is not clear. These contrasting results suggest that a regulatory or compensating mechanism is employed *in vivo* to regulate lysosomal pH, but it may not be sufficient to compensate in all conditions/cell types. Interestingly, while knocking out ClC-7 does not appear to affect lysosomal pH, suggesting that transporter is not involved in lysosomal pH, our results clearly show that ClC-7 is important in lysosomal pH because the Y715C mutation results in hyperacidic lysosomes (Fig. 5).

Mice expressing a mutant form of ClC-7 that uncouples Cl^- and H^+ transport ("Unc"), essentially turning the transporter into a channel, are reported to have less severe osteopetrosis symptoms and regain coat color (102). Because a Cl^- shunt was unable to

compensate for the loss of ClC-7, but the steady state lysosomal pH was similar to WT, this suggests that the transporter plays a specific role in regulating the luminal [Cl^-], possibly controlling the activity of enzymes. In agreement with this argument, molecular simulations comparing a lysosomal Cl^- channel to an antiporter indicate the transporter accumulates a higher concentration of Cl^- than the channel (106). Interestingly, a recent paper suggests the importance of high lysosomal Cl^-, arguing that luminal [Cl^-] in several lysosomal disease models is reduced and that lowering luminal [Cl^-] reduces the activity of two lysosomal enzymes (107). However, [Cl^-]-dependent enzymatic activity has not been noted in other lysosomal proteins. As opposed to [Cl^-]-reducing effects other LSDs may exhibit, the Y715C mutant protein may be increasing the lysosomal [Cl^-] based on the electrophysiology characteristics the mutant has compared to WT (Fig 4). The mutant protein appears to conduct about three times the current as WT, in addition to having altered gating, possibly affecting the enzymatic activity of the lysosome. Additionally, increasing the rate of Cl^- transport may be influencing pH, resulting in the observed hyperacidification of patient lysosomes (Fig 5).

A change in the lysosomal pH and/or an increase in luminal [Cl^-] may change the size and ionic homeostasis of the lysosome (27). Using a mathematical model of lysosomal acidification, Ishida et al. predicted that a mixture of cations and Cl^- acting as counterions would result in the observed lysosomal size (106). However, only using Cl^- would likely increase the overall number of luminal ions, in turn increasing lysosomal size, possibly creating some of the small vacuoles we observed. This may be happening in the patient lysosomes. Changes in lysosomal size, ionic composition, or membrane potential may have a variety of effects on lysosomal function and trafficking. For example, if luminal

[Ca^{2+}] was reduced, lysosomal Ca^{2+} channels may not be able to function properly and could affect, among other things, organelle fusion (27). Some vacuole formation has been observed in cells with non-functional TRPML-1, a Ca^{2+} channel in lysosomes that signals and regulates lysosomal fusion, but the quantity of vacuoles is not as T715C *de novo* patients (CITE). Additionally, the effects on lysosomal pH in TRPML-1 mutants is undetermined: different groups have reported hypoacidification, hyperacidification, and no change to lysosomal pH (162). However, even with an effect on trafficking, the patient cells have many acidic lysosome-like compartments containing Oregon Green dextran, implying some level of endosome to lysosome trafficking is likely to have occurred. Interestingly, the patient cells appear to endocytose dye at a faster rate than the control (Fig 5C), possibly indicating increased endocytosis at the plasma membrane.

We do not know the physical and structural effects of the Y715C mutation on the ClC-7 protein. Changing a tyrosine to a cysteine may have removed a physphorylation site, caused a structural change in ClC-7, and/or introduced a sulfur group capable of making unwelcome disulfide bonds with another part of the protein structure. These changes may affect way ClC-7 interacts with other proteins or lipids. Mice expressing a non-conducting ClC-7 mutant ("Td") still have severe osteopetrosis like a KO animal, but regain their coat color, suggesting that the presence of the protein is sufficient to recover activity (116). Interestingly, the patients' *de novo* mutation affects human pigmentation, suggesting that this Y715C may be involved in some sort of signaling pathway or complex. A new finding by Gayle et al. hints at a new form of ClC-7 regulation or a protein-protein interaction (117). PIKfyve is a phosphoinositol kinase that interacts with a scaffolding complex to phosphorylate PI3P to generate $PI(3,5)P_2$, a lipid that assists in

endolysomal trafficking and regulation (118). Treatment with the PIKfyve inhibitor apilimod has selective cytotoxic activity in B-cell non-Hodgkin lymphoma (B-NHL) compared to normal cells, but knocking out ClC-7 or Ostm1 (its β-subunit) abolished the killing effect. The reason for this is unknown, but suggests that ClC-7 could be regulated by $PI(3,5)P_2$, is a downstream target PIKfyve, or interacts with the PIKfyve complex. Interestingly, treating cells with apilimod also induces vacuole formation and, although the cells look different than the Y715C patient cells, it is possible that the *de novo* mutation may somehow be related to this pathway.

We explored a possible therapy treatment for the patient by treating with chloroquine, a malaria drug that increases lysosomal pH. We induced a small shift in the lysosomal pH of the patient to a less acidic pH (Fig 6), moving it closer to the range of the WT pH. We did not see an effect on the vacuoles in the cytoplasm, but we only treated up to 72hrs and longer treatment courses may be necessary to at least partially reverse the vacuole phenotype. Thus, chloroquine presents a possible FDA-approved therapeutic treatment to help alleviate some of the symptoms of the patients.

ACKNOWLEDGMENTS

The authors have no conflicts of interest to declare. We thank the patients, their families and the treating physicians for their cooperation, encouragement and interest. This work was supported by the Intramural Research Programs of the NHGRI and NINDS. The CD63 (H5C6), Lamp1 (H4A3) and Lamp2 (H4B4) antibodies developed by Dr. JT August and

JEK Hildreth (Johns Hopkins University School of Medicine) were obtained from the Developmental Studies Hybridoma Bank, created by the NICHD of the NIH and maintained at The University of Iowa, Department of Biology, Iowa City, IA 52242. We thank Dr. Forbes Porter at the NIH for NPC25 patient fibroblast lines.

URLs.

1000 Genomes Project 11_2010 data release project, ftp://ftp-trace.ncbi.nih.gov/1000genomes/ftp/release/20100804/; http://www.crisprscan.org/; CRISPRscan; Gene Ontology, http://www.geneontology.org/; Exome Aggregation Consortium (ExAC), Cambridge, MA (URL: http://exac.broadinstitute.org) [date accessed (March, 2017)]; NHLBI Exome Sequencing Project EVS v.0.0.30, http://evs.gs.washington.edu/EVS/; FastQC, http://www.bioinformatics.babraham.ac.uk/projects/fastqc/; http://liulab.dfci.harvard.edu/MACS/00README.html;

Chapter 5: Concluding remarks

Organelles within the endocytic pathway must strictly maintain their internal pH to function properly. While luminal pH is generated and maintained by the V-type ATPase (V-ATPase) (4), the voltage-shunting counterions also required to facilitate organelle acidification are not clear. Further, the mechanism used to regulate organelle pH is not known and, if counterion movement is a rate-limiting step in acidification, could be a means of regulation. In most endosomal organelles, Cl^- has emerged as the primary counterion candidate.

Counterion movement in endosomes is still not fully understood and part of the work in this thesis sought to use clathrin-coated vesicles (CCVs), a subset of early endosomes, as a model system of endosomal acidification. We successfully isolated a sample of highly enriched bovine brain CCVs that exhibited V-ATPase facilitated acidification and required the presence of Cl^-, but was independent of the monovalent cations present. Our findings were very similar to the acidification properties previously reported in both brain and liver CCVs (21, 22, 24), except while other studies found that acidification was partially influenced by the cation present (22), our vesicles displayed no reliance on cations. Thus, we have the cleanest preparation of CCVs, which further highlights the importance of Cl^- in acidification. While we were unable to identify the Cl^- transporting protein responsible for acidification, we did explore solubilization conditions that may be useful in future CCV studies.

In addition to looking at the counterion requirements of CCVs, we functionally confirmed that CCVs are primarily composed of synaptic vesicles (SVs). This result suggests that the protein facilitating brain CCV acidification is likely to be vGLUT1, a

glutamate transporter with a Cl^- permeability that, like the CCVs, requires a small [Cl^-] to facilitate glutamate uptake (67, 141). However, CCVs are present throughout the body, while vGLUT1 is primarily expressed in neurons. Since both brain and liver CCVs need Cl^- to acidify, vesicles from non-neuronal sources may have organ specific Cl^- transporting proteins and/or counterion requirements. In fact, liver CCVs have a slightly different counterion requirement profile in that they do not require Cl^- for acidification, but its presence greatly enhances the extent of acidification (21), arguing that liver CCVs utilize a different method to acidify the lumen. The Cl^- acidification in liver may result from trafficking Cl^- transporting proteins, like intracellular ClCs, around the cell. Previous work has indicated the ClC-3, -4, and -5 interact with clathrin (83), and our mass spectroscopy results also show that ClC-4 is present in the sample in low quantities. Examining CCVs from other organs could provide further insight into the role of Cl^- and counterions in these early endosomes.

Similar to endosomes, Cl^- is also a major candidate counterion in lysosomes. Much of this thesis was spent on determining if ClC-7, a $2Cl^-/H^+$ transporter, plays a role in lysosomal acidification. Early studies have shown that isolated lysosomes appear to be permeable to Cl^- and K^+, and that both ions assist with acidification, although Cl^- seems to function as the primary counterion (18-20, 23, 92, 95). The primary Cl^- permeation pathway through the lysosomal membrane is provided by ClC-7 and siRNA knockdown of the transporter in HeLa cells, U2OS cells (S.B. Lioi and J.A. Mindell; unpublished work), and cultured glial macrophages all result in hypoacidic lysosomes (44, 115). Together, these data argue that ClC-7 mediates counterion movement in lysosomes and assists in acidification. However, several different studies evaluating the lysosomal pH of

murine primary cells that lack either ClC-7 or its β-subunit Ostm1 reveal no significant pH change compared to WT, even though the mice themselves have severe osteopetrosis and lysosomal storage defects (94, 99, 100, 102, 116). Thus, the role that ClC-7 plays in lysosomal physiology is currently under debate.

We created a ClC-7 liver specific KO mouse to address these conflicting results, for the first time directly comparing the acidification properties of isolated lysosomes to the lysosomal pH of cultured cells derived from the same tissue. The isolated WT lysosomes exhibited Cl^--dependent acidification that was absent in KO lysosomes. Additionally, we found that H^+-driven $^{36}Cl^-$-uptake is abolished in isolated KO lysosomes in our experiments, making it unlikely that another protein is providing an alternative Cl^- permeability pathway in the lysosomal membrane of this system. However, the lysosomal pH in cultured KO hepatocytes was similar to WT. We explored the ability of hepatocytic lysosomes to respond to stressful conditions by measuring pH after autophagy induction and after organelle alkalization by a weak base. Again, the lysosomal pH of KO primary hepatocytes matched that of the WT in both situations. The unaltered pH in KO hepatocytes is perplexing, but agrees with the existing body of published data obtained from several different ClC-7 KO cell types (47, 94, 100, 102).

While we did not find an obvious role for ClC-7 in hepatocytic lysosomal pH, we observed indications that ClC-7 affects metabolism. The KO mouse typically had noticeable fat lining the gut that was absent in WT. Additionally, the body weight and the liver weight of the KO mouse were 25-30% heavier than WT. These results are consistent with those published by Weinert et al., who showed an increase in an autophagy marker when a non-conducting mutant ClC-7 was expressed in place of the WT (163). ClC-7

may be involved in the vast signaling pathway of mTORC1, the major regulator of autophagy and metabolism in the cell, which resides at the lysosomal membrane and senses and responds to changes in amino acid levels. Expanding our studies to look at various autophagy markers/characteristics in the ClC-7 KO mouse liver, and other KO tissues, may increase our understanding of the role of the transporter.

We characterized the pH lysosomes in cells from two patients with a *de novo* Y715C mutation in a single allele of ClC-7. All other reported detrimental mutations in ClC-7 and its β-subunit Ostm1 have resulted in osteopetrosis and lysosomal storage disease, but these two patients do not have osteopetrosis and, instead, display hypopigmentation, a delay in gross and fine motor skills, abnormal liver/spleen/kidneys, and failure to thrive. Unexpectedly, we found that the *de novo* patient fibroblasts had hyperacidic lysosomes compared to a neonatal control. Electrophysiological measurements of the mutant transporter showed altered gating and larger current, indicative of an increase in the turnover rate of transport, and suggesting that an increase in Cl^- transport provides additional counterions for acidification. Thus, we present strong evidence showing that ClC-7 is important in lysosomal pH.

How could a single, heterozygous mutation in one allele cause such a significant impact? The Y715C mutation, located in the cytoplasmic CBS domain of ClC-7, could change the structure of the transporter, result in loss of a phosphorylation site, and/or introduce an unwanted disulfide bond. A recent paper suggests that ClC-7 functions downstream of PIKfyve, a phosphoinositol kinase that phosphorylates PI3P to generate $PI(3,5)P_2$ (117). ClC-7 could itself be a target of the PIKfyve kinase, may be interacting with the PIKfyve scaffolding complex, or could be regulated by $PI(3,5)P_2$, an important

lysosomal signaling lipid known to regulate other membrane proteins. Interestingly, treatment with apilimod also induces vacuole formation in various cell types, although the vacuoles look different than the Y715C patient cells, and our unpublished results show that apilimod treatment results in hyperacidic lysosomes as well (M.R. Weston and J.A. Mindell, unpublished results). Future experiments exploring the effects of apilimod on WT, ClC-7 KO, and the Y715C mutant may lend insight as to the interaction of PIKfyve and $PI(3,5)P_2$ with ClC-7, and its influence on lysosomal pH.

We still do not know how to reconcile the conflicting results of how KO ClC-7 lysosomes cultured from multiple tissues have a normal steady state pH, but hypoacidic lysosomes are observed after the KD of ClC-7 with siRNA also occur. Possibly a mechanism to compensate for the loss of ClC-7 develops in the KO cells, but the KD cells lack enough time to acquire this ability. Measuring lysosomal pH in an inducible ClC-7 KO cell line over time could clarify this question and, if lysosomal pH does recover, comparing RNA expression at different time points may reveal if a change in protein expression is responsible, potentially indicating a compensatory mechanism.

An alternative compensation mechanism for ClC-7 may be a factor that transiently associates with the lysosome on the cytoplasmic side of the membrane, but is lost upon lysosome isolation. Our lab added cytoplasm back to isolated lysosomes, but saw no change in acidification, making the cytoplasmic factor hypothesis less likely (unpublished results, A. Amin and J.A. Mindell). Therefore, because the ClC-7 KO hepatocyte lysosomes appear to have little to no Cl^- conductance across their membranes, the KO lysosomes likely use cations as counterions. Yet, how the lysosome is supplied with cations to allow acidification is unclear. While no cation channel has been shown to

regulate lysosomal pH under quiescent conditions, the loss of either TMEM175 or TPC1/2 (K^+ and Na^+ channels, respectively) has been shown to result in hypoacidic lysosomes upon starvation (110, 113). Comparing the expression levels of these cation channels in WT and ClC-7 KO lysosomes may indicate if these proteins are over expressed in the organelle.

ClC-7 asymmetrically affects different processes in the body and the way various tissues and cell types compensate for the loss of ClC-7 is unknown. In osteoclasts, the resorption lacuna, an external compartment similar to lysosomes, appears less acidic (99). Perhaps tissues most affected by a loss of ClC-7, such as brain and bone, either compensate differently or place a higher demand on their lysosomes then macrophages and fibroblasts, where KO lysosomal pH has primarily been evaluated. Although our starvation experiments in KO hepatocytes were not able to reveal a role for ClC-7, exploring other means of exerting stress on lysosomes may yet hint as to its function and should be pursued.

The lysosomal luminal [Cl^-] may be important for both acidification and general lysosomal physiology. Mice expressing a ClC-7 containing a mutation that uncouples Cl^- and H^+ movement, effectively changing the transporter to a Cl^- channel, is only able to partially compensate for the loss of the transporter, suggesting that ClC-7 is needed to provide sufficient luminal [Cl^-] (102). A mathematical model of lysosomal acidification supports this idea with simulations that predict the $2Cl^-/H^+$ antiporter can generate a larger luminal [Cl^-] than a Cl^- channel (106). The need for luminal [Cl^-] is unknown, but only a few lysosomal enzymes have reported Cl^--dependent activity. However, a change in the lysosomal pH and/or an increase in luminal [Cl^-] may alter the size, ionic

homeostasis, or membrane potential of the lysosome (27). If the Y715C mutant transports a greater number of Cl^- ions, this may boost the total internal ion composition, causing an increase in lysosomal size and potentially creating some of the small vacuoles observed in the patient cells. Developing methods to measure ionic concentrations in lysosomes will help move the field forward and assist in modeling, calculating membrane potential and clarifying if any cation(s) are present at sufficient concentrations to act as a counterion during lysosomal acidification.

Many aspects in lysosomal physiology and pH regulation are open to debate. How lysosomal pH is regulated is still unknown, and finding a transporter whose absence affects lysosomal pH under quiescent conditions will be enlightening. Perhaps the reason the absence of one protein does not affect general lysosomal pH is that regulation is performed by many proteins working together. Interestingly, the Y715C mutation may be an exception in that it lowers lysosomal pH, a situation for which the cell might not have any prevention mechanisms.

The experiments described in this thesis, using pH-sensitive dyes to measure lysosomal pH in various systems, have provided us clues as to the mechanism lysosomes use to acidify and have shown a role for ClC-7 in this process. Additionally, these experiments have suggested a potential treatment for the *CLCN7* Y715C patients, and I hope that our research will help alleviate their symptoms. Ultimately, I hope this body of work will lead to a better understanding of organelle acidification, the counterions involved, and mechanisms of organellar pH regulation.

LITERATURE CITED

1. Jentsch TJ. Discovery of CLC transport proteins: cloning, structure, function and pathophysiology. J Physiol-London. 2015;593(18):4091-109.
2. Huotari J, Helenius A. Endosome maturation. Embo Journal. 2011;30(17):3481-500.
3. Feng LA, Campbell EB, Hsiung YC, MacKinnon R. Structure of a Eukaryotic CLC Transporter Defines an Intermediate State in the Transport Cycle. Science. 2010;330(6004):635-41.
4. Forgac M. Vacuolar ATPases: rotary proton pumps in physiology and pathophysiology. Nature Reviews Molecular Cell Biology. 2007;8(11):917-29.
5. Grabe M, Wang HY, Oster G. The mechanochemistry of V-ATPase proton pumps. Biophysical Journal. 2000;78(6):2798-813.
6. Maxson ME, Grinstein S. The vacuolar-type H+-ATPase at a glance - more than a proton pump. J Cell Sci. 2014;127(23):4987-93.
7. Kane PM. Disassembly and reassembly of the yeast vacuolar H(+)-ATPase in vivo. J Biol Chem. 1995;270(28):17025-32.
8. Wieczorek H, Gruber G, Harvey WR, Huss M, Merzendorfer H, Zeiske W. Structure and regulation of insect plasma membrane H+V-ATPase. Journal of Experimental Biology. 2000;203(1):127-35.
9. Sautin YY, Lu M, Gaugler A, Zhang L, Gluck SL. Phosphatidylinositol 3-kinase-mediated effects of glucose on vacuolar H+-ATPase assembly, translocation, and acidification of intracellular compartments in renal epithelial cells. Mol Cell Biol. 2005;25(2):575-89.
10. Trombetta ES, Ebersold M, Garrett W, Pypaert M, Mellman I. Activation of lysosomal function during dendritic cell maturation. Science. 2003;299(5611):1400-3.
11. Manolson MF, Proteau D, Preston RA, Stenbit A, Roberts BT, Hoyt MA, et al. The Vph1 Gene Encodes a 95-Kda Integral Membrane Polypeptide Required for Invivo Assembly and Activity of the Yeast Vacuolar H+-Atpase. Journal of Biological Chemistry. 1992;267(20):14294-303.
12. Manolson MF, Wu BG, Proteau D, Taillon BE, Roberts BT, Hoyt MA, et al. Stv1 Gene Encodes Functional Homolog of 95-Kda Yeast Vacuolar H+-Atpase Subunit Vph1p. Journal of Biological Chemistry. 1994;269(19):14064-74.
13. Kawasaki-Nishi S, Nishi T, Forgac M. Yeast V-ATPase complexes containing different isoforms of the 100-kDa a-subunit differ in coupling efficiency and in vivo dissociation. Journal of Biological Chemistry. 2001;276(21):17941-8.
14. Toei M, Saum R, Forgac M. Regulation and Isoform Function of the V-ATPases. Biochemistry. 2010;49(23):4715-23.

15. Smith AN, Borthwick KJ, Karet FE. Molecular cloning and characterization of novel tissue-specific isoforms of the human vacuolar H+-ATPase C, G and d subunits, and their evaluation in autosomal recessive distal renal tubular acidosis. Gene. 2002;297(1-2):169-77.

16. Smith AN, Jouret F, Bord S, Borthwick KJ, Al-Lamki RS, Wagner CA, et al. Vacuolar H+-ATPase d2 subunit: Molecular characterization, developmental regulation, and localization to specialized proton pumps in kidney and bone. J Am Soc Nephrol. 2005;16(5):1245-56.

17. Lee SH, Rho J, Jeong D, Sul JY, Kim T, Kim N, et al. v-ATPase V-0 subunit d2-deficient mice exhibit impaired osteoclast fusion and increased bone formation. Nat Med. 2006;12(12):1403-9.

18. Ohkuma S, Moriyama Y, Takano T. Electrogenic Nature of Lysosomal Proton Pump as Revealed with a Cyanine Dye. Journal of Biochemistry. 1983;94(6):1935-43.

19. Harikumar P, Reeves JP. The Lysosomal Proton Pump Is Electrogenic. Journal of Biological Chemistry. 1983;258(17):403-10.

20. Ohkuma S, Moriyama Y, Takano T. Identification and characterization of a proton pump on lysosomes by fluorescein-isothiocyanate-dextran fluorescence. Proc Natl Acad Sci U S A. 1982;79(9):2758-62.

21. Vandyke RW, Steer CJ, Scharschmidt BF. Clathrin-Coated Vesicles from Rat-Liver - Enzymatic Profile and Characterization of Atp-Dependent Proton Transport. Proceedings of the National Academy of Sciences of the United States of America-Biological Sciences. 1984;81(10):3108-12.

22. Vandyke RW, Scharschmidt BF, Steer CJ. Atp-Dependent Proton Transport by Isolated Brain Clathrin-Coated Vesicles - Role of Clathrin and Other Determinants of Acidification. Biochim Biophys Acta. 1985;812(2):423-36.

23. Vandyke RW. Acidification of Rat-Liver Lysosomes - Quantitation and Comparison with Endosomes. Am J Physiol. 1993;265(4):C901-C17.

24. Xie XS, Stone DK, Racker E. Determinants of clathrin-coated vesicle acidification. J Biol Chem. 1983;258(24):14834-8.

25. Stauber T, Jentsch TJ. Chloride in Vesicular Trafficking and Function. In: Julius D, editor. Annual Review of Physiology, Vol 75. Annual Review of Physiology. 75. Palo Alto: Annual Reviews; 2013. p. 453-77.

26. Mindell JA. Lysosomal Acidification Mechanisms. In: Julius D, Clapham DE, editors. Annual Review of Physiology, Vol 74. Annual Review of Physiology. 74. Palo Alto: Annual Reviews; 2012. p. 69-86.

27. Xu HX, Ren DJ. Lysosomal Physiology. In: Julius D, editor. Annual Review of Physiology, Vol 77. Annual Review of Physiology. 77. Palo Alto: Annual Reviews; 2015. p. 57-80.

28. Yamashiro DJ, Fluss SR, Maxfield FR. Acidification of endocytic vesicles by an ATP-dependent proton pump. J Cell Biol. 1983;97(3):929-34.

29. de Duve C, Pressman BC, Gianetto R, Wattiaux R, Appelmans F. Tissue fractionation studies. 6. Intracellular distribution patterns of enzymes in rat-liver tissue. Biochem J. 1955;60(4):604-17.

30. Straus W. Occurrence of Phagosomes and Phago-Lysosomes in Different Segments of the Nephron in Relation to the Reabsorption, Transport, Digestion, and Extrusion of Intravenously Injected Horseradish Peroxidase. J Cell Biol. 1964;21(3):295-308.

31. Tycko B, Maxfield FR. Rapid acidification of endocytic vesicles containing alpha 2-macroglobulin. Cell. 1982;28(3):643-51.

32. Vanrenswoude J, Bridges KR, Harford JB, Klausner RD. Receptor-Mediated Endocytosis of Transferrin and the Uptake of Fe in K562-Cells - Identification of a Non-Lysosomal Acidic Compartment. Proceedings of the National Academy of Sciences of the United States of America-Biological Sciences. 1982;79(20):6186-90.

33. Galloway CJ, Dean GE, Marsh M, Rudnick G, Mellman I. Acidification of Macrophage and Fibroblast Endocytic Vesicles Invitro. Proceedings of the National Academy of Sciences of the United States of America-Biological Sciences. 1983;80(11):3334-8.

34. Vandyke RW, Belcher JD. Acidification of 3 Types of Liver Endocytic Vesicles - Similarities and Differences. Am J Physiol. 1994;266(1):C81-C94.

35. Jentsch TJ. CLC chloride channels and transporters: From genes to protein structure, pathology and physiology. Critical Reviews in Biochemistry and Molecular Biology. 2008;43(1):3-36.

36. White MM, Miller C. A voltage-gated anion channel from the electric organ of Torpedo californica. J Biol Chem. 1979;254(20):10161-6.

37. Jentsch TJ, Steinmeyer K, Schwarz G. Primary structure of *Torpedo marmorata* chloride channel isolated by expression cloning in Xenopus oocytes. Nature. 1990;348(6301):510-4.

38. Dutzler R, Campbell EB, Cadene M, Chait BT, MacKinnon R. X-ray structure of a ClC chloride channel at 3.0 angstrom reveals the molecular basis of anion selectivity. Nature. 2002;415(6869):287-94.

39. Dutzler R, Campbell EB, MacKinnon R. Gating the selectivity filter in ClC chloride channels. Science. 2003;300(5616):108-12.

40. Park E, Ampbell EBC, MacKinnon R. Structure of a CLC chloride ion channel by cryo-electron microscopy. Nature. 2017;541(7638):19.

41. Accardi A, Miller C. Secondary active transport mediated by a prokaryotic homologue of ClC Cl- channels. Nature. 2004;427(6977):803-7.

42. Picollo A, Pusch M. Chloride/proton antiporter activity of mammalian CLC proteins ClC-4 and ClC-5. Nature. 2005;436(7049):420-3.

43. Scheel O, Zdebik AA, Lourdel S, Jentsch TJ. Voltage-dependent electrogenic chloride/proton exchange by endosomal CLC proteins. Nature. 2005;436(7049):424-7.

44. Graves AR, Curran PK, Smith CL, Mindell JA. The Cl(-)/H(+) antiporter ClC-7 is the primary chloride permeation pathway in lysosomes. Nature. 2008;453(7196):788-92.

45. Neagoe I, Stauber T, Fidzinski P, Bergsdorf EY, Jentsch TJ. The Late Endosomal ClC-6 Mediates Proton/Chloride Countertransport in Heterologous Plasma Membrane Expression. Journal of Biological Chemistry. 2010;285(28):21689-97.

46. Estevez R, Bottger T, Stein V, Birkenhager R, Otto E, Hildebrandt F, et al. Barttin is a Cl- channel beta-subunit crucial for renal Cl- reabsorption and inner ear K+ secretion. Nature. 2001;414(6863):558-61.

47. Lange PF, Wartosch L, Jentsch TJ, Fuhrmann JC. ClC-7 requires Ostm1 as a beta-subunit to support bone resorption and lysosomal function. Nature. 2006;440(7081):220-3.

48. Jeworutzki E, Lopez-Hernandez T, Capdevila-Nortes X, Sirisi S, Bengtsson L, Montolio M, et al. GlialCAM, a Protein Defective in a Leukodystrophy, Serves as a CIC-2 Cl- Channel Auxiliary Subunit. Neuron. 2012;73(5):951-61.

49. Poroca DR, Pelis RM, Chappe VM. CIC Channels and Transporters: Structure, Physiological Functions, and Implications in Human Chloride Channelopathies. Front Pharmacol. 2017;8:25.

50. Hara-Chikuma M, Wang YH, Guggino SE, Guggino WB, Verkman AS. Impaired acidification in early endosomes of CIC-5 deficient proximal tubule. Biochemical and Biophysical Research Communications. 2005;329(3):941-6.

51. Novarino G, Weinert S, Rickheit G, Jentsch TJ. Endosomal Chloride-Proton Exchange Rather Than Chloride Conductance Is Crucial for Renal Endocytosis. Science. 2010;328(5984):1398-401.

52. Steinmeyer K, Schwappach B, Bens M, Vandewalle A, Jentsch TJ. Cloning and functional expression of rat CLC-5, a chloride channel related to kidney disease. Journal of Biological Chemistry. 1995;270(52):31172-7.

53. Gunther W, Piwon N, Jentsch TJ. The CIC-5 chloride channel knock-out mouse - an animal model for Dent's disease. Pflugers Archiv-European Journal of Physiology. 2003;445(4):456-62.

54. Hara-Chikuma M, Wang YH, Guggino SE, Guggino WB, Verkman AS. Impaired acidification in early endosomes of ClC-5 deficient proximal tubule. Biochemical and Biophysical Research Communications. 2005;329(3):941-6.

55. Smith AJ, Lippiat JD. Direct endosomal acidification by the outwardly rectifying CLC-5 Cl-/H+ exchanger. J Physiol-London. 2010;588(12):2033-45.

56. Smith AJ, Lippiat JD. Voltage-dependent charge movement associated with activation of the CLC-5 2Cl(-)/1H(+) exchanger. Faseb Journal. 2010;24(10):3696-705.

57. Stauber T, Weinert S, Jentsch TJ. Cell Biology and Physiology of CLC Chloride Channels and Transporters. Compr Physiol. 2012;2(3):1701-44.

58. Mohammad-Panah R, Harrison R, Dhani S, Ackerley C, Huan LJ, Wang YC, et al. The chloride channel ClC-4 contributes to endosomal acidification and trafficking. Journal of Biological Chemistry. 2003;278(31):29267-77.

59. Mohammad-Panah R, Wellhauser L, Steinberg BE, Wang YC, Huan LJ, Liu XD, et al. An essential role for ClC-4 in transferrin receptor function revealed in studies of fibroblasts derived from Clcn4-null mice. J Cell Sci. 2009;122(8):1229-37.

60. Rickheit G, Wartosch L, Schaffer S, Stobrawa SM, Novarino G, Weinert S, et al. Role of ClC-5 in Renal Endocytosis Is Unique among ClC Exchangers and Does Not Require PY-motif-dependent Ubiquitylation. Journal of Biological Chemistry. 2010;285(23):17595-603.

61. Zhao ZF, Li XH, Hao JF, Winston JH, Weinman SA. The ClC-3 chloride transport protein traffics through the plasma membrane via interaction of an N-terminal dileucine cluster with clathrin. Journal of Biological Chemistry. 2007;282(39):29022-31.

62. Stobrawa SM, Breiderhoff T, Takamori S, Engel D, Schweizer M, Zdebik AA, et al. Disruption of ClC-3, a chloride channel expressed on synaptic vesicles, leads to a loss of the hippocampus. Neuron. 2001;29(1):185-96.

63. Dickerson LW, Bonthius DJ, Schutte BC, Yang BL, Barna TJ, Bailey MC, et al. Altered GABAergic function accompanies hippocampal degeneration in mice lacking ClC-3 voltage-gated chloride channels. Brain Res. 2002;958(2):227-50.

64. Yoshikawa M, Uchida S, Ezaki J, Rai T, Hayama A, Kobayashi K, et al. CLC-3 deficiency leads to phenotypes similar to human neuronal ceroid lipofuscinosis. Genes Cells. 2002;7(6):597-605.

65. Hara-Chikuma M, Yang BX, Sonawane ND, Sasaki S, Uchida S, Verkman AS. ClC-3 chloride channels facilitate endosomal acidification and chloride accumulation. Journal of Biological Chemistry. 2005;280(2):1241-7.

66. Schenck S, Wojcik SM, Brose N, Takamori S. A chloride conductance in VGLUT1 underlies maximal glutamate loading into synaptic vesicles. Nature Neuroscience. 2009;12(2):156-62.

67. Preobraschenski J, Zander JF, Suzuki T, Ahnert-Hilger G, Jahn R. Vesicular glutamate transporters use flexible anion and cation binding sites for efficient accumulation of neurotransmitter. Neuron. 2014;84(6):1287-301.

68. Riordan JR, Rommens JM, Kerem B, Alon N, Rozmahel R, Grzelczak Z, et al. Identification of the cystic fibrosis gene: cloning and characterization of complementary DNA. Science. 1989;245(4922):1066-73.

69. Bear CE, Li CH, Kartner N, Bridges RJ, Jensen TJ, Ramjeesingh M, et al. Purification and functional reconstitution of the cystic fibrosis transmembrane conductance regulator (CFTR). Cell. 1992;68(4):809-18.

70. Haggie PM, Verkman AS. Defective organellar acidification as a cause of cystic fibrosis lung disease: reexamination of a recurring hypothesis. Am J Physiol-Lung Cell Mol Physiol. 2009;296(6):L859-L67.

71. Rowe SM, Miller S, Sorscher EJ. Mechanisms of disease: Cystic fibrosis. N Engl J Med. 2005;352(19):1992-2001.

72. Barasch J, Kiss B, Prince A, Saiman L, Gruenert D, al-Awqati Q. Defective acidification of intracellular organelles in cystic fibrosis. Nature. 1991;352(6330):70-3.

73. Fuster DG, Alexander RT. Traditional and emerging roles for the SLC9 Na+/H+ exchangers. Pflugers Arch. 2014;466(1):61-76.

74. Kondapalli KC, Prasad H, Rao R. An inside job: how endosomal Na+/H+ exchangers link to autism and neurological disease. Front Cell Neurosci. 2014;8:21.

75. Donowitz M, Tse CM, Fuster D. SLC9/NHE gene family, a plasma membrane and organellar family of Na+/H+ exchangers. Mol Asp Med. 2013;34(2-3):236-51.

76. Nakamura N, Tanaka S, Teko Y, Mitsui K, Kanazawa H. Four Na+/H+ exchanger isoforms are distributed to Golgi and post-Golgi compartments and are involved in organelle pH regulation. Journal of Biological Chemistry. 2005;280(2):1561-72.

77. Roth TF, Porter KR. Yolk Protein Uptake in the Oocyte of the Mosquito Aedes Aegypti. L. J Cell Biol. 1964;20(2):313-32.

78. Royle SJ. The cellular functions of clathrin. Cell Mol Life Sci. 2006;63(16):1823-32.

79. McMahon HT, Boucrot E. Molecular mechanism and physiological functions of clathrin-mediated endocytosis. Nature Reviews Molecular Cell Biology. 2011;12(8):517-33.

80. Xie XS, Crider BP, Stone DK. Isolation and reconstitution of the chloride transporter of clathrin-coated vesicles. J Biol Chem. 1989;264(32):18870-3.

81. Xie XS, Stone DK. Isolation and reconstitution of the clathrin-coated vesicle proton translocating complex. J Biol Chem. 1986;261(6):2492-5.

82. Barrera NP, Robinson CV. Advances in the Mass Spectrometry of Membrane Proteins: From Individual Proteins to Intact Complexes. In: Kornberg RD, Raetz CRH, Rothman JE, Thorner JW, editors. Annual Review of Biochemistry, Vol 80. Annual Review of Biochemistry. 80. Palo Alto: Annual Reviews; 2011. p. 247-71.

83. Stauber T, Jentsch TJ. Sorting Motifs of the Endosomal/Lysosomal CLC Chloride Transporters. Journal of Biological Chemistry. 2010;285(45):34537-48.

84. de Duve C. The lysosome turns fifty. Nat Cell Biol. 2005;7(9):847-9.

85. Berthet J, De Duve C. Tissue fractionation studies. I. The existence of a mitochondria-linked, enzymically inactive form of acid phosphatase in rat-liver tissue. Biochem J. 1951;50(2):174-81.

86. Lubke T, Lobel P, Sleat DE. Proteomics of the lysosome. Biochim Biophys Acta-Mol Cell Res. 2009;1793(4):625-35.

87. Lüllmann-Rauch R. History and Morphology of the Lysosome. Lysosomes Medical Intelligence Unit Boston, MA: Springer; 2005.

88. Luzio JP, Pryor PR, Bright NA. Lysosomes: fusion and function. Nature Reviews Molecular Cell Biology. 2007;8(8):622-32.

89. Eskelinen EL, Saftig P. Autophagy: A lysosomal degradation pathway with a central role in health and disease. Biochim Biophys Acta-Mol Cell Res. 2009;1793(4):664-73.

90. Parenti G, Andria G, Ballabio A. Lysosomal Storage Diseases: From Pathophysiology to Therapy. In: Caskey CT, editor. Annual Review of Medicine, Vol 66. Annual Review of Medicine. 66. Palo Alto: Annual Reviews; 2015. p. 471-86.

91. Pillay CS, Elliott E, Dennison C. Endolysosomal proteolysis and its regulation. Biochem J. 2002;363:417-29.

92. Dellantone P. Evidence for an Atp-Driven Proton Pump in Rat-Liver Lysosomes by Basic-Dyes Uptake. Biochemical and Biophysical Research Communications. 1979;86(1):180-9.

93. DiCiccio JE, Steinberg BE. Lysosomal pH and analysis of the counter ion pathways that support acidification. Journal of General Physiology. 2011;137(4):385-90.

94. Steinberg BE, Huynh KK, Brodovitch A, Jabs S, Stauber T, Jentsch TJ, et al. A cation counterflux supports lysosomal acidification. Journal of Cell Biology. 2010;189(7):1171-86.

95. Cuppoletti J, Auresfischer D, Sachs G. The Lyososomal H+ Pump - 8-Azido-Atp Inhibition and the Role of Chloride in H+ Transport. Biochim Biophys Acta. 1987;899(2):276-84.

96. Di A, Brown ME, Deriy LV, Li CY, Szeto FL, Chen YM, et al. CFTR regulates phagosome acidification in macrophages and alters bactericidal activity. Nat Cell Biol. 2006;8(9):933-U52.

97. Haggie PM, Verkman AS. Unimpaired Lysosomal Acidification in Respiratory Epithelial Cells in Cystic Fibrosis. Journal of Biological Chemistry. 2009;284(12):7681-6.

98. Brandt S, Jentsch TJ. ClC-6 and ClC-7 are two novel broadly expressed members of the CLC chloride channel family. Febs Letters. 1995;377(1):15-20.

99. Kornak U, Kasper D, Bosl MR, Kaiser E, Schweizer M, Schulz A, et al. Loss of the ClC-7 chloride channel leads to osteopetrosis in mice and man. Cell. 2001;104(2):205-15.

100. Kasper D, Planells-Cases R, Fuhrmann JC, Scheel O, Zeitz O, Ruether K, et al. Loss of the chloride channel ClC-7 leads to lysosomal storage disease and neurodegeneration. Embo Journal. 2005;24(5):1079-91.

101. Vaananen HK, Zhao H, Mulari M, Halleen JM. The cell biology of osteoclast function. J Cell Sci. 2000;113(3):377-81.

102. Weinert S, Jabs S, Supanchart C, Schweizer M, Gimber N, Richter M, et al. Lysosomal Pathology and Osteopetrosis upon Loss of H+-Driven Lysosomal Cl- Accumulation. Science. 2010;328(5984):1401-3.

103. Wartosch L, Fuhrmann JC, Schweizer M, Stauber T, Jentsch TJ. Lysosomal degradation of endocytosed proteins depends on the chloride transport protein ClC-7. Faseb Journal. 2009;23(12):4056-68.

104. McDonald JK, Reilly TJ, Zeitman BB, Ellis S. Cathepsin C: a chloride-requiring enzyme. Biochem Biophys Res Commun. 1966;24(5):771-5.

105. Cigic B, Pain RH. Location of the binding site for chloride ion activation of cathepsin C. Eur J Biochem. 1999;264(3):944-51.

106. Ishida Y, Nayak S, Mindell JA, Grabe M. A model of lysosomal pH regulation. Journal of General Physiology. 2013;141(6):705-20.

107. Chakraborty K, Leung K, Krishnan Y. High lumenal chloride in the lysosome is critical for lysosome function. eLife. 2017;6:e28862.

108. Wang WY, Zhang XL, Gao Q, Xu HX. TRPML1: An Ion Channel in the Lysosome. In: Nilius B, Flockerzi V, editors. Mammalian Transient Receptor Potential. Handbook of Experimental Pharmacology. 222. Berlin: Springer-Verlag Berlin; 2014. p. 631-45.

109. Dong XP, Cheng XP, Mills E, Delling M, Wang FD, Kurz T, et al. The type IV mucolipidosis-associated protein TRPML1 is an endolysosomal iron release channel. Nature. 2008;455(7215):992-U78.

110. Cang CL, Zhou YD, Navarro B, Seo YJ, Aranda K, Shi L, et al. mTOR Regulates Lysosomal ATP-Sensitive Two-Pore Na+ Channels to Adapt to Metabolic State. Cell. 2013;152(4):778-90.

111. Wang X, Zhang XL, Dong XP, Samie M, Li XR, Cheng XP, et al. TPC Proteins Are Phosphoinositide-Activated Sodium-Selective Ion Channels in Endosomes and Lysosomes. Cell. 2012;151(2):372-83.

112. Cang CL, Bekele B, Ren DJ. The voltage-gated sodium channel TPC1 confers endolysosomal excitability. Nat Chem Biol. 2014;10(6):463-9.

113. Cang CL, Aranda K, Seo YJ, Gasnier B, Ren DJ. TMEM175 Is an Organelle K+ Channel Regulating Lysosomal Function. Cell. 2015;162(5):1101-12.

114. Cao Q, Zhong XZ, Zou YJ, Zhang Z, Toro L, Dong XP. BK Channels Alleviate Lysosomal Storage Diseases by Providing Positive Feedback Regulation of Lysosomal Ca2+ Release. Dev Cell. 2015;33(4):427-41.

115. Majumdar A, Capetillo-Zarate E, Cruz D, Gouras GK, Maxfield FR. Degradation of Alzheimer's amyloid fibrils by microglia requires delivery of ClC-7 to lysosomes. Molecular Biology of the Cell. 2011;22(10):1664-76.

116. Weinert S, Jabs S, Hohensee S, Chan WL, Kornak U, Jentsch TJ. Transport activity and presence of ClC-7/Ostm1 complex account for different cellular functions. EMBO Rep. 2014;15(7):784-91.

117. Gayle S, Landrette S, Beeharry N, Conrad C, Hernandez M, Beckett P, et al. Identification of apilimod as a first-in-class PIKfyve kinase inhibitor for treatment of B-cell non-Hodgkin lymphoma. Blood. 2017;129(13):1768-78.

118. Li XR, Garrity AG, Xu HX. Regulation of membrane trafficking by signalling on endosomal and lysosomal membranes. J Physiol-London. 2013;591(18):4389-401.

119. Ikonomov OC, Sbrissa D, Delvecchio K, Xie Y, Jin JP, Rappolee D, et al. The phosphoinositide kinase PIKfyve is vital in early embryonic development: preimplantation lethality of PIKfyve-/- embryos but normality of PIKfyve+/- mice. J Biol Chem. 2011;286(15):13404-13.

120. Poet M, Kornak U, Schweizer M, Zdebik AA, Scheel O, Hoelter S, et al. Lysosomal storage disease upon disruption of the neuronal chloride transport protein CIC-6. Proceedings of the National Academy of Sciences of the United States of America. 2006;103(37):13854-9.

121. Zoncu R, Bar-Peled L, Efeyan A, Wang SY, Sancak Y, Sabatini DM. mTORC1 Senses Lysosomal Amino Acids Through an Inside-Out Mechanism That Requires the Vacuolar H+-ATPase. Science. 2011;334(6056):678-83.

122. Zoncu R, Efeyan A, Sabatini DM. mTOR: from growth signal integration to cancer, diabetes and ageing. Nature Reviews Molecular Cell Biology. 2011;12(1):21-35.

123. Puertollano R. mTOR and lysosome regulation. F1000Prime Reports. 2014;6:52.

124. Zhou J, Tan SH, Nicolas V, Bauvy C, Yang ND, Zhang JB, et al. Activation of lysosomal function in the course of autophagy via mTORC1 suppression and autophagosome-lysosome fusion. Cell Res. 2013;23(4):508-23.

125. Schultz ML, Tecedor L, Chang M, Davidson BL. Clarifying lysosomal storage diseases. Trends in neurosciences. 2011;34(8):401-10.

126. Chalhoub N, Benachenhou N, Rajapurohitam V, Pata M, Ferron M, Frattini A, et al. Grey-lethal mutation induces severe malignant autosomal recessive osteopetrosis in mouse and human. Nat Med. 2003;9(4):399-406.

127. Cleiren E, Benichou O, Van Hul E, Gram J, Bollerslev J, Singer FR, et al. Albers-Schonberg disease (autosomal dominant osteopetrosis, type II) results from

mutations in the CICN7chloride channel gene. Hum Mol Genet. 2001;10(25):2861-7.

128. Leisle L, Ludwig CF, Wagner FA, Jentsch TJ, Stauber T. ClC-7 is a slowly voltage-gated 2Cl(-)/1H(+)-exchanger and requires Ostm1 for transport activity. Embo Journal. 2011;30(11):2140-52.

129. Gunther W, Piwon N, Jentsch TJ. The ClC-5 chloride channel knock-out mouse - an animal model for Dent's disease. Pflugers Arch. 2003;445(4):456-62.

130. Maritzen T, Keating DJ, Neagoe I, Zdebik AA, Jentsch TJ. Role of the Vesicular Chloride Transporter ClC-3 in Neuroendocrine Tissue. J Neurosci. 2008;28(42):10587-98.

131. Maycox PR, Link E, Reetz A, Morris SA, Jahn R. Clathrin-coated vesicles in nervous tissue are involved primarily in synaptic vesicle recycling. J Cell Biol. 1992;118(6):1379-88.

132. Morimoto R, Hayashi M, Yatsushiro S, Otsuka M, Yamamoto A, Moriyama Y. Co-expression of vesicular glutamate transporters (VGLUT1 and VGLUT2) and their association with synaptic-like microvesicles in rat pinealocytes. J Neurochem. 2003;84(2):382-91.

133. Nandi PK, Irace G, Van Jaarsveld PP, Lippoldt RE, Edelhoch H. Instability of coated vesicles in concentrated sucrose solutions. Proc Natl Acad Sci U S A. 1982;79(19):5881-5.

134. Cheng YF, Boll W, Kirchhausen T, Harrison SC, Walz T. Cryo-electron tomography of clathrin-coated vesicles: Structural implications for coat assembly. Journal of Molecular Biology. 2007;365(3):892-9.

135. Pearse BM. Coated vesicles from human placenta carry ferritin, transferrin, and immunoglobulin G. Proc Natl Acad Sci U S A. 1982;79(2):451-5.

136. Palmgren MG. Acridine orange as a probe for measuring pH gradients across membranes: Mechanism and limitations. Analytical Biochemistry. 1991;192(2):316-21.

137. Linsdell P, Evagelidis A, Hanrahan JW. Molecular determinants of anion selectivity in the cystic fibrosis transmembrane conductance regulator chloride channel pore. Biophysical Journal. 2000;78(6):2973-82.

138. Keen JH, Willingham MC, Pastan IH. Clathrin-coated vesicles: isolation, dissociation and factor-dependent reassociation of clathrin baskets. Cell. 1979;16(2):303-12.

139. Mulberg AE, Tulk BM, Forgac M. Modulation of coated vesicle chloride channel activity and acidification by reversible protein kinase A-dependent phosphorylation. J Biol Chem. 1991;266(31):20590-3.

140. Arai H, Pink S, Forgac M. Interaction of anions and ATP with the coated vesicle proton pump. Biochemistry. 1989;28(7):3075-82.

141. Maycox PR, Deckwerth T, Hell JW, Jahn R. Glutamate uptake by brain synaptic vesicles. Energy dependence of transport and functional reconstitution in proteoliposomes. J Biol Chem. 1988;263(30):15423-8.

142. Tycko B, Keith CH, Maxfield FR. Rapid acidification of endocytic vesicles containing asialoglycoprotein in cells of a human hepatoma line. J Cell Biol. 1983;97(6):1762-76.

143. Li WC, Ralphs KL, Tosh D. Isolation and Culture of Adult Mouse Hepatocytes. In: Ward A, Tosh D, editors. Mouse Cell Culture: Methods and Protocols. Methods in Molecular Biology. 633. Totowa: Humana Press Inc; 2010. p. 185-96.

144. Sengupta S, Peterson TR, Laplante M, Oh S, Sabatini DM. mTORC1 controls fasting-induced ketogenesis and its modulation by ageing. Nature. 2010;468(7327):1100-4.

145. Xiong J, Zhu MX. Regulation of lysosomal ion homeostasis by channels and transporters. Sci China-Life Sci. 2016;59(8):777-91.

146. Jentsch TJ, Poet M, Fuhrmann JC, Zdebik AA. Physiological functions of CLC Cl- channels gleaned from human genetic disease and mouse models. Annual Review of Physiology. Annual Review of Physiology. 67. Palo Alto: Annual Reviews; 2005. p. 779-807.

147. Jentsch TJ. Chloride and the endosomal-lysosomal pathway: emerging roles of CLC chloride transporters. J Physiol-London. 2007;578(3):633-40.

148. Uchida S, Sasaki S, Furukawa T, Hiraoka M, Imai T, Hirata Y, et al. Molecular-Cloning of a Chloride Channel That Is Regulated by Dehydration and Expressed Predominantly in Kidney Medulla. Journal of Biological Chemistry. 1993;268(6):3821-4.

149. Steinmeyer K, Ortland C, Jentsch TJ. Primary structure and functional expression of a developmentally regulated skeletal muscle chloride channel. Nature. 1991;354(6351):301-4.

150. Kieferle S, Fong PY, Bens M, Vandewalle A, Jentsch TJ. 2 Highly Homologous Members of the Clc Chloride Channel Family in Both Rat and Human Kidney. Proceedings of the National Academy of Sciences of the United States of America. 1994;91(15):6943-7.

151. Thiemann A, Grunder S, Pusch M, Jentsch TJ. A chloride channel widely expressed in epithelial and non-epithelial cells. Nature. 1992;356(6364):57-60.

152. Gunther W, Luchow A, Cluzeaud F, Vandewalle A, Jentsch TJ. ClC-5, the chloride channel mutated in Dent's disease, colocalizes with the proton pump in endocytotically active kidney cells. Proceedings of the National Academy of Sciences of the United States of America. 1998;95(14):8075-80.

153. Devuyst O, Christie PT, Courtoy PJ, Beauwens R, Thakker RV. Intra-renal and subcellular distribution of the human chloride channel, CLC-5, reveals a pathophysiological basis for Dent's disease. Hum Mol Genet. 1999;8(2):247-57.

154. Tifft CJ, Adams DR. The National Institutes of Health undiagnosed diseases program. Current Opinion in Pediatrics. 2014;26(6):626-33.

155. Gahl WA, Wise AL, Ashley EA. The Undiagnosed Diseases Network of the National Institutes of Health A National Extension. Jama-Journal of the American Medical Association. 2015;314(17):1797-8.

156. Markello TC, Han T, Carlson-Donohoe H, Ahaghotu C, Harper U, Jones M, et al. Recombination mapping using Boolean logic and high-density SNP genotyping for exome sequence filtering. Mol Genet Metab. 2012;105(3):382-9.

157. Gahl WA, Markello TC, Toro C, Fajardo KF, Sincan M, Gill F, et al. The National Institutes of Health Undiagnosed Diseases Program: insights into rare diseases. Genet Med. 2012;14(1):51-9.

158. Gahl WA, Tifft CJ. The NIH Undiagnosed Diseases Program: lessons learned. Jama. 2011;305(18):1904-5.

159. Malicdan MCV, Vilboux T, Stephen J, Maglic D, Mian L, Konzman D, et al. Mutations in human homologue of chicken talpid3 gene (KIAA0586) cause a hybrid ciliopathy with overlapping features of Jeune and Joubert syndromes. J Med Genet. 2015;52(12):830-9.

160. Silberberg SD, Chang T-H, Swartz KJ. Secondary Structure and Gating Rearrangements of Transmembrane Segments in Rat P2X₄ Receptor Channels. The Journal of General Physiology. 2005;125(4):347.

161. De Duve C, De Barsy T, Poole B, Trouet A, Tulkens P, Van Hoof Fo. Lysosomotropic agents. Biochemical Pharmacology. 1974;23(18):2495-531.

162. Zeevi DA, Frumkin A, Bach G. TRPML and lysosomal function. Biochimica et Biophysica Acta (BBA) - Molecular Basis of Disease. 2007;1772(8):851-8.

163. Sartelet A, Stauber T, Coppieters W, Ludwig CF, Fasquelle C, Druet T, et al. A missense mutation accelerating the gating of the lysosomal Cl-/H+-exchanger ClC-7/Ostm1 causes osteopetrosis with gingival hamartomas in cattle. Dis Model Mech. 2014;7(1):119-28.

CURRICULUM VITAE

Mary R. Weston
maryrweston@gmail.com

Education

2010-2017 **Ph.D., Biology**
Johns Hopkins University and the National Institutes of Health Graduate Partnership Program
Bethesda, MD

Degree conferral date: 12/2017
Advisor: Dr. Joseph Mindell
Thesis title: Investigating the role of chloride in endocytic organelle acidification

2005-2009 **B.A., Biochemistry**
Minors: Mathematics, Economics
DePauw University
Greencastle, IN

Research Experience

2010-2017 **Pre-doctoral Trainee**
Membrane Transport Biophysics Section, NINDS, National Institutes of Health, Bethesda, MD
Advisor: Dr. Joseph Mindell
Research synopsis: Investigating the role of chloride in endocytic organelle acidification, specifically focusing on the role of chloride transporter ClC-7 in lysosomal acidification.

2009-2010 **Biological Systems Specialist 1**
Idaho National Laboratory
Idaho Falls, Idaho
Principle Investigators: Dr. Garold Gresham and Dr. Allison Ray
Description of work: Optimized a Near Infrared Spectroscopy (NIR) method to identify various structural components in biomass and

determine the recalcitrance of biomass exposed to various drying and pretreatment conditions.

2009 **Summer Research Intern**
Idaho National Laboratory
Principle Investigators: Dr. Allison Ray
Project goal: Evaluate the recalcitrance of biomass exposed to various drying and pretreatment conditions.

2008 **SULI Department of Energy Summer Intern**
Idaho National Laboratory
Principle Investigator: Dr. Francisco Roberto
Project goal: devise a method to metabolically engineer Alicyclobacillus acidocaldarius, a thermophillic bacterium, to produce biodegradable plastics

Teaching Experience

2011 **Teaching Assistant,** Cell biology Lab
The Johns Hopkins University, Baltimore, MD (January 2011-May 2011)

2010 **Teaching Assistant,** Biochemistry Lab
The Johns Hopkins University, Baltimore, MD (August 2010-Dec. 2010)

2008 **Teaching Assistant,** Tae Kwon Do Class
DePauw University, Greencastle, IN (January 2008-May 2008)

Select Poster Presentations

- **M.R. Weston** and J.A. Mindell. *Investigating the effects of ClC-7 on lysosomal pH maintenance.* The National Cancer Institute and University of Maryland, Baltimore combined student symposium (Jan. 2016).
- S.B. Lioi, **M.R. Weston**, and J.A. Mindell. *siRNA knockdown of ClC-7 produces a lysosomal pH increase*. Biophysical Society annual meeting (Feb. 2015).
- **M.R. Weston** and J.A. Mindell. *Characterizing a chloride permeable protein present in clathrin-coated vesicles.* The NINDS annual retreat (May 2014).
  Awarded first place, graduate student division.
- **M.R. Weston** and J.A. Mindell. *Characterizing a chloride permeable protein present in clathrin-coated vesicles.* The Biophysical Society Annual Meeting (Feb. 2014).

- **M.R. Weston** and J.A. Mindell. *Characterizing a chloride permeable protein present in clathrin-coated vesicles.* The SGP Annual Meeting: The Enigmatic Chloride Ion (Sept. 2013).
- **M.R. Weston** and F.F. Roberto. *Metabolic engineering of* Alicyclobacillus acidocaldarius *via electroporation for the production of biodegradable plastics.* Invited poster for the SERCh Competition, hosted by the Dept. of Energy at Oak Ridge National Laboratory (Oct. 2008). Awarded travel grant.

Involvement and Leadership Experience

2013-2017	Member of the Biophysical Society
2015-2016	Organization Committee for the NIH Career Symposium
2013-2014	Organization Committee for the NIH Career Symposium
2013-2016	Editor and contributor of the GSChronicles, an NIH graduate student newspaper
2015	Participated in the 2015 JHU JHUGCC biotech case competition
2014-2016	Helped organize and participate in the NINDS 'Backyard brains' activity for Take Your Child to Work Day
2012	Organized and led the JHU-NIH partnership program student recruitment
2016-2017	Member of the 'Lasker Lessons in Leadership' seminar series Seminar series for selected pre- and post-doctoral fellows that provides strategies to develop both scientific and general leadership skills
2015	Completed the NIH Workplace Dynamics series 5 workshops that provide leadership and management training to promote better interpersonal communication
2015	Completed the NIH Translational Science Training Program (TSTP) Training course that intertwines interdisciplinary scientific content, understanding of the drug development process, professional skills development, clinical trial terminology, and career exploration.